An EPR Study of the Protein Proaerolysin

By

Michael James McAlduff
B.Sc., Saint Francis Xavier University, 1999

A Thesis Submitted in Partial Fulfillment of the
Requirements for the Degree of

MASTER OF SCIENCE

In the Department of Chemistry

We accept this dissertation as conforming
To the required standard

Dr. T. E. Gough, Supervisor (Department of Chemistry)

Dr. J. T. Buckley, Supervisor (Department of Biochemistry and Microbiology)

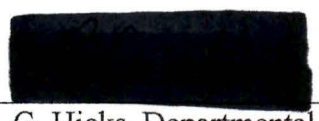

Dr. R. G. Hicks, Departmental Member (Department of Chemistry)

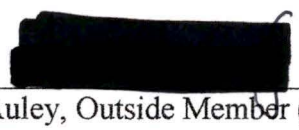

Dr. A. McAuley, Outside Member (Department of Chemistry)

Supervisors: Dr. T. E. Gough, and Dr. J. T. Buckley

Abstract

The purpose of this thesis was to investigate the protein proaerolysin and its active form aerolysin. The nitroxyl spin label (1-oxyl-2,2,5,5-tetramethylpyrrolidine-3-yl)methylmethanethiosulfonate was used to selectively label the protein at cysteines located throughout the protein. Four mutants were chosen because of their location in the protein. Variants 300C PA, 445C PA, 241C PA, and 242C PA were all labeled successfully with the spin label. Their EPR spectra were analyzed to determine what kind of motion was occurring in the aqueous phase. Various additives were used in the hope of identifying large changes in the EPR spectra and attributing them to some change in the structure of the protein. Trypsin, protease K, and SDS were all added to at least one of the mutants. Temperature studies were carried out on 445C PA + MTSL in the proaerolysin and aerolysin forms and correlation times were determined to be on the order of 10^{-11}-10^{-12} seconds. Simulations were performed on the spin label to determine some physical parameters; these simulations were found to be a good basis for comparing spectra of labeled protein and free spin in solution.

Examiners:

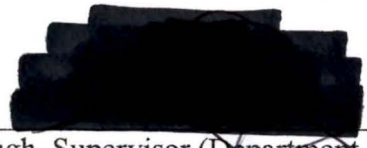

Dr. T. E. Gough, Supervisor (Department of Chemistry)

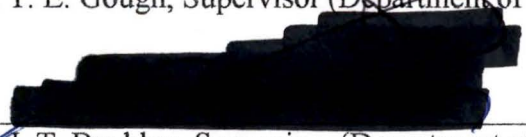

Dr. J. T. Buckley, Supervisor (Department of Biochemistry and Microbiology)

Dr. R. G. Hicks, Departmental Member (Department of Chemistry)

[redacted]

Dr. A. McAuley, Outside Member (Department of Chemistry)

Table of Contents

List of Figures

List of Tables

List of Abbreviations

241C PA Proaerolysin with an amino acid at position 241 replaced with a cysteine

242C PA Proaerolysin with an amino acid at position 242 replaced with a cysteine

300C PA Proaerolysin with an amino acid at position 300 replaced with a cysteine

445C PA Proaerolysin with an amino acid at position 445 replaced with a cysteine

AFC Automatic frequency control

EPR Electron Paramagnetic Resonance

MTSL (1-oxyl-2,2,5,5-tetramethylpyrrolidine-3-yl)methylmethanethiosulfonate

PA Proaerolysin

SDSL site directed spin labeling

Acknowledgements

I would like to thank my supervisors Dr. Terry Gough and Dr. Tom Buckley for their help and guidance during my master's. I would also like to thank all the members of Dr. Buckley's lab who were always helpful and patient when trying to demonstrate a biochemistry technique to a chemist. I would like to thank my committee members for taking the valuable time to prepare for my defense. A special thanks to Mr. Terry Wiley for helping when the EPR was not working properly.

I would like to also thank the people who provided distractions over the past few years. Roommates and other graduate students in chemistry were always ready to take part in social activities outside of work. Special thanks go to Matt Lukeman, Stephan O'Leary, and Craig Jeffrey for the memories. Finally, I would like to thank my folks for their editorial help.

Chapter 1: Introduction

1.1 Principles of EPR

1.1.1 Angular Momentum

For atoms, the model for orbital angular momentum is the motion of a particle on the surface of a sphere. The total orbital angular momentum is quantized, as well as the orbital angular momentum along one direction fixed in space, usually the z direction. The orbital angular momentum for an electron is of the form $[l\,(l+1)]^{1/2}\hbar$, where l is an integer, 0, 1, 2, 3, …, etc. The z-component of orbital angular momentum is $M_l\hbar$. The allowed values of M_l are the integers $0, \pm1, \pm2, \ldots \pm l$, giving $2l + 1$ allowed values of M_l.[1]

To distinguish the spin angular momentum from the orbital angular momentum the quantum number S is used. The electron spin angular momentum has a magnitude given by $[S\,(S+1)]^{1/2}\hbar$ and the component $M_S\hbar$ is restricted to the $2S + 1$ values. The allowed values of M_S range in unit increments from –S up to +S. For a single electron the spin angular momentum is S = ½. An electron can take only two orientations with respect to a specific axis. An α electron is an electron with $m_s = +1/2$. A β electron is an electron with $m_s = -1/2$. The vector representing the magnitude of the spin angular momentum lies at an angle of 55° to the z-axis. When more than one electron is in a given system M_s can take on the values 1, 3/2, 2, etc.[1]

Similar to the orbital and spin angular momenta, the nuclear spin angular momentum is quantized. The nuclear spin quantum number, I, may be half-integral or integral.

1.1.2 Relation Between Magnetic Moments and Angular Momenta

The magnetic dipole moment is what is important in the present study. Magnetic moment and angular momentum are proportional to one another. The magnetic moment is given by

$$\mu_z = \gamma M_I \hbar . \qquad (1)$$

The coefficient of proportionality γ is called the magnetogyric ratio. In EPR spectroscopy γ = -ge/2mc, where g is a factor which is required for all cases other than those involving pure orbital angular momentum. There is an associated orbital magnetic moment of eh/4πmc arising from the quantization of the orbital angular momentum. For the electron, this value is given by the symbol μ_B which is called the Bohr magneton.[2] The value of g can be determined by the Landé formula.

$$g = 1 + \frac{J(J+1) + S(S+1) - L(L-1)}{2J(J+1)} \qquad (2)$$

For electron spin the value of g is very close to 2, for a free electron $g_e = 2.00232$. The extra 0.00232 comes from the interactions of the electron with the fluctuations of the electromagnetic field around the electron.[3] In equation 2, J is the quantum number for the total angular momentum of an atom, and takes on the values J = L+S, L+S-1… |L-S|.[1] The electron spin magnetic moment μ_z along the direction of the magnetic field **H** is

$$\mu_z = \gamma M_S \hbar = - g\mu_B M_S. \qquad (3)$$

Since there is a negative charge on the electron, there is a negative sign in equation 3.[2]

1.1.3 Energy of Magnetic Dipoles in a Magnetic Field

The next consideration will be that of a set of noninteracting magnetic dipoles in a fixed magnetic field which could represent either nuclear or electronic dipoles. The classical energy of a magnetic dipole in a magnetic field is given by:

$$W = -\boldsymbol{\mu}\cdot\mathbf{H} = -\mu H \cos(\boldsymbol{\mu}, \mathbf{H}). \quad (4)$$

W is the energy, $\boldsymbol{\mu}$ is the dipole moment of a magnet in a field **H**, and ($\boldsymbol{\mu}$, **H**) is the angle between $\boldsymbol{\mu}$ and **H**. The classical description would allow ($\boldsymbol{\mu}$, **H**) to have any value, but electrons and nuclei behave quantum mechanically, therefore only certain values are allowed.[2] Equation 4 becomes $W = -\mu_z H$, where μ_z is the magnetic component. This equation when combined with equation 3 gives a set of energies

$$W = g\mu_B H M_S. \quad (5)$$

M_S can have the values +1/2 and –1/2 giving two possible values for W, $\pm$ 1/2 $g\mu_B H$. These are referred to as the Zeeman energies and, if the photon energy *hv* matches the energy-level separation ΔW, then transitions between two Zeeman levels can be stimulated by an electromagnetic field of the suitable frequency *v*. The change in energy between two Zeeman levels is given by:

$$\Delta W = hv = g\mu_B H. \quad (6)$$

The magnetic dipole selection rules are $\Delta M_s = \pm 1$, $\Delta M_I = 0$, and $H_1 \perp H_0$.[2]

1.2 Instrumentation

Electromagnetic radiation can be thought of as coupled electric and magnetic fields that are oscillating perpendicular to one another and to the direction of propagation. It is the electric field component that interacts with molecules. For absorption to occur,

the energy of a quantum must correspond to the separation between energy levels in the molecule. EPR is a technique that can only be used when species have a net electron spin angular momentum. The many species which may be studied by EPR include free radicals (solid, liquid, or gaseous phases), point defects in solids such as F-defects, biradicals, and transition-metals ions.[2]

One expects that a molecule that has magnetic dipoles would interact with the magnetic component of microwave radiation. When the molecule is irradiated over a wide range of frequencies, only minimal absorption arises from a magnetic interaction due to zero-field splittings. When the molecule is placed in a static magnetic field then absorption arises from magnetic dipole transitions.[2]

A possible experimental arrangement for the detection of magnetic dipolar transitions is the spectrometer shown in Figure 1.1. Absorption will occur when the energy of a quantum of incident radiation matches the energy-level separation of a molecule between its ground state and an excited state. The requirement of a static magnetic field is the unique aspect for most magnetic dipolar transitions, except for zero-field splittings of triplets. In the absence of a magnetic field the energy levels are degenerate.

The most important component of an EPR spectrometer is the resonant cavity that contains the sample. The fundamental resonant frequency is the frequency at which one-half of a wavelength corresponds to a cavity dimension. Considerable microwave energy may be stored in the mode of a resonant cavity even though the energy density associated with a traveling wave is usually small. The wavelength of a microwave is on the order of centimeters; therefore, the size of a resonant microwave cavity will be large. In a cavity,

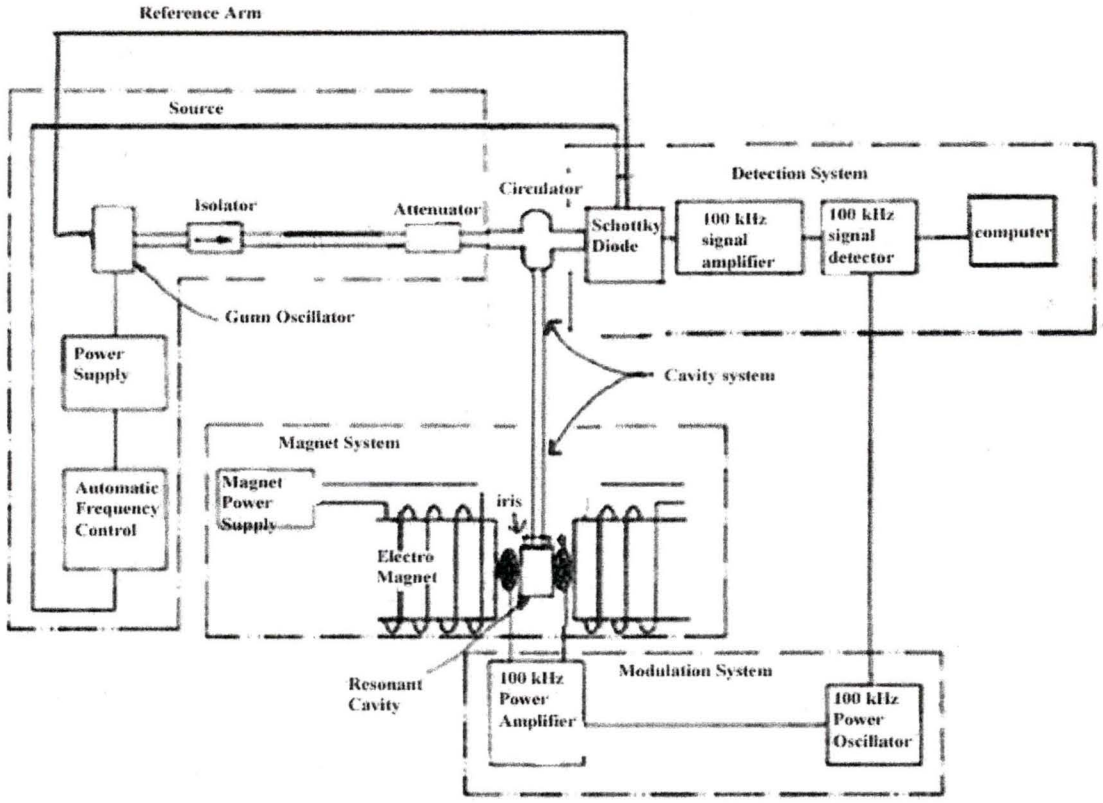

Figure 1.1: EPR spectrometer blocked according to function[2]

one has to consider both electric (E_1) and magnetic (H_1) fields. The E_1 and H_1 fields have different locations for their maxima; their locations depend on the cavity mode. To be useful a cavity mode should: (a) allow a high-energy density, and (b) placement of the sample at a maximum of H_1 and a minimum E_1.[2] Cavities are characterized by their Q or quality factor. This parameter is an indication of how efficiently the cavity can store microwave energy. The higher the Q value, the more sensitive the spectrometer becomes. The Q factor is defined as

$$Q = \frac{2\pi(energy\ stored)}{energy\ dissipated\ per\ cycle} \qquad (7),$$

where the energy dissipated per cycle is the amount of energy lost during one microwave period. The Q value for the spectrometer used in this study, the Bruker EMX EPR, is 18,000 for an empty cavity, but drops to 2,000 when a sample is introduced. Therefore, the cavity effectively amplifies the signal 2,000 times. Energy can be lost to the side walls of the cavity because the microwaves generate electrical currents in the side walls of the cavity, which in turn generates heat. Energy can also be lost to the sample as the microwaves heat the sample. The Q factor can be easily measured because there is another way of expressing Q (Figure 1.2):

$$Q = \frac{\nu_{res}}{\Delta\nu}, \qquad (8)$$

where ν_{res} is the resonant frequency of the cavity and $\Delta\nu$ is the width at half height of the resonance. A consequence of the resonance is that there will be a standing wave inside the cavity. Standing electromagnetic waves have their electric and magnetic field components exactly out of phase in space. Where the magnetic field is a maximum, the

electric field is a minimum and vice versa. The spatial distribution of the amplitudes of the electric and magnetic fields of the fundamental mode are shown in Figure 1.3 for the EMX EPR cavity.[2]

A small hole referred to as an iris couples microwave energy in and out of the sample. The fractional reflection of microwave energy from the cavity should be reduced to some small value; thus the reflected power at the sample resonance is enhanced. The setting of the iris depends upon the size and nature of the sample.[2] Critical coupling corresponds to a maximum power transfer from the microwave source to the cavity. Reflection of some fraction of the incident energy can occur due to discontinuities in the waveguide or imperfect matching of microwave elements, therefore standing waves arise. One would like the power appearing at the detector to come only from reflections originating at the microwave cavity since reflections from other sources decrease instrument sensitivity. The sample absorbs microwave energy; the Q is lowered because of increased losses and the coupling changes due to the change of the impedance of the cavity. The cavity is no longer critically coupled, resulting in microwaves being reflected back to the bridge, giving an EPR signal.[2]

A circulator is a nonreciprocal device that causes little loss to waves traveling in the forward direction, but it attenuates waves moving in the reverse direction. The circulator is constructed from ferrite components and small magnets. Due to the magnetic field, electrons of the ferrite precess about the magnetic field with Larmor frequency. In certain propagation directions, microwaves are absorbed due to resonance effects. The circulator is used to direct microwave power to the cavity and to direct the signal reflected from the cavity to the detector (Figure 1.4).[5]

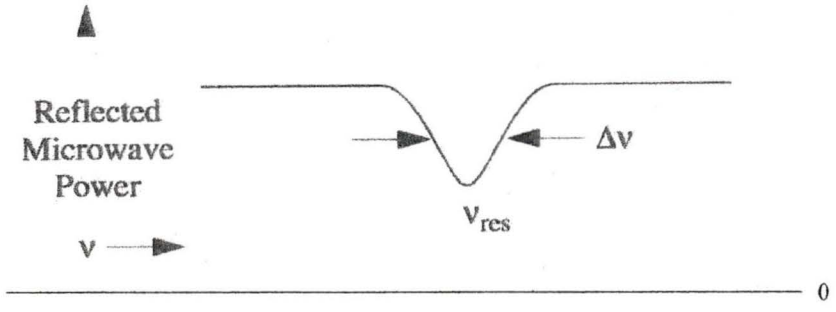

Figure 1.2: Reflected microwave power from a resonant cavity[4]

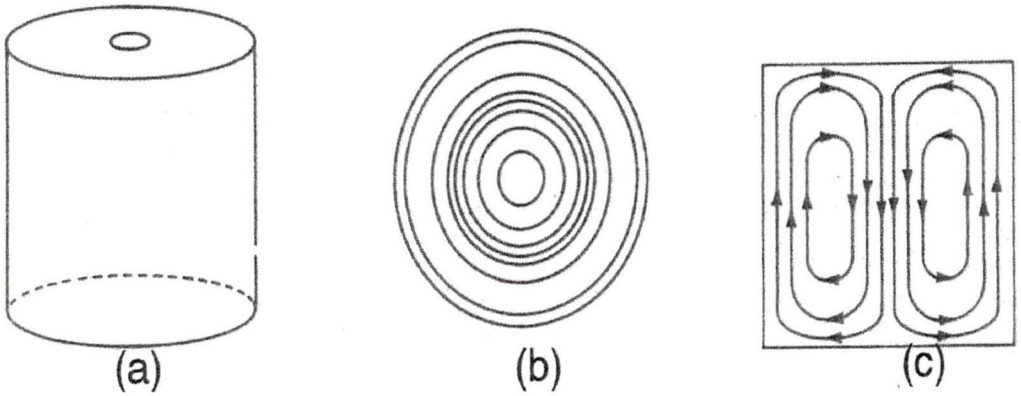

Figure 1.3: (a) the cavity, (b) the electric field and (c) the magnetic field patterns in the EMX EPR .[2]

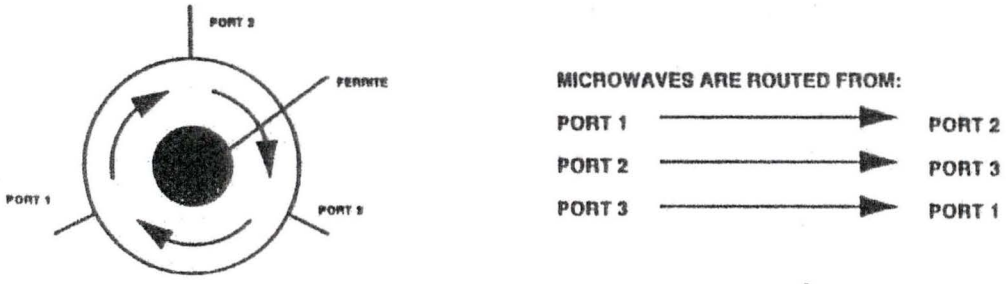

Figure 1.4: Circulator for an EMX EPR[5]

The EMX EPR spectrometer employs a gunn oscillator as the source of microwave radiation. The gunn oscillator was developed by Berteaud, 1976; Bott and Fawcett, 1968; Eastman, 1972; Kroemer, 1972; and Shurmer, 1971.[6] It consists of two gunn diodes and a varactor that are coupled to a cylindrical cavity with variable dimensions. The varactor is a semiconductor diode with the properties of a voltage-dependent capacitor. The frequency is determined by the dimensions of the cavity and the varactor. Since the dimensions and the varactor voltage depend on each other they are controlled simultaneously by a servo mechanism. The total frequency range of the EMX bridge is 9.1 GHz to 9.9 GHz. The principles of operation are that, if one applies a suitable gunn voltage, the gunn element shows a region of negative resistance which causes oscillations at various frequencies. An additional resonance circuitry is able to reduce this frequency band to one specific frequency. The frequency fine adjustment is done by the varactor (automatic frequency control) (Figure 1.5). Owing to the resonant absorption by the cavity, there will be a sharp dip at that region of the mode that corresponds to the cavity resonance frequency. The gunn oscillator is tuned so that the dip occurs at the center of the mode.[5]

Because the energy density in the resonant cavity is very sensitive to the frequency of the incident radiation, the gunn oscillator frequency should be very stable. The resonant linewidth of the cavity should be large compared to frequency variations. An automatic-frequency-control system may be used for stabilization. The gunn oscillator frequency may be readily "locked" to the resonant frequency of the sample cavity. The output of the microwave source cannot be varied easily so the next component is a variable attenuator. The variable attenuator is a device that blocks the

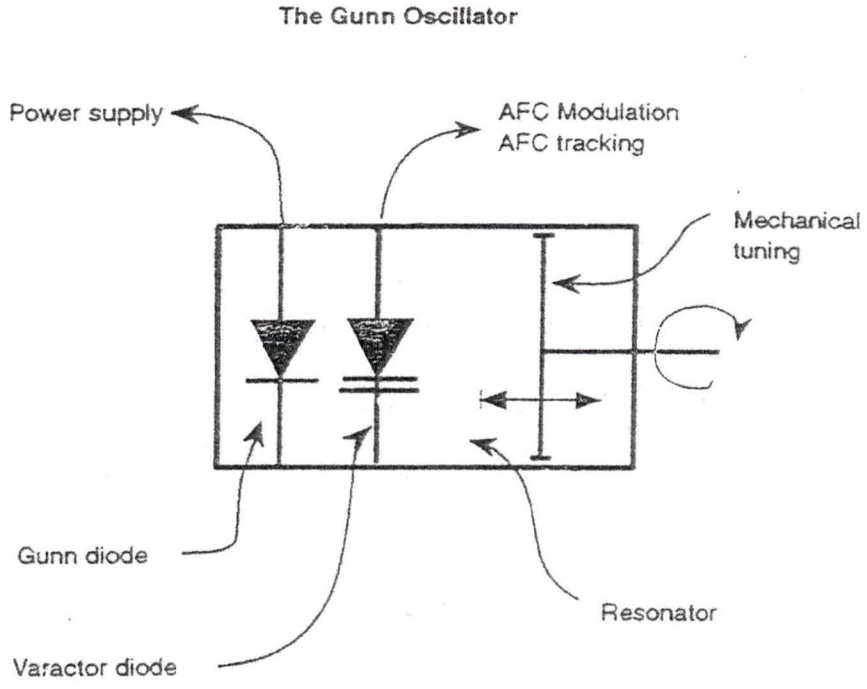

Figure 1.5: The Gunn Oscillator[5]

flow of microwave radiation. The attenuator allows for the precise and accurate control of the microwave power that the sample sees.[4]

A Schottky diode is used to detect the reflected microwaves by converting the microwave power to an electrical current. A reference arm makes sure the detector operates at the proper level by supplying the detector with some extra microwave power or "bias". Some of the source power is split off into the reference arm, where a second reference attenuator controls the power level, and thus the diode current. To ensure that the reference arm microwaves are in phase with the reflected signal microwaves when the two signals combine at the detector diode there is a phase shifter.[4]

The main disadvantage of the EMX EPR outlined in Figure 1.1 is the contribution of 1/f noise components to the output signal from the detector. To limit the noise-contributing components to frequencies very close to the modulation frequency, a small-amplitude magnetic field modulation is used. The most commonly used modulation frequency is 100 kHz. This frequency is obtained by placing small Helmholtz coils on each side of the cavity along the axis of the static field.[2] A microwave diode detector produces noise that is inversely proportional to the frequency of the detected signal ("1/f noise"). The widespread use of 100 kHz as a modulation frequency is because 100 kHz is the highest frequency where the line of interest will not be broadened. 100 kHz corresponds to a linewidth of approximately 0.1 gauss. The amplitude of the 100 kHz signal is proportional to the slope of the Figure 1.6 at the center of the modulating field when the amplitude of the field modulation is small compared to the linewidth. The magnetic field is modulated between H_a and H_b and the detector current oscillates

sinusoidally between i_a and i_b. For small modulation amplitudes the output signal appears as the first derivative of the absorption signal.[2]

The signal to noise ratio can be improved by signal averaging. Signal averaging involves addition of spectra obtained by repetitive scans. The spectrum is divided into equal intervals with each portion stored in a separate channel of a time-averaging computer. The signal stored in each channel rises in proportion to n, the number of scans. The noise signal will increase in proportion to $\sqrt{n}$. Therefore, the signal-to-noise ratio improves in proportion to $\sqrt{n}$.[2]

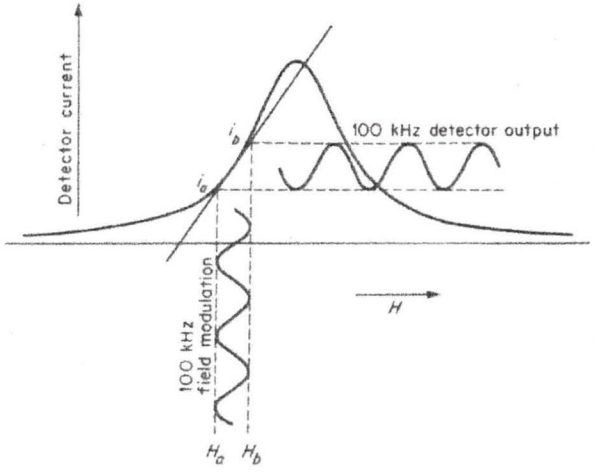

Figure 1.6: 100 kHz modulation[2]

1.3 The Spin Hamiltonian

The Hamiltonian operator of a system is a quantum mechanical operator whose eigenvalues are the energies of the states of the system. The spin Hamiltonian is

$$\mathcal{H} = \mu_B \mathbf{S}\cdot\mathbf{g}\cdot\mathbf{H} + \mathbf{S}\cdot\mathbf{A}\cdot\mathbf{I} - g_N\mu_N\mathbf{I}\cdot\mathbf{H}. \quad (9)$$

The first term is the electronic Zeeman term. The **g**-tensor

> "is a symmetric tensor composed of the free-electron g-value plus an anisotropic correction due to the spin-orbit coupling." (p. 155)[1]

The **A**-tensor is the magnetic hyperfine interaction, and consists of an isotropic and anisotropic component.[1]

1.3.1 The Zeeman term

The spin Hamiltonian reduces to equation 10 when zero-field splittings and nuclear effects are ignored

$$\mathcal{H} = \mu_B \mathbf{S}\cdot\mathbf{g}\cdot\mathbf{H}\,. \quad (10)$$

There is a reference frame that diagonalizes **g** and the Hamiltonian becomes

$$\mathcal{H} = \mu_B [S_x S_y S_z]\cdot\begin{bmatrix} g_1 & 0 & 0 \\ 0 & g_2 & 0 \\ 0 & 0 & g_3 \end{bmatrix}\cdot\begin{bmatrix} H_x \\ H_y \\ H_z \end{bmatrix} \quad (11)$$

$$\mathcal{H} = \mu_B (g_1 S_x H_x + g_2 S_y H_y + g_3 S_z H_z). \quad (12)$$

The energy levels will then be given by

$$E = \mu_B S_H H(g_1^2 \sin^2\theta\cos^2\phi + g_2^2 \sin^2\theta\sin^2\phi + g_3^2\cos^2\theta)^{1/2} = \mu_B g_H S_H H\,, \quad (13)$$

with the θ and ϕ being the polar and azimuthal angles respectively.

The g-value in the direction of **H** is

$$g_H = (g_1^2 \sin^2\theta\cos^2\phi + g_2^2 \sin^2\theta\sin^2\phi + g_3^2\cos^2\theta)^{1/2}\,. \quad (14)$$

In a solution, molecules are tumbling and rotating. Therefore the different g-values average to

$$g^2 = \frac{1}{3}(g_1^2 + g_2^2 + g_3^2). \quad (15)$$

In a symmetric environment the g-tensor has axial symmetry;

$$g_1 = g_2 = g_\perp \quad \text{and} \quad g_3 = g_{//}.$$

Then g_H reduces to

$$g_H = (g_\perp^2 \sin^2\theta + g_{//}^2 \cos^2\theta)^{1/2}. \quad (16)$$

In solution, the average value is given by equation 17[1]

$$g = \frac{1}{3}(2g_\perp + g_{//}). \quad (17)$$

1.3.2 Electron spin-nuclear spin interaction

A splitting of the Zeeman levels can occur because of the existence of nuclei with magnetic moments other than zero (nuclear spin I = 1/2, 1, 3/2,...). This is because the nuclear spins also quantize in the magnetic field at the nucleus. The electron experiences both the external magnetic field and the field at the electron due to the nuclear magnetic moments. This effect is represented by the term

$$\mathbf{S \cdot A \cdot I} \quad (18)$$

where **A** is the hyperfine coupling tensor, **S** is the electron spin vector operator, and **I** is the nuclear spin vector operator. The electronic transitions $\Delta m_S = \pm 1$ do not change the population of the nuclear levels. Therefore, the EPR permitted transitions occur at $\Delta m_I = 0$. The electron Zeeman level given by equation 10 is then split into $2I + 1$ levels.

> "If the electron Zeeman term is large as compared with the hyperfine term..., the coupling tensor **A** does not depend on **H**." (p. 164)[1]

In small fields the electron Zeeman and hyperfine terms are on the same order, and **S·A·I** does not apply because of the strong **I-S** contact interaction coupling. Thus there is a resulting effective spin.[1]

$$\mathbf{F} = \mathbf{S} + \mathbf{I} \tag{19}$$

This is illustrated in Figure 1.7 for S = I = ½.

The levels do not converge to a single value as can be seen in Figure 1.7 but move toward the zero-field energy levels for F = 1, a triplet state, and F = 0, a singlet state. Equation 18 can be used without restriction because of the use of strong fields in most EPR research.[1]

The hyperfine tensor consists of two parts: an isotropic and an anisotropic part. The isotropic term occurs when the electron density at the nucleus is not zero. It is known as the Fermi or contact term, *a*, and is proportional to the s-character of unpaired electrons in ions and atoms. The anisotropic term, also known as the dipolar interaction **B**, is caused by the magnetic interaction between electronic and nuclear spins. The diagonal form of the hyperfine tensor is written

$$\mathbf{A} = \begin{bmatrix} a+B_1 & 0 & 0 \\ 0 & a+B_2 & 0 \\ 0 & 0 & a+B_3 \end{bmatrix} = a + \begin{bmatrix} B_1 & 0 & 0 \\ 0 & B_2 & 0 \\ 0 & 0 & B_3 \end{bmatrix} = a + \mathbf{B} \tag{20}$$

The contact term is shown in equation 21,

$$a = a_s^{\,2} g \mu_B g_N \mu_N (8\pi / 3) \mathbf{S} \cdot \mathbf{I} \delta (\mathbf{r}_e - \mathbf{r}_N) . \tag{21}$$

Where a_s^2 is the probability that the electron is in an s state and $\delta(\mathbf{r}_e - \mathbf{r}_N)$ is the Dirac delta function. Equation 21 can be rewritten as a function of the value at the nucleus of the normalized electron spin density $\vartheta(\mathbf{r}_N)$,

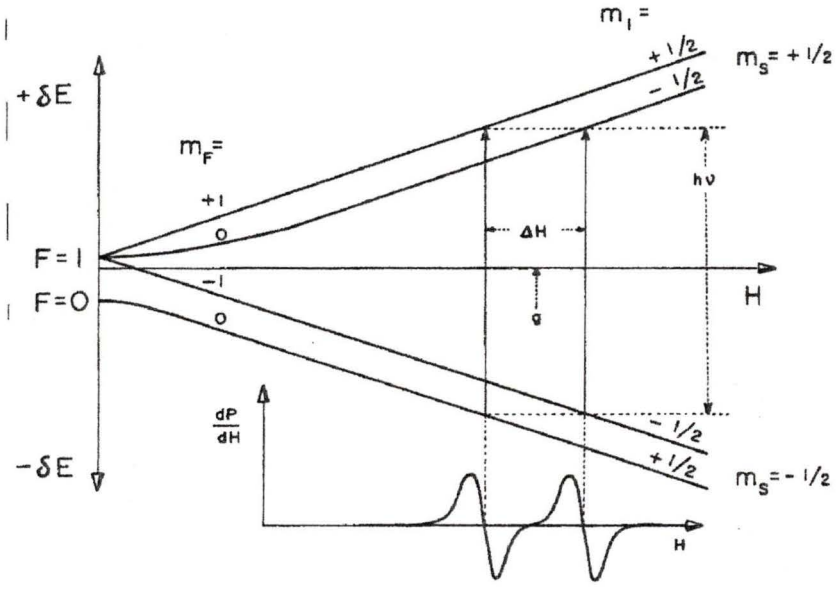

Figure 1.7: Energy level diagram for S = ½ and I = ½.[1]

$$a = a_s^{\,2} g\mu_B g_N \mu_N (8\pi/3)\vartheta(\mathbf{r}_N) \tag{22}$$

because the delta function is zero for $\mathbf{r}_e \neq \mathbf{r}_N$.

The anisotropic hyperfine term is

$$\mathbf{S}\cdot\mathbf{B}\cdot\mathbf{I} = -(1-a_s^{\,2})g\mu_B g_N \mu_N \left[\frac{\mathbf{S}\cdot\mathbf{I}}{|\mathbf{r}|^3} - \frac{3\mathbf{S}\cdot\mathbf{rr}\cdot\mathbf{I}}{|\mathbf{r}|^5}\right] \tag{23}$$

where $(1 - a_s^{\,2})$ is the probability that the electron is not in an s state.[1]

According to McMillan,[1] if the hyperfine coupling is different in the x, y, and z directions, then the hyperfine term of the Hamiltonian is

$$\mathcal{H}_{\text{hf}} = [S_x S_y S_z]\cdot\begin{bmatrix} A_1 & 0 & 0 \\ 0 & A_2 & 0 \\ 0 & 0 & A_3 \end{bmatrix}\cdot\begin{bmatrix} I_x \\ I_y \\ I_z \end{bmatrix} \tag{24}$$

and the hyperfine coupling energies are the eigenvalues

$$\begin{aligned} E_{1(\text{hf})} &= A_1 m_S m_I \\ E_{2(\text{hf})} &= A_2 m_S m_I \\ E_{3(\text{hf})} &= A_3 m_S m_I. \end{aligned} \tag{25}$$

For axial symmetry, the Hamiltonian due to the hyperfine interaction is

$$\mathcal{H}_{\text{hf}} = [S_x S_y S_z]\cdot\begin{bmatrix} A_\perp & 0 & 0 \\ 0 & A_\perp & 0 \\ 0 & 0 & A_{//} \end{bmatrix}\cdot\begin{bmatrix} I_x \\ I_y \\ I_z \end{bmatrix}. \tag{26}$$

The effective spin Hamiltonian for S = ½ is

$$\mathcal{H} = \mu_B[\, g_\perp^{\,2}\sin^2\theta + g_{//}^{\,2}\cos^2\theta]^{1/2}\,\mathbf{H}\cdot\mathbf{S} + A_{//}S_zI_z + A_\perp(S_xI_x + S_yI_y) \tag{27}$$

and the eigenvalues of the spin Hamiltonian are[1]

$$E_{\perp} = \mu_B g_{\perp} H m_S + A_{\perp} m_S m_I \quad (28)$$

$$E_{//} = \mu_B g_{//} H m_S + A_{//} m_S m_I .$$

The hyperfine tensor values are

$$A_1 = a + B_1 \quad (29)$$

$$A_2 = a + B_2 \quad (30)$$

$$A_3 = a + B_3. \quad (31)$$

The contact term is

$$a = \frac{1}{3}(A_1 + A_2 + A_3) \quad (32)$$

and in axial symmetry it is

$$a = \frac{1}{3}(A_{//} + 2A_{\perp}).^{1} \quad (33)$$

1.4 Broadening Mechanisms

1.4.1 Bloch equations

The Bloch equations introduce the relaxation times T_1 and T_2. In our cavity the electron magnetic moments precess about H_{eff}. H_{eff} is the field that results from the external magnetic field and the instantaneous value of the oscillatory field H_1. Turning off H_1 will leave the electronic magnetic moment pointing in a direction between H_1 and H_0. The electron magnetic moment starts to precess about H_0. The direction of H_0 is the z-axis; the component of the magnetization along z will increase as the magnetization vector **M** moves toward the z-axis. This process is called spin-lattice relaxation; it occurs in a time T_1, because it requires that the dipole give up energy to the lattice. The component perpendicular to the z-axis will also change. When H_1 is turned off, the coherence of the individual components is lost and $M_{\perp}$ starts to decay. This process is

called spin-spin relaxation, occurs in a time T_2, and involves spin-spin rather than spin-lattice interaction. Both relaxations are exponential, and in a frame rotating with $M_\perp$ are given by

$$\left(\frac{d}{dt}\right)M_z = \left(\frac{1}{T_1}\right)(M_0 - M_z) + \gamma(\boldsymbol{M}\times\boldsymbol{H})_z = -\gamma(M_x H_1 \sin\omega t - M_y H_1 \cos\omega t) + \frac{(M_0 - M_z)}{T_1} \tag{34}$$

$$\left(\frac{d}{dt}\right)M_x = \gamma(\boldsymbol{M}\times\boldsymbol{H})_x - \left(\frac{1}{T_2}\right)M_x = +\gamma(M_y H_0 + M_z H_1 \sin\omega t) - \frac{M_x}{T_2} \tag{35}$$

$$\left(\frac{d}{dt}\right)M_y = \gamma(\boldsymbol{M}\times\boldsymbol{H})_y - \left(\frac{1}{T_2}\right)M_y = \gamma(-M_z H_1 \cos\omega t + M_x H_0) - \frac{M_y}{T_2} \tag{36}$$

where ω is the frequency of rotation about the z axis. Equations 34-36 are Bloch's equations.[7] The $\gamma(\mathbf{M}\times\mathbf{H})$ term in each equation comes from the driving of $\mathbf{M}$ by the torque.[1]

1.4.2 Line broadening

The relaxation effects of the dipolar interactions can be treated as a time-dependent perturbation using the results of Redfield theory.[8] The spin Hamiltonian gives resonance lines centered at the fields

$$H_m = \hbar\omega / \beta g(\theta,\phi) - A(\theta,\phi)m / \beta g(\theta,\phi), \tag{37}$$

where m is the allowed values of the nuclear magnetic quantum number, and

$$g(\theta,\phi) = (g_x^{\,2}c_x^{\,2} + g_y^{\,2}c_y^{\,2} + g_z^{\,2}c_z^{\,2})^{1/2}, \tag{38}$$

$$A(\theta,\phi) = (A_x^{\,2}g_x^{\,2}c_x^{\,2} + A_y^{\,2}g_y^{\,2}c_y^{\,2} + A_z^{\,2}g_z^{\,2}c_z^{\,2})^{1/2} / g(\theta,\phi), \tag{39}$$

with

$$\begin{aligned} c_x &= \sin\theta\cos\phi, \\ c_y &= \sin\theta\sin\phi, \\ c_z &= \cos\theta. \end{aligned} \tag{40}$$

The composite line shape may be obtained by averaging over all possible orientations,

$$L(H) = \int_0^{2\pi}\int_0^{\pi} L(\theta, \phi, H) \sin\theta \, d\theta \, d\phi \,, \tag{41}$$

where $L(\theta, \phi, H)$ is the individual component line shape. The results of fluctuating magnetic fields on the relaxation times of resonance lines can be predicted by Redfield theory.[8] The Redfield theory gives the linewidth, δH,

$$\delta H = g\beta\tau[\langle H_{z'}^{\,2}\rangle + \langle H_{y'}^{\,2}\rangle/(1+\omega_0^{\,2}\tau^2)]/\hbar\,, \tag{42}$$

where $\langle H_{z'}^{\,2}\rangle$ and $\langle H_{y'}^{\,2}\rangle$ are the mean-square components of the fluctuating field parallel and perpendicular to the laboratory field H.[8]

> "The field component $H_{z'}$ makes random jumps in time between two extreme values $\pm H_{z'}$, corresponding to the effective spin state of the paramagnetic center producing the field. Thus the mean-square field $\langle H_{z'}^{\,2}\rangle$ is simply equal to $H_{z'}^{\,2}$." (p. 2610)[8]

If $\tau\omega_0 >> 1$, then the second term involving $H_{y'}$ may be neglected.[8]

If the magnetic environment of the unpaired electron is changed due to chemical processes, then the EPR line could be broadened. If a free radical can exist in two forms, A and B, and there is no interconversion between the two forms two lines will appear in the EPR spectrum, Figure 1.8(a). If interconversion occurs broadening of the lines result. As the rate of interconversion from form A to form B increases more broadening results and the lines move closer together until the result is a single spectrum.[2] This result is

illustrated in Figure 1.8. In the limit of slow interconversion the relation between the linewidth Γ and the mean lifetime is[2]

$$\Gamma = \Gamma_0 + \frac{1}{2\tau g_e}. \tag{43}$$

where Γ_0 is the width without interconversion. The mean lifetime, τ, can be written in terms of τ_A and τ_B,

$$\tau = \frac{\tau_A \tau_B}{\tau_A + \tau_B}. \tag{44}$$

Therefore, if $\tau_A = \tau_B$, the mean lifetime of species A or B is 2τ.[2]

Figure 1.8b shows the spectrum when the interconversion has increased the linewidth by a factor of 2. As the rate of interconversion increases, the lines continue to broaden and begin to move toward their midpoint. The relationship between shift and lifetime is given by equation 45

$$(\delta H_0^2 - \delta H_e^2)^{1/2} = \frac{\sqrt{2}}{g_e \tau}. \tag{45}$$

Here δH_0 is the line separation without interconversion and δH_e the line separation when there is interconversion. This is illustrated in Figure 1.8c. The two lines continue to broaden and shift with increasing rate of interconversion until they give a single line, as shown in Figure 1.8d.[2]

As the interconversion becomes very fast, the width of the line becomes proportional to τ and to the mean square of δH_0.

$$\Gamma = \Gamma_0 + g_e \frac{\tau \left\langle (\delta H_0)^2 \right\rangle}{4} \tag{46}$$

Figures 1.8d and 1.8e show this point. At the fast interconversion limit the line narrows to the limiting width Γ_0.[2]

The lines will converge to a position given by the weighted mean. If the two forms have probabilities p_A and p_B, then

$$\langle H \rangle = \frac{p_A H_A + p_B H_B}{p_A + p_B} \tag{47}$$

and the linewidth is[2]

$$\Gamma = \Gamma_0 + g_e \tau p_A p_B \left\langle \left(\delta H_0\right)^2 \right\rangle \tag{48}$$

1.4.3 Inhomogeneous and Homogeneous Broadening

Inhomogeneous broadening results from the unpaired electron being in slightly different magnetic fields depending on location in the magnetic field. At any time a small fraction of the spins are in resonance. The observed line is a superposition of individual components each slightly shifted from the others. The observed line has approximately a Gaussian shape that can be written by equation 49

$$y = a \exp(-bx^2). \tag{49}$$

Inhomogeneous broadening can arise in a number of ways. Inhomogeneous broadening can be caused by an inhomogeneous magnetic field. Anisotropic interactions in randomly oriented systems in the solid state may also cause inhomogeneous line broadening. In this case the distribution of local magnetic fields resulting from the anisotropic g and hyperfine interactions gives rise to the inhomogeneity. Finally, another cause of inhomgeneous broadening can be unresolved hyperfine structure; for example, the four methyl groups surrounding the nitroxide on the label used in this study, may

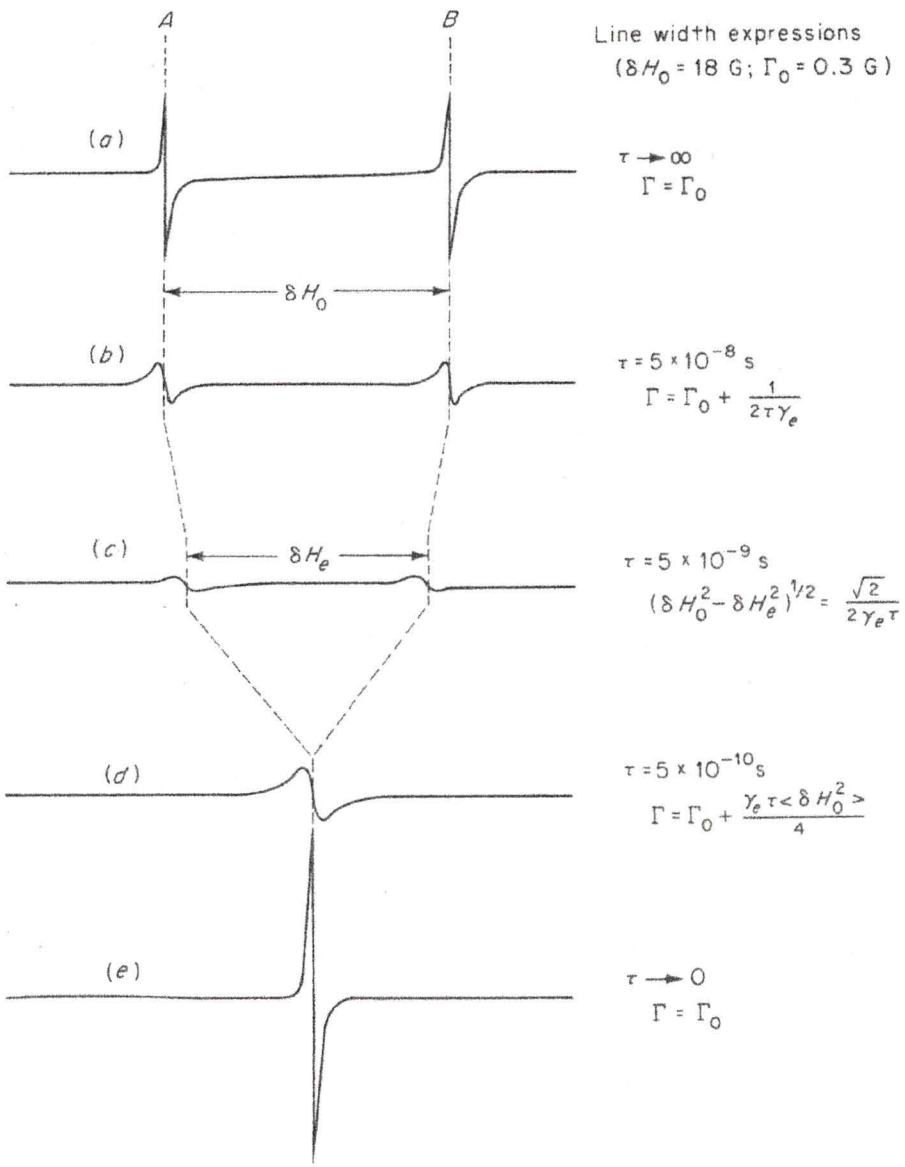

Figure 1.8: The effect of increasing rate of interconversion between form A and B of a free radical[2]

cause inhomogeneous line broadening.[2]

For homogeneous broadening,[2] the static and the time-average magnetic field can be considered to be the same at each electron dipole. However, the instantaneous magnetic field is not the same at each electron dipole. The line shape is therefore the same for each electron dipole. The line has a lorentzian shape which can be written in the following form.

$$y = \frac{a}{a + bx^2} \tag{50}$$

Electron spin-electron spin dipolar interaction is the first mechanism which will be considered. Spin-spin interaction occurs except in very dilute solutions. There is a magnetic field associated with the electron magnetic moment. The magnitude of this field at the electron can take any value between $\pm 2\mu_e/r^3$ depending on orientation where r is the distance to another unpaired electron. Electron spin-nuclear spin interactions are produced by magnetic nuclei near the radical. In a liquid of low viscosity anisotropic interactions with magnetic nuclei are averaged to zero. When the radical is tumbling slowly the anisotropy of g and hyperfine interactions can contribute to the spin-spin relaxation time via the mean square of the fluctuating field.[2]

1.5 Correlation times

When an unpaired electron interacts with a nucleus of spin I, the observed spectrum will consist of $2I + 1$ hyperfine components. Each component is identified by the nuclear quantum number M which characterizes the sublevels involved in the transitions.

> "For a Lorentzian curve, the peak-to-peak height of the first derivative varies with the inverse square of the width, and therefore the

relative heights of two lines having the same intensity but different widths is given by

$$I_1 / I_2 = [T_2(1) / T_2(2)]^2 . \qquad (51)$$

The linewidth variations have to be ascribed in most cases to the fluctuations of the anisotropic terms of the magnetic Hamiltonian caused by molecular motions." (p. 29)[9]

When the spectral lines result from hyperfine interaction with a single nucleus, then the dependence of the linewidth $1/T_2$ on the quantum number M specifying the transition is

$$[T_2(M)]^{-1} = A + BM + CM^2 . \qquad (52)$$

A, B, and C are linewidth parameters. The A value is a constant term including all line-broadening effects which are the same for all hyperfine components. The B coefficient arises from the product of the g and hyperfine tensors. These coefficients cause the spectrum to appear asymmetric. The C coefficient is a function only of hyperfine anisotropy. The B and C values provide information on the rotational correlation time for tumbling of the radical in the liquid. Therefore, it is worthwhile to rewrite equation 52

$$[T_2(0)]^{-1}[T_2(0) / T_2(\pm 1) - 1] = C \pm B \qquad (53)$$

where $[T_2(0)]^{-1}$ is the width of the central line (M = 0). Values of $T_2(0)/T_2(\pm 1)$ come from the square root of the ratios of the peak heights of our spectrum. The B and C parameters are related to τ_c in the following way;

$$B = \frac{4}{15} f(\Delta\gamma) H_0 \tau_c \qquad C = \frac{1}{8} f^2 \tau_c \qquad (54, 55)$$

where

$$f = \frac{4}{3}\pi(A_{//} - A_{\perp}) \qquad (56)$$

all the hyperfine terms have units of MHz, and

$$\Delta\gamma = \beta_e \hbar^{-1}\left[g_{rr} - \frac{1}{2}(g_{pp} + g_{qq})\right]. \qquad (57)$$

The correlation time is regarded as the time for one rotation through one radian about a principal axis.[9]

1.6 The nitroxide spin label

In the present study g values for a nitroxide spin label will be considered. Systems with an n-fold axis of symmetry ($n \geq 3$) are described as having axial symmetry, $x = y$. Two components of the g value which are the approximations $g_{\perp}$ and $g_{//}$ are to be considered. Figure 1.10 shows how the g components are oriented with respect to the symmetry axis.

Figure 1.11 shows the dipole-dipole interaction that is set up in the molecule. This interaction is dependent on the orientation of the p orbital with respect to the magnetic field.

In this case the dipolar energy is written as[10]

$$E_{dipolar} = \frac{\mu_1 \mu_2}{r^3}(3\cos^2\theta - 1) \qquad (58)$$

and solved for the case where $\theta = 0°$

$$2\frac{\mu_1\mu_2}{r^3} = 2A_{aniso}, \qquad (59)$$

and when $\theta = 90°$

$$-\frac{\mu_1\mu_2}{r^3} = -A_{aniso}. \qquad (60)$$

$A_{\perp}$ and $A_{//}$ are the two extreme cases one can obtain for the hyperfine interaction. From the above it is seen that

$$A_{\perp} = a_{iso} - A_{aniso} \quad \text{and} \quad A_{//} = a_{iso} + 2A_{aniso}.$$

Consider the nitroxide radical which contains a single nucleus with spin I = 1. This is a simple case since the g tensor and the hyperfine tensor have the same principal axes, and each tensor is approximately axially symmetric.

Figure 1.12(a) illustrates the spectrum obtained for a rapidly tumbling liquid at 260K. Figure 1.12(b) illustrates the spectrum obtained from a solution of lower temperature that has not yet reached the rigid limit. Figure 1.12 (c) shows the line shape for a solution that is at its rigid limit. The widths are different for each line.

Figure 1.13 shows how the g and a values combine together. From equation 45 the linewidth is proportional to the mean square of the shift in line positions, thus the three lines have different widths and the high-field line is broader than the low-field line.[2] Figure 1.14 shows several nitroxide spin labels along with their g and A values. In Figure 1.14 the x-axis is taken as being along the N-O bond, the z-axis along the 2p π orbital of the nitrogen, and the y-axis perpendicular to the other two.

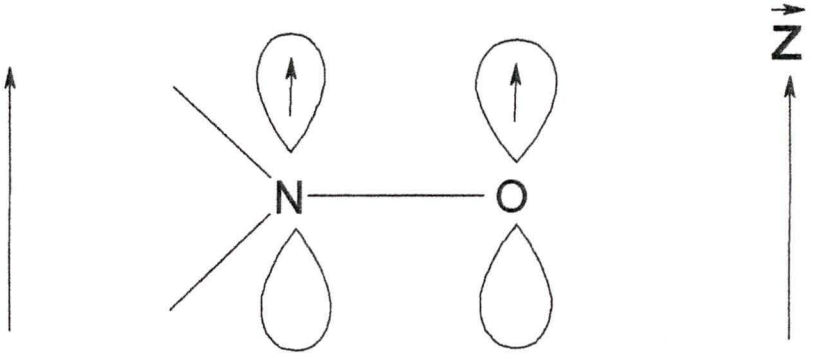

Figure 1.9: Nitroxyl group orientation, the z direction is parallel to the symmetry axis

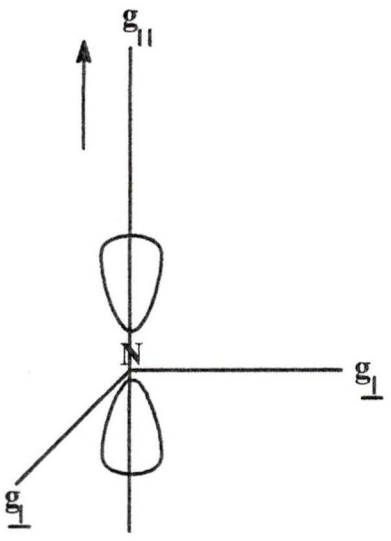

Figure 1.10: the orientation of $g_{\perp}$ and $g_{//}$ with respect to the symmetry axis, the black arrow gives the direction of the symmetry axis, which is parallel to $g_{//}$.

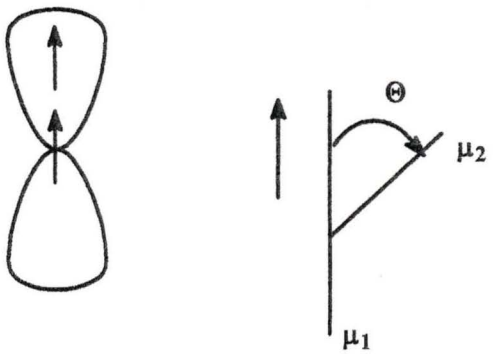

Figure 1.11: Dipole-dipole interaction

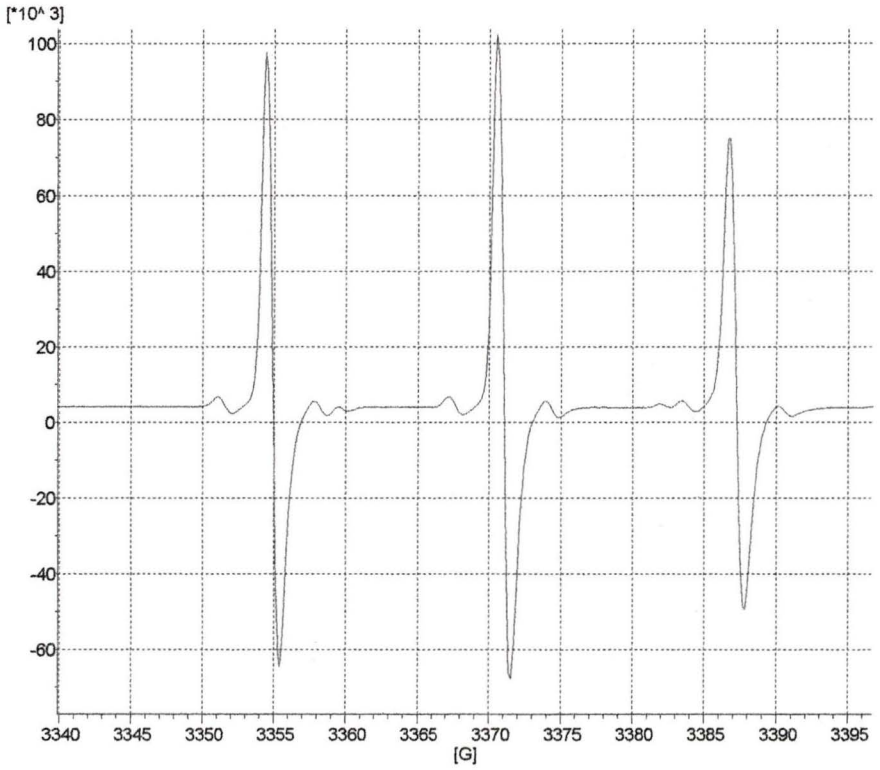

1.12(a) EPR spectrum of 50 μM deuterated MTSL in water, run in capillary tube at 260K

Figure 1.12: Spectra showing the effect of varying the temperature

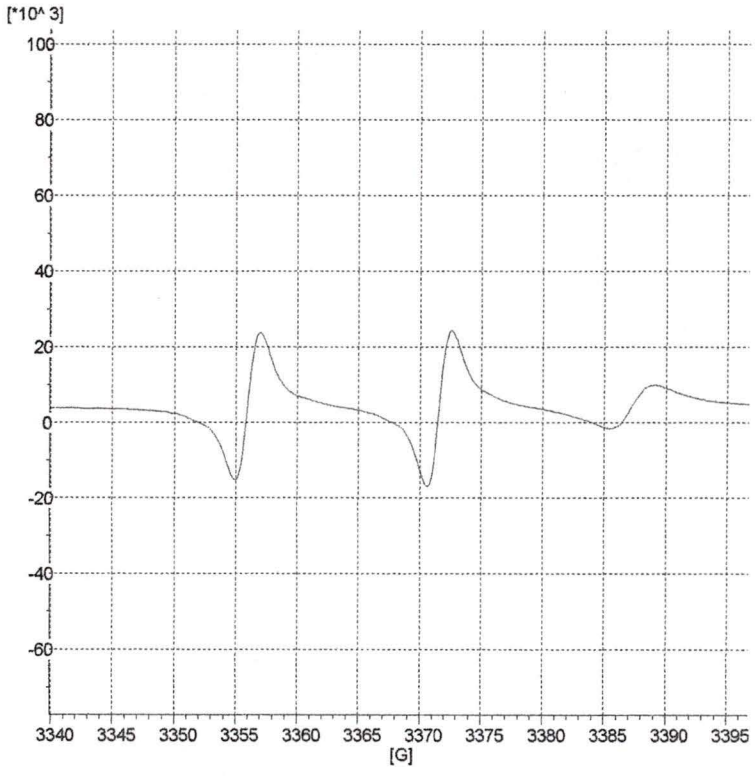

1.12 (b) EPR spectrum of 50 μM deuterated MTSL, run in capillary tube at 240K

Figure 1.12: Spectra showing the effect of varying the temperature

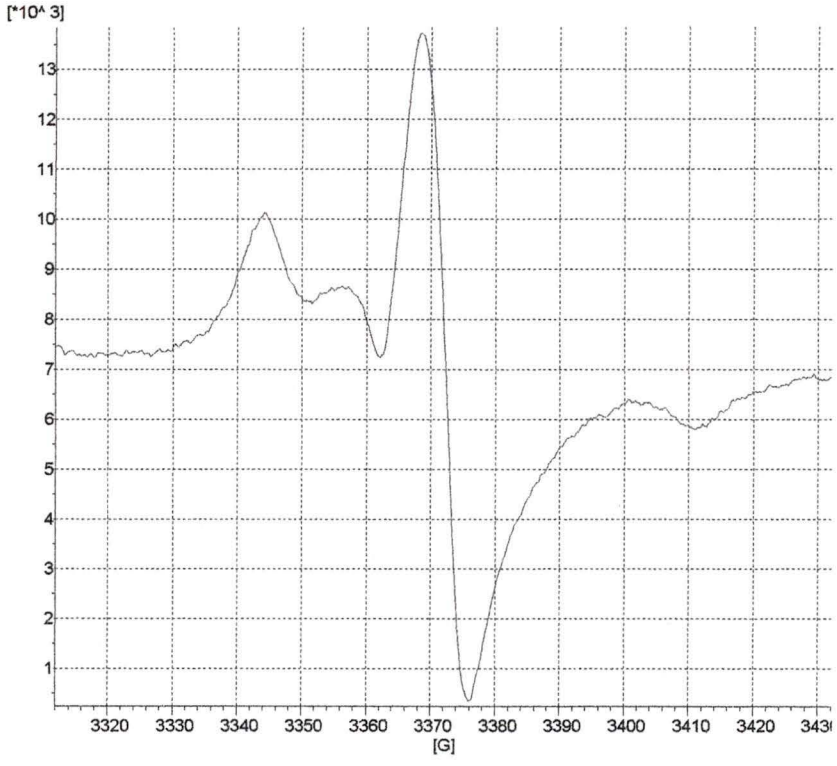

1.12 (c) EPR spectrum of 50 μM deuterated MTSL in water, run in capillary tube at 215K

Figure 1.12: Spectra showing the effect of varying the temperature

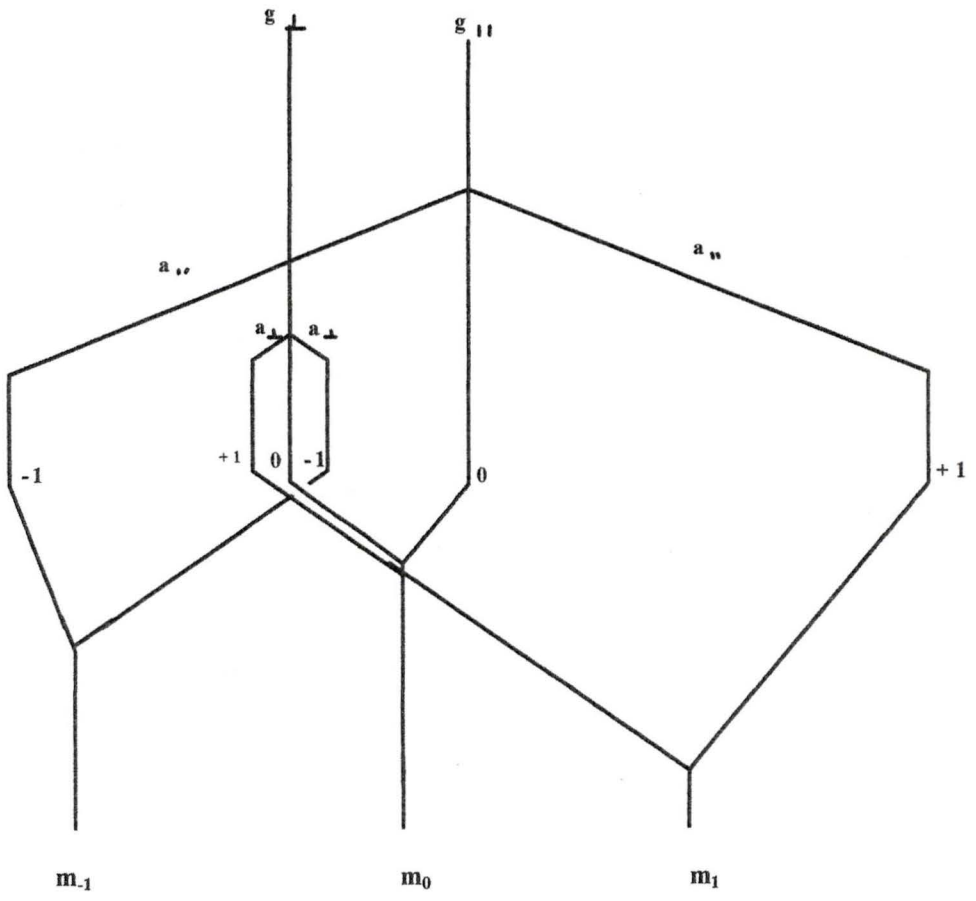

Figure 1.13: Schematic representation of how the g and a values combine.

	g_{xx}	g_{yy}	g_{zz}	A_{xx} (G)	A_{yy}(G)	A_{zz}(G)
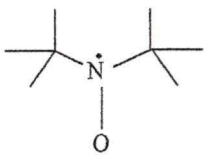	2.0088	2.0062	2.0027	7.6	6.0	31.8
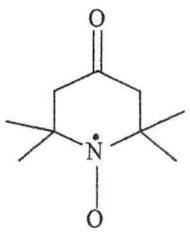	2.0104	2.0074	2.0026	5.2	5.2	31
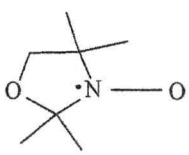	2.0088	2.0058	2.0022	5.9	5.4	32.9
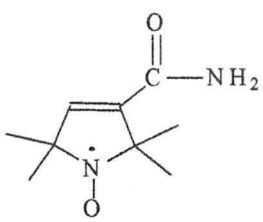	2.0086	2.0066	2.0032	-	-	31

Figure 1.14: Values of a and g for various spin labels[9]

1.7 The Channel-Forming Toxin Aerolysin

In this thesis the protein proaerolysin will be studied. The protein is studied in two forms, the inactive form of the protein is proaerolysin while the active form is aerolysin.

> "Aerolysin is secreted as a soluble protein by bacteria in the genus *Aeromonas*." (p. 362)[11]

Aerolysin can exist in solution even at concentrations above 50 mg/mL. Bacteria secrete the protein into the environment in the pro form. The protein can be activated under the proper conditions and in the active form the protein can form a highly stable transmembrane channel.[11] Proaerolysin has an approximate molar mass of 52 kDa and is made of a single chain of 470 amino acids. Proaerolysin is a dimer in the crystal and in solution. The monomer has a bilobal shape with a large elongated lobe joined onto a smaller globular-shaped lobe. The small lobe consists of a single domain, domain 1, and the larger lobe consists of three domains, domains 2, 3, and 4. The large lobe is approximately 110 Å long with a thickness between 20 and 45 Å. The protein is composed of 40% β-sheet structure and 17% α-helix. The β-sheet structure consists of eight antiparallel β-sheets made of twenty β-strands.[12] In the dimer, the elongated lobes lie side by side while the two smaller domains clasp each other in a cross over fashion. Interactions between hydrophobic residues observed in the monomer-monomer interface provide a driving force for the association of the monomers. The protein contains two disulfide bonds; one is in the small lobe and it appears essential for toxin activity and the other bridge joins the two cysteines at the top of the large lobe in domain 2. Proaerolysin contains no free SH groups.[11]

Several steps are involved in the process of converting proaerolysin from an inactive water-soluble protein to a transmembrane channel. The steps include activation of the protoxin, binding to specific receptors, oligomerization, and insertion into the membrane bilayer.[11]

Proaerolysin is approximately 4.5 kDa larger than aerolysin which is due to the presence of additional 40-50 amino acids at the C-terminus. Activation is achieved by proteolytic nicking of proaerolysin in a highly mobile region at the tip of the large lobe in domain 4. Enzymes like trypsin, chymotrypsin, and thermolysin all have cut sites in this region of the protein. The rest of the molecule is more resistant to proteolytic attack. Once it is formed the distal C-terminal peptide dissociates from the rest of the toxin molecule and plays no further role in channel formation. Aerolysin remains a dimer and appears to have a very similar structure to proaerolysin.

Aerolysin then binds to receptors on the cell surface, thus increasing the effective concentration and promoting oligomerization. Oligomerization is a concentration-dependent process that can occur even in solution. However, this only occurs at concentrations higher than approximately 10 μM and most of the oligomers that form in solution aggregate and precipitate. The oligomer is a heptamer that forms an amphipathic barrel. It is not completely understood at this point how the oligomer inserts into a membrane. The result of the channel formation however is osmotic swelling and cell lysis. Aerolysin is more active against cells that have certain receptors, but it can form a channel in any lipid bilayer. Aerolysin could, therefore, kill the bacteria that secret it. In order to avoid killing itself, the bacteria secret the protein in the inactive pro- form.[11]

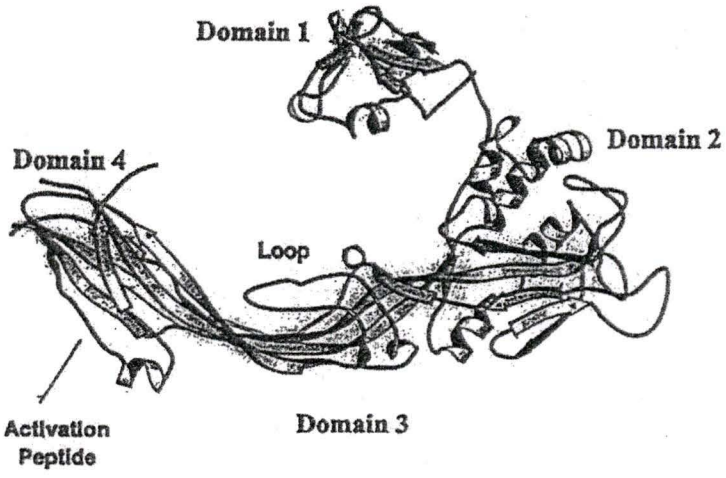

Figure 1.15: A single strand of proaerolysin[11]

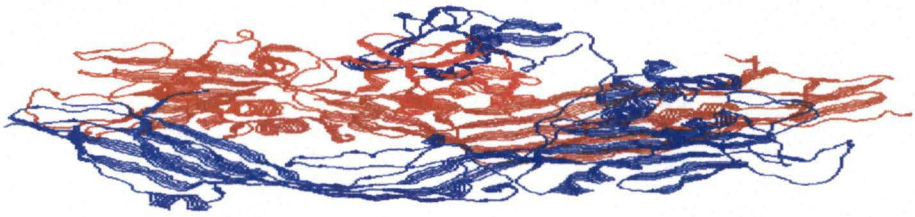

Figure 1.16: The Proaerolysin dimer

Chapter 2: EPR's uses in Biochemistry; a Review of the Literature

Experiments using spin labels attached to biological molecules were first explored by Ohnishi and McConnell in 1965.[13] They used the chloropromazine to study what occurred when aromatic molecules were inserted into DNA. Later studies used nitroxyl radicals because the EPR spectra were more easily interpreted and the radicals were more stable than chloropromazine. It was noticed that organic functional group reactions did not destroy the nitroxyl radical. Therefore, nitroxyl radicals containing various functional groups could be created. This facilitated selective labeling of specific locations in biomolecules.[13]

NMR and crystallographic methods can be used to determine new protein structures. Unfortunately, questions concerning structure still exist that cannot be solved by these methods.

> "Notable examples are the structure and dynamics of high molecular weight proteins in solution, and the investigation of conformational transitions and protein folding in real-time. In addition, no general approach is available for crystallization of membrane proteins, and few structures are known for these important molecules. Site directed spin labeling (SDSL) provides a means for approaching these areas of interest, allowing resolution at the level of the backbone fold." (p. 779)[14]

Site directed spin labeling allows for the placement of a nitroxide side chain at a specific location in a molecule. The electron paramagnetic resonance spectrum of the nitroxide is obtained. Spin labeling at different positions throughout the molecule should allow one to learn about the dynamics of the molecule as well as gain some structural information about the molecule.[14]

The structure of a protein can be changed by altering the DNA sequence of the cloned gene for that protein. An amino acid may be replaced by site-directed

mutagenesis. Site-directed mutagenesis allows one to make specific changes and to examine the effects of these changes.[15] In this study, amino acids at specific locations in the protein (241, 242, 300, and 445) are replaced with a cysteine residue. Cysteine is the only naturally occurring amino acid that has a sulfhydryl group. The sulfhydryl group reacts with the appropriate spin label to give a nitroxide radical on the protein at a specific location. The most commonly used reagent is (1-oxyl-2,2,5,5-tetramethylpyrroline-3-methyl)-methanethiosulfonate. Its reaction is shown in Figure 2.1.

From the EPR spectrum of a labeled protein several parameters can be determined. The first parameter that can be determined is the solvent accessibility of the side chain, Π. Another parameter is the side chain mobility, M_s. Also, from an EPR spectrum a polarity index for the side chain's immediate environment can be determined. Finally, the distance, r, between the side chain and another paramagnetic center in the protein can be estimated.[14]

The collision frequency of nitroxide side chain with paramagnetic reagents in solution can be used to determine the solvent accessibility of a nitroxide side chain. Paramagnetic reagents that are commonly used in solvent accessibility studies are molecular oxygen and metal ion complexes like Ni(II)ethylenediaminediacetate (NiEDDA) and Ni(II)acetonylacetonate (NiAA). The solvent accessibility, Π, of a nitroxide side chain can be used to identify the type of secondary structure and orientation in the protein. Therefore, if the amino acids in a protein are sequentially labeled with a nitroxide side chain, then the solvent accessibility can be used to determine secondary structure. The helical membrane protein bacteriorhodopsin was the first

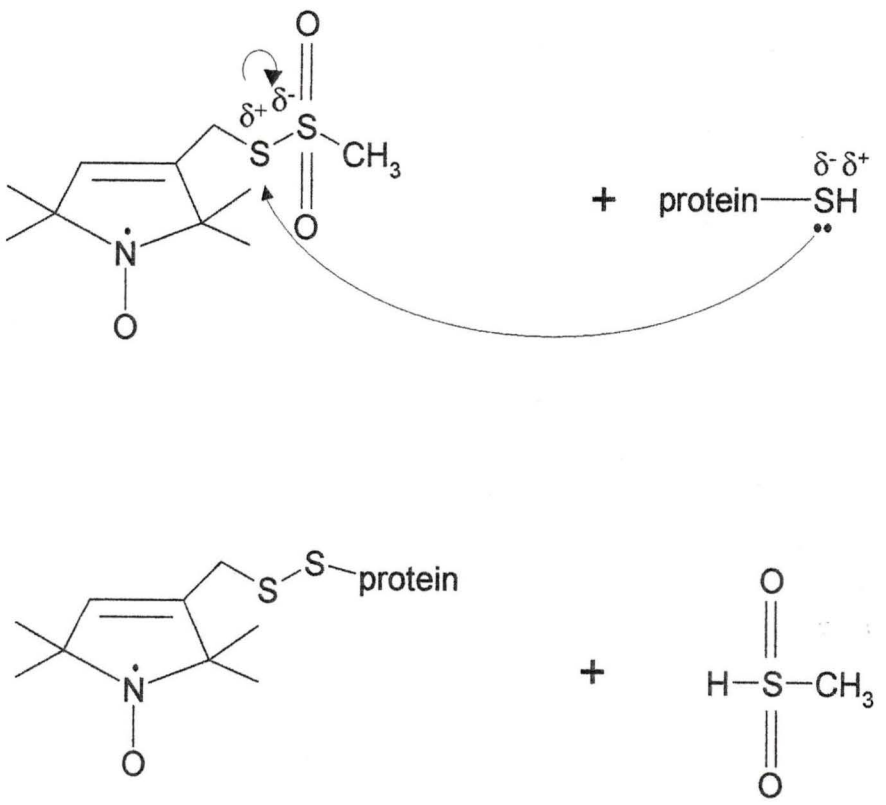

Figure 2.1: MTSL and its reaction with a protein

protein that showed the ability to use solvent accessibility to determine secondary structure and topography.[16] Altenbach et al.[17] showed that $\Phi = \ln[\Pi(O_2)/\Pi(NiAA)]$ is a linear function of depth in a membrane and thus they could determine the distance between the nitroxides and the aqueous/membrane interface.

Mchaourab et al.[18] describe the general relationship between structure and side chain mobility. The peak-to-peak width of the middle resonance, ΔH_0, and the spectral second moment, $\langle H^2 \rangle$, both provide insight into the structure and side chain mobility.

> "The numerical value of these quantities at X-band frequencies is determined primarily by the degree of averaging of the anisotropic **g** tensor and the anisotropic hyperfine tensor." (p. 7701)[18]

The second moment and linewidth increase when the frequency of nitroxide rotational motion is decreased. Similarly, molecular ordering about an axis can be related to the second moment and the linewidth. The second moment and linewidth can be used as simple measures of mobility for a nitroxide side chain. The reciprocal of these two quantities are used because one would like them to increase with increased mobility. Figure 2.2 is a plot of the reciprocal second moment versus the reciprocal central line width. The values were obtained from the spectra of spin labeled side chains of T4 lysozyme. Buried sites are located in the low-mobility region of Figure 2.2 because of the dense packed interior of the protein. Tertiary interaction sites have mobilities between helix surface sites and buried sites. Loop sites have the highest mobilities. There are overlaps between sites which are due to the effects of backbone dynamics.[18]

The hyperfine values of a nitroxide depend on the polarity of the environment. The equilibrium in Figure 2.3 will shift toward the right in a hydrophobic environment. This shift leaves much of the unpaired electron density associated with the oxygen atom.

Therefore, interaction of the free electron with the nitrogen nucleus is smaller leading to a lower isotropic coupling constant. In a polar environment the equilibrium shifts to the left; the coupling constant increases because of the increased electron-nitrogen nuclear interaction. Lassman et al.[9] developed a hydrophobicity parameter, h.

$$h = \frac{A_{zz}(H_2O) - A_{zz}(sample)}{A_{zz}(H_2O) - A_{zz}(decalin)} \tag{61}$$

They showed from spectra of the strongly immobilized nitroxides that the splitting between the low field maxima and the high field minima ($2A_{zz}$) can be positively associated with the isotropic coupling constant. They used $2A_{zz}$ in water and $2A_{zz}$ in decalin as extremes. The hydrophobicity increases from zero for a purely polar environment to one for an environment with the hydrophobicity of decalin.[9]

Through magnetic interactions the distance between a spin label and a paramagnetic species can be determined. The theory behind this is well documented for two extreme cases. The first case is the slow motion limit of the spin systems.[19] This can be accomplished by freezing the sample as a result of which the spectrum is inhomogeneously broadened because of static dipolar interactions. The second case is the fast motion limit.[20] In the fast motion regime, rapid diffusion of the protein averages the dipolar interactions. The spectrum is homogeneously broadened because of relaxation effects in the fast motional case.

The parallel magnetic field component a distance r away from a magnetic dipole is

$$H_{z'} = \mu(1 - 3\cos^2\theta_R')/r^3, \tag{62}$$

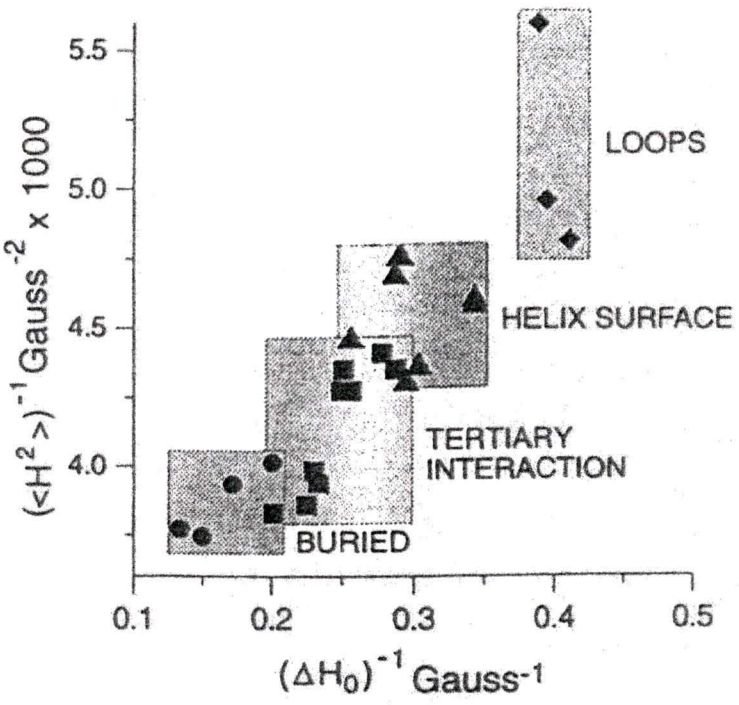

Figure 2.2: Reciprocal second moment versus the reciprocal central linewidth for the spectra of spin labeled side chains of T4 lysozyme representing helix surface, loop, tertiary interaction sites, and buried sites. [18]

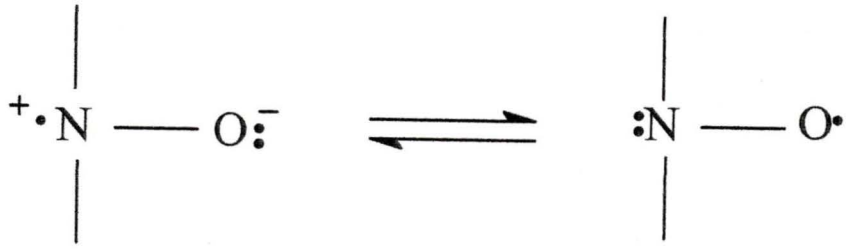

Figure 2.3: Polarity of nitroxyl group

θ_R' is the azimuthal angle between the dipole position and the field direction. θ_R' is related to the other angles through

$$\cos\theta_R' = \sin\theta_R \sin\theta \cos(\phi_R - \phi) + \cos\theta_R \cos\theta \ , \qquad (63)$$

θ_R and ϕ_R are the azimuthal and polar angles indicating the position of the dipole. The linewidth is

$$\delta H(\theta,\phi) = C(1 - 3\cos^2\theta_R')^2 + \delta H_0 , \qquad (64)$$

where

$$C = g\beta\mu^2\tau / r^6\hbar \qquad (65)$$

and δH_0 is the natural linewidth without dipolar broadening. C may be determined if one has a sample containing two spins which can be compared to a system that is identical except that the relaxing spin is replaced with a diamagnetic species. Once one knows C, then it should be straightforward to determine distances.[8]

Nitroxide-nitroxide and metal ion-nitroxide dipolar interactions are two ways that site directed spin labeling can be used to determine inter-residue distances. In the limit of slow motion, distances between two nitroxides can be estimated from static dipolar interactions. In this case one can determine distances within 10-25 Å.[21-23] When a protein of high molecular weight is being considered, dipolar interactions can be used to determine distances because the protein's rotational diffusion is so slow.

For lower molecular weight proteins, less than 15 kDa, interspin distances can be estimated from spectral linebroadening and Redfield theory.[20] This method has been used to study the structure of T4 lysozyme in solution.[24] Distances were found to be consistent with a hinge-bending angle corresponding to an open state of the active site as opposed to the closed state observed in the crystal structure of the wild-type protein.

The lactose permease of *Escherichia coli* is a membrane transport protein. The molecule is made of twelve transmembrane helices connected by hydrophilic loops (Figure 2.4). Sun et al.[25] in 1999 looked at the proximity between periplasmic loops in the lactose permease of *E. coli* as determined by site-directed spin labeling. The (1-oxyl-2,2,5,5-tetramethylpyrroline-3-methyl)-methanethiosulfonate labeled mutants were analyzed by EPR spectroscopy, and interspin distance was estimated from the extent of line shape broadening in the double-labeled proteins. They were able to make a correlation between distances estimated by site-directed cross-linking, previous work, and EPR. EPR results were able to show that site-directed thiol cross-linking is a reflection of proximity.

Bacteriorhodopsin is a protein that has also been studied by EPR spectroscopy. Altenbach et al.[26] labeled 18 consecutive positions of the residues 125 to 142. In Figure 2.5 these residues are portions of the intramembrane helices D and E and the loop that connects them. Through consecutive labeling the authors hoped to obtain some insight into the environment in which the residues were situated. They used power saturation EPR spectroscopy to obtain an estimate of the relative collision frequency of each spin label with O_2 and chromium oxalate. O_2 was chosen because it could freely diffuse into the membrane while the chromium oxalate was membrane impermeable.

> "Power saturation curves were measured as the vertical peak-to-peak amplitude (A) of the first derivative M_I=0 line as a function of the incident power (P) in the range of 0.1 to 36 mW. The resulting data were fitted to the function;
>
> $$A = I \cdot P^{1/2} \cdot [1 + (2^{\frac{1}{\varepsilon}} - 1)P / P_{1/2}]^{-\varepsilon},$$
>
> with ***I***, $P_{1/2}$, and ε as adjustable parameters. This function describes the saturation parameter of a first derivative EPR signal of arbitrary homogeneity. ***I*** is a scaling factor, $P_{1/2}$ is the power where the first derivative amplitude is reduced to half of its unsaturated value, and ε is a

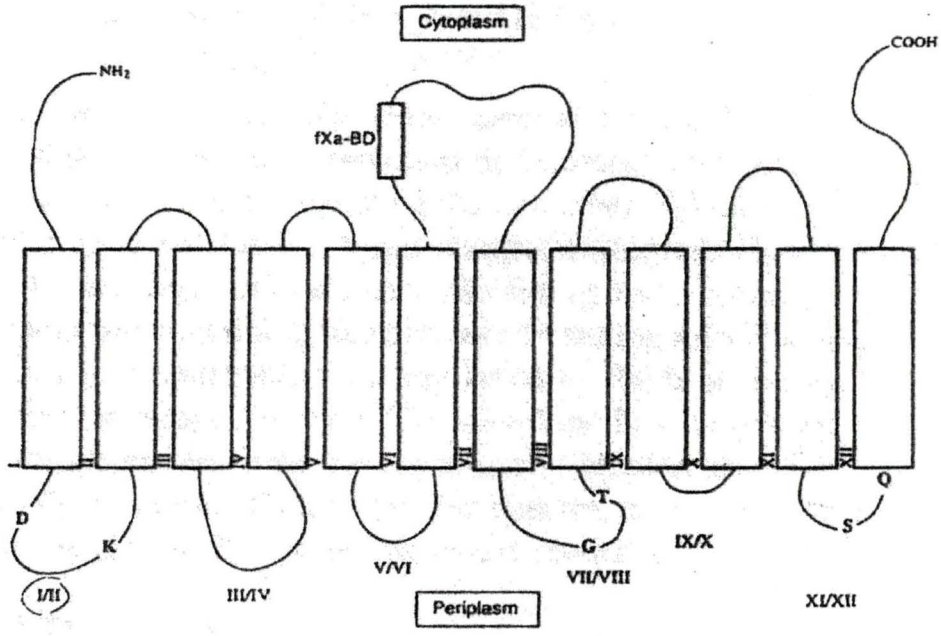

Figure 2.4: "Secondary structure model of lac permease of *E. Coli* showing positions of Cys mutants in the periplasmic loops."[25] The twelve hydrophobic transmembrane helices are shown as rectangles.[25]

measure of the homogeneity of saturation of the resonance line." (p. 1667)[17]

$\Delta P_{1/2}$ values were determined for the residues, where $\Delta P_{1/2}$ is the difference between the $P_{1/2}$ values with and without relaxing agents. The results show that residues 129 to 131 form a short water-exposed loop, and residues 132 to 142 are in the membrane.[26] In 1991, Greenhalgh et al.[27] were able to determine the location with respect to the aqueous boundaries of three mutants of bacteriorhodopsin labeled with (1-oxyl-2,2,5,5-tetramethylpyrroline-3-methyl)-methanethiosulfonate (Figure 2.5). Their results showed that Tyr-79 was at the aqueous-protein interface on the extracellular side of helix C. Val-101 was close to the aqueous boundary on the intracellular side of the protein. Asp-96 was estimated to be within 7 Å of the aqueous medium on the intracellular side of the membrane. Arg-82 and Asp-85 were determined to be within 5 Å and 9 Å of the aqueous boundary on the extracellular side of the membrane.

EPR provides an opportunity to measure distances upon addition of a second paramagnetic center. Site-directed mutagenesis allows one to incorporate both metal-binding sites and nitroxide spin labels into a single protein. Voss et al.[28] in 1995, reported that three mutants of T4 lysozyme were labeled with (1-oxyl-2,2,5,5-tetramethylpyrroline-3-methyl)-methanethiosulfonate at positions 71, 76, and 80 and their EPR spectra were analyzed in the presence of Cu (II). The results showed that Cu (II)-induced relaxation effects on the nitroxide could be analyzed in terms of interspin distance in the range 10-25 Å. The results are in good agreement with Leigh theory both under rigid lattice conditions and in the presence of rapid spin label motion at room temperature. The main advantage of this method is that intramolecular distances can be estimated at room temperature, and a single metal ion provides a reference site for the

estimation of distances to nitroxide sites. Voss et al.[29] in 1995 spin labeled several mutants of the lactose permease of *Escherichia coli.* The results showed that positions 103, 111, and 121 are 8, 14, and >23 Å from the metal binding site.

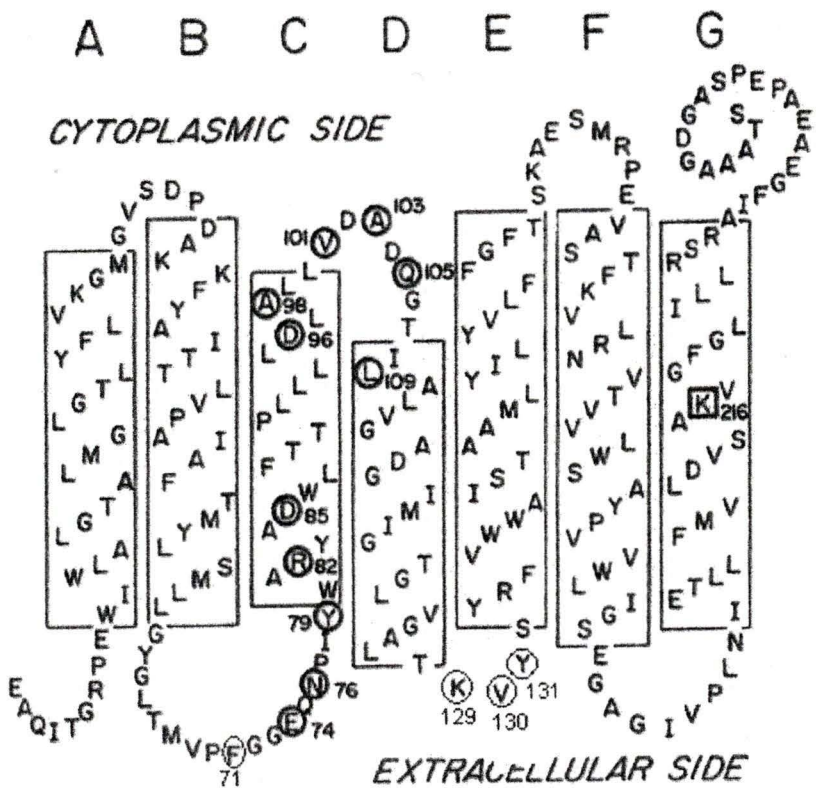

Figure 2.5: "Secondary structure of bacteriorhodopsin. The boxed regions A-G represent the seven transmembrane α-helical segments."[27]

Chapter 3: Objective

The purpose of this thesis was to investigate the protein proaerolysin and its active form aerolysin. The labeling process is explained in chapter 4 along with the methods of testing the protein after labeling. In chapter 5, the results of the labeling process along with various experiments performed on the protein variants are presented. Variants 300C PA, 445C PA, 241C PA, and 242C PA were all labeled successfully with the spin label. These four variants were chosen because of their location in the protein. Their EPR spectra were analyzed to determine what kind of motion was occurring in the aqueous phase. Experiments were run that looked at the total and segmental motion of the protein. Various additives were used in the hope of identifying large changes in the EPR spectra and attributing them to some change in the structure of the protein. Trypsin, protease K, and SDS were all added to at least one of the mutants. Temperature studies were carried out on 445C PA + MTSL in the proaerolysin and aerolysin forms and correlation times were determined to be on the order of 10^{-11}-10^{-12} seconds. Simulations were performed on the spin label to determine some physical parameters; these simulations were found to be a good basis for comparing spectra of labeled protein and free spin in solution.

Chapter 4: Materials and Methods

4.1 Materials

The nitroxyl spin label (1-oxyl-2,2,5,5-tetramethylpyrrolidine-3-yl)methylmethanethiosulfonate (MTSL), was obtained from Reanal Finechemical Company in Budapest, Hungary. The deuterated form of the reagent was obtained from Toronto Research Chemicals Inc. in Toronto, Canada. This reagent was chosen for several reasons. First, the nitroxyl is very stable and inert because of the four surrounding methyl groups. Second, the EPR spectrum of this compound comprises three sharp lines resulting from the coupling of the unpaired electron spin with the nitrogen nuclear spin, I = 1. Third, and probably most important, the reagent is SH reactive, which means it will react with proteins containing a SH group. Temed, ammonium persulfate (APS), HEPES (N-[2-Hydroxyethyl]piperazine-N'-[2-ethane sulfonic acid]), trypsin, and trypsin inhibitor were obtained from Sigma. Prestained low range molecular mass standard was obtained from Biorad. Sodium dodecyl sulfate was obtained from Fisher Scientific. Sodium chloride was obtained from EM Science. The disodium salt of EDTA (Ethylenediaminetetraacetic acid) was obtained from ACP. Sodium dihydrogen orthophosphate was obtained from BDH Inc. Horse blood was obtained from PML Microbiologicals.

4.2 Method of Labeling

In this study, a proaerolysin variant is a protein that has undergone site-directed mutagenesis to replace a specific amino acid in the protein with a cysteine residue. Twelve ml of the protein concentrate was thawed out and centrifuged for ten minutes at 10000 rpm and 4°C. Dissolving 10.6 mg of MTSL in 1.00 ml of reagent grade DMSO made a 40.0 mM stock solution. Sixty μl of 40.0 mM MTSL dissolved in DMSO was

then added to the supernatant to make a final concentration of 200 μM. The solution of protein and spin label was incubated at 37°C for 1 h. The solution was then applied to a Sephadex G25 column. This column had beads that are 100-300 μm in diameter, equilibrated with a buffer of 20 mM NaH_2PO_4, 0.3 M NaCl, pH 6.0. The solution was applied with a flow rate of 5 ml/5 minutes. The labeled protein was eluted with a buffer of 20 mM NaH_2PO_4, 0.3 M NaCl, pH 6.0. The protein was collected in 5 ml aliquots. The protein elutes between 60 and 120 ml detected by reading the absorbance at 280 nm. This wavelength was chosen because, as can be seen in the plot of absorbance vs wavelength for proaerolysin (Figure 4.1), the maximum in the UV spectrum occurs at 280 nanometers. The post G25 sample of protein was then applied to a hydroxyapatite column at a flow rate of 5 ml/20 minutes. The protein was eluted with a linear gradient formed by 150 mM NaH_2PO_4, 0.3 M NaCl, pH 6.0 and 20 mM NaH_2PO_4, 0.3 M NaCl, pH 6.0. The sample was eluted at an approximate phosphate concentration of between 70 mM and 100 mM. An ammonium sulphate precipitation to 60% of saturation at 4°C was performed on the protein solution that came off the hydroxyapatite column and the mixture was incubated on ice for 2 h. After 2 h the mixture was centrifuged for ten minutes at 10000 rpm and 4°C. The supernatant was discarded and the protein pellet was resuspended in 15 ml of 20 mM Hepes, 1 mM EDTA, pH 7.4. This resuspended solution was applied to a DEAE column at a flow rate of 5 ml/20 minutes. The DEAE sample was eluted with a linear gradient of 20 mM Hepes, 1 mM EDTA, 0.4 M NaCl, pH 7.4

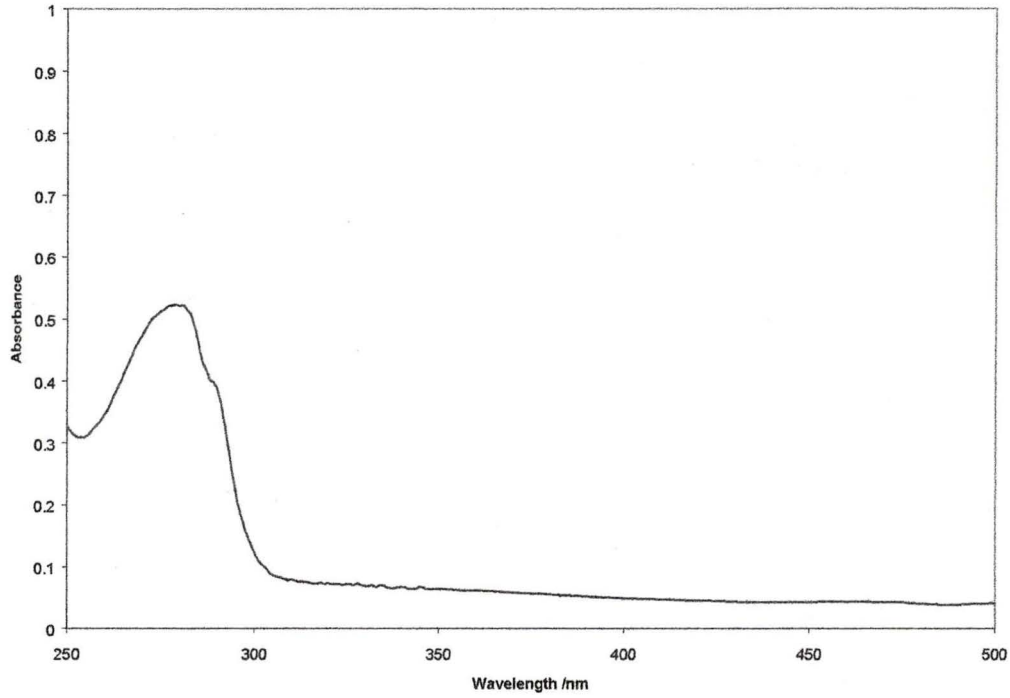

Figure 4.1: Plot of Absorbance vs Wavelength for Proaerolysin, OD280 0.521

and 20 mM Hepes, 1 mM EDTA, 0.1 M NaCl, pH 7.4. The protein comes off between 150 and 250 ml. The protein was named by denoting the amino acid number that was replaced with a cysteine. For example, one of the variants used in this study was 300C PA. The nomenclature arises because the amino acid at position 300 in proaerolysin was replaced with a cysteine.

4.3 Methods of Protein Analysis

Once a variant had been labeled, several techniques were used to determine whether or not the process had any detrimental effect on the protein. First, the variant was run on a SDS-PAGE gel. Electrophoresis is a method available for the separation of proteins based on the migration of charged proteins in an electric field. Electrophoresis in the presence of SDS separates proteins almost exclusively on the basis of molecular weight, with smaller proteins migrating more rapidly. After electrophoresis, the proteins were visualized by adding a dye such as Coomassie blue that binds to most proteins but not to the gel itself.[30] SDS polyacrylamide gels were prepared as described by Neville.[31] Sample buffer for SDS PAGE contained 8% SDS, 20% β-mercaptoethanol, 40% glycerol, 108 mM H_2SO_4, and 220 mM Tris-HCl pH 6.1 with bromophenol blue. Prior to use, sample buffer was diluted 1:4 in liquid samples. A 12% separating gel and a 3% stacking gel were used. Gels were run at 16 mA constant current until the proteins had stacked. Then they were run at 40 mA until the dye front reached the bottom of the gel. Gels were fixed and stained in 0.03% Coomassie blue, 25% isopropanol, and 10% acetic acid for 30 minutes. They were gradually de-stained by transferring to solutions containing progressively lower Coomassie blue concentrations. In preparation for drying, gels were de-stained fully by washing for 1 to 2 h in 10% acetic acid. A sample of wild

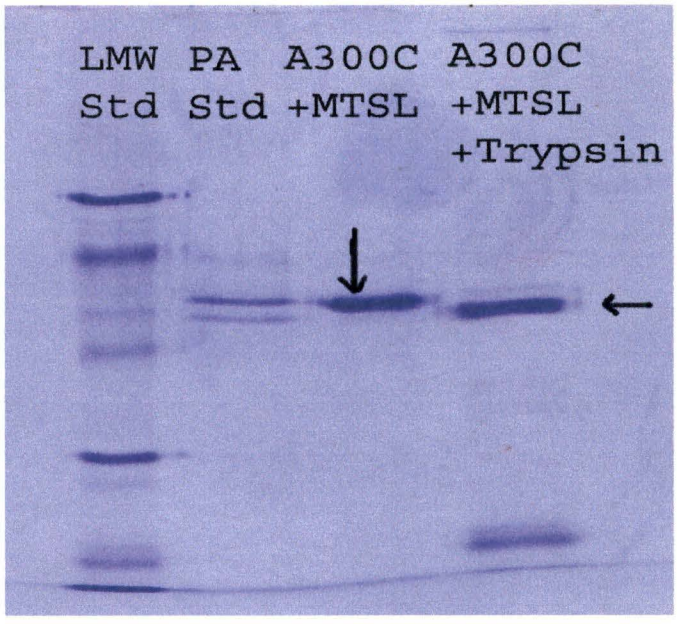

Figure 4.2: SDS-page gel of 1.66 μM 300C PA + MTSL with and without trypsin added LMW Std included 97.4, 66.2, 45.0, 31.0, 21.5, and 14.4 kDa proteins[32], the bottom of the 300C PA + MTSL + trypsin lane has a blue band at the bottom of the gel that denotes the presence of trypsin.

type is compared to a sample of the variant after labeling. This shows whether or not the protein has broken down during the labeling process. A SDS-PAGE gel also gives an idea of how much conversion of proaerolysin to aerolysin there has been. Aerolysin is approximately 4.5 kDa smaller then proaerolysin and it migrates below proaerolysin. The vertical arrow in Figure 4.2 is pointing at the band of 300C PA + MTSL. Since this band is in the same horizontal plane as the higher band in the proaerolysin standard most of the 300C PA is in the form of proaerolysin. The horizontal arrow in Figure 4.2 is pointing at the band of 300C PA + MTSL + trypsin. Since this band is in the same horizontal plane as the lower band in the proaerolysin standard the protein is in the form of aerolysin. After labeling, virtually all of the protein in the 300C PA sample migrates as a single band corresponding to proaerolysin. There is no evidence of breakdown as a result of the labeling process. The results in Figure 4.2 show that the 300C PA can be nearly entirely converted to aerolysin by trypsin treatment. There is no evidence of smaller products, which would result if labeling had affected folding of proaerolysin.

SDS-PAGE was used to determine if degradation or incorrect folding resulted from labeling with MTSL. In order to determine whether activity was affected, hemolytic titres were performed before and after labeling.[33] Ten μl of protein with an OD_{280} of 0.2 was used in the titre. Ten μl of 20 μg/ml trypsin was used to activate the protein for 10 min in a total volume of 100 μl. The final volume was made up to 200 μl with HBS (20 mM Hepes, 0.15 M NaCl, pH 7.4). After incubating for 10 min at room temperature, the samples were serially diluted 1 in 2 with HBS in 96-well microtitre plates. 100 μl of 0.8% red blood cells were added to all wells and the plates were incubated at 37°C for 1 h. During the 1 h incubation the plates were checked at the 5, 10,

15, 30, and 60 minute marks to determine the number of lysed wells. In Figure 4.3 the wells that are solid circles are red blood cells that have not been lysed by aerolysin. The wells that have a dot in the center are red blood cells that have been lysed. Looking at the bottom row, one sees that all the wells are dark solid circles, this means that the protein in these wells has not been converted to aerolysin. Looking at the row containing 300C PA, one sees that all the wells have a dot in the center of the circle, this means that the protein in these wells has been converted to aerolysin. The most concentrated aerolysin occurs in the first column at the far left of Figure 4.3, where the initial protein concentration had an OD_{280} of 0.2. The successive columns have been serially diluted 1 in 2. Wild type proaerolysin was placed in the first two rows as a standard with trypsin added to the first row and not to the second. In the next four rows were placed the variants of interest, alternating between unlabeled and labeled protein. The third and fourth rows contained 300C PA while the fifth and sixth contained 445C PA. The activity of the variant is a comparison of the length of time wild type aerolysin takes to lyse a certain concentration of blood cells with the length of time the variant aerolysin takes to lyse that same concentration of blood cells. If the protein had activity before labeling and less activity after the labeling process, then the label had an undesirable effect on the protein. Wild type was active with and without trypsin added, as can be seen in Figure 4.2 the wild type standard proaerolysin contained both proaerolysin and aerolysin. Therefore there was activity in the second row even though trypsin was not added. A decrease in activity was seen with the labeled 300C PA variant whereas there was an increase in activity with the labeled 445C PA variant.

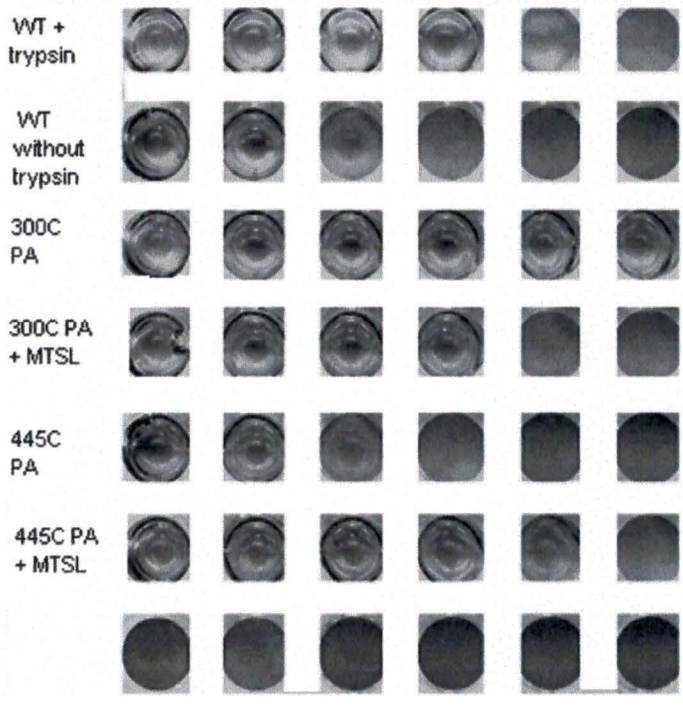

Figure 4.3: Hemolytic titre showing the effect of labeling, [protein] = 1.66 μM in the first column. The titre shows if the labeling process has affected the activity of the protein by comparing labeled and unlabeled proteins.

4.4 EPR analysis

The EMX EPR was used to study the nitroxyl spin label either by itself in solution or when attached to a protein. Two different sample containers were used, depending on the amount of protein available for a given experiment. One was a flat cell that requires 500 μl of sample. The other was a capillary tube that has an external diameter of 2 ml and is sealed at one end; it requires 40 μl of the sample. Unless otherwise stated all spectra were run at a power of 31.8 mW, 100 scans were run, each scan taking 41.9 seconds, and the modulation amplitude was 2 G.

First, a spectrum was obtained for the spin label alone in buffer solution. This spectrum contained three sharp lines as expected for a rapidly rotating nitroxyl group (Figure 4.4). The spectrum of the labeled protein was then obtained. In contrast to the spectrum in Figure 4.4 the high field line was very broad, the low field line was broad, and the central line was sharp. Figure 4.5 is evidence that the label's movements were restricted by attachment to the 52 kDa protein.

Proaerolysin has no free SH groups so if an EPR signal was obtained then the molecule was labeled at the desired location. This was proved by using the above labeling process to label wild type proaerolysin, and since no signal was seen in the EPR spectrum labeling was only occurring at the desired site (Figure 4.6). Figure 4.7 shows the EPR spectrum of an empty capillary tube for comparison with Figure 4.6.

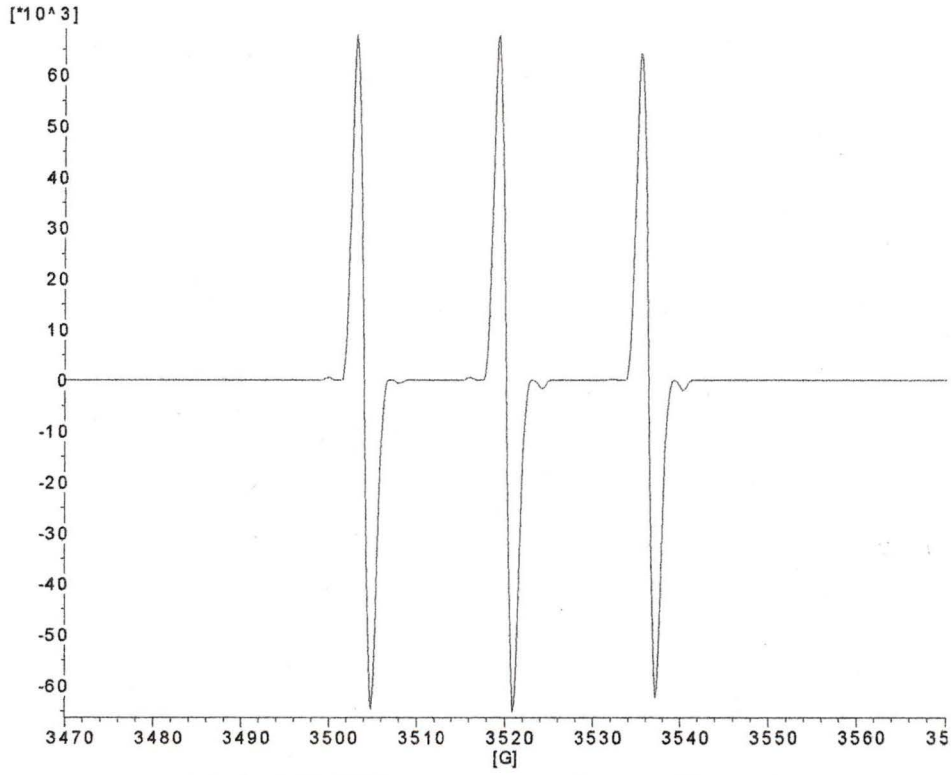

Figure 4.4: 5 μM MTSL in water, run in a capillary tube at 293K

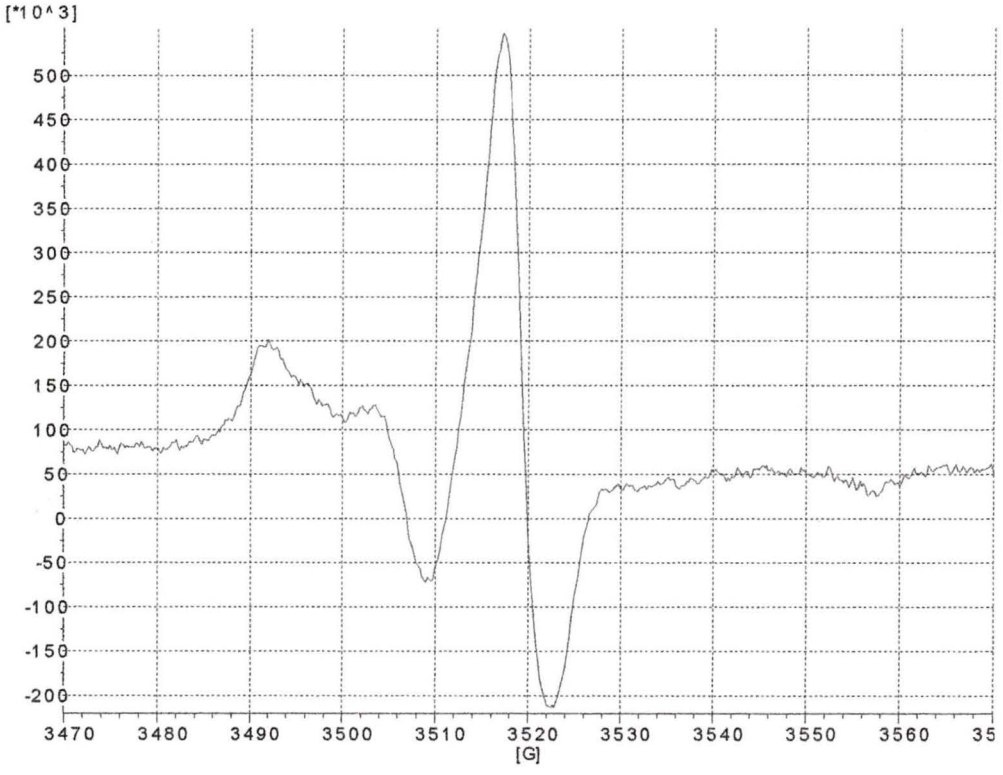

Figure 4.5: 5.3 μM 300C PA + MTSL in buffered solution in capillary tube at RT

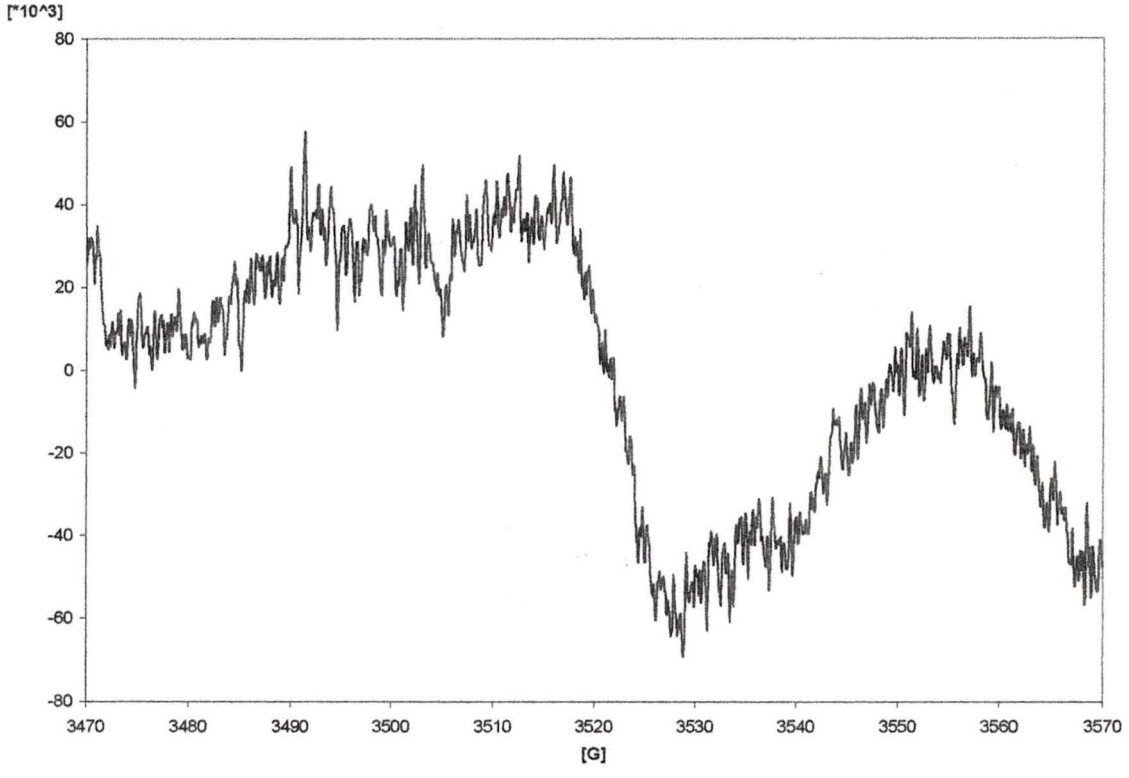

Figure 4.6: 10 μM wild type proaerolysin + MTSL run in capillary tube at RT

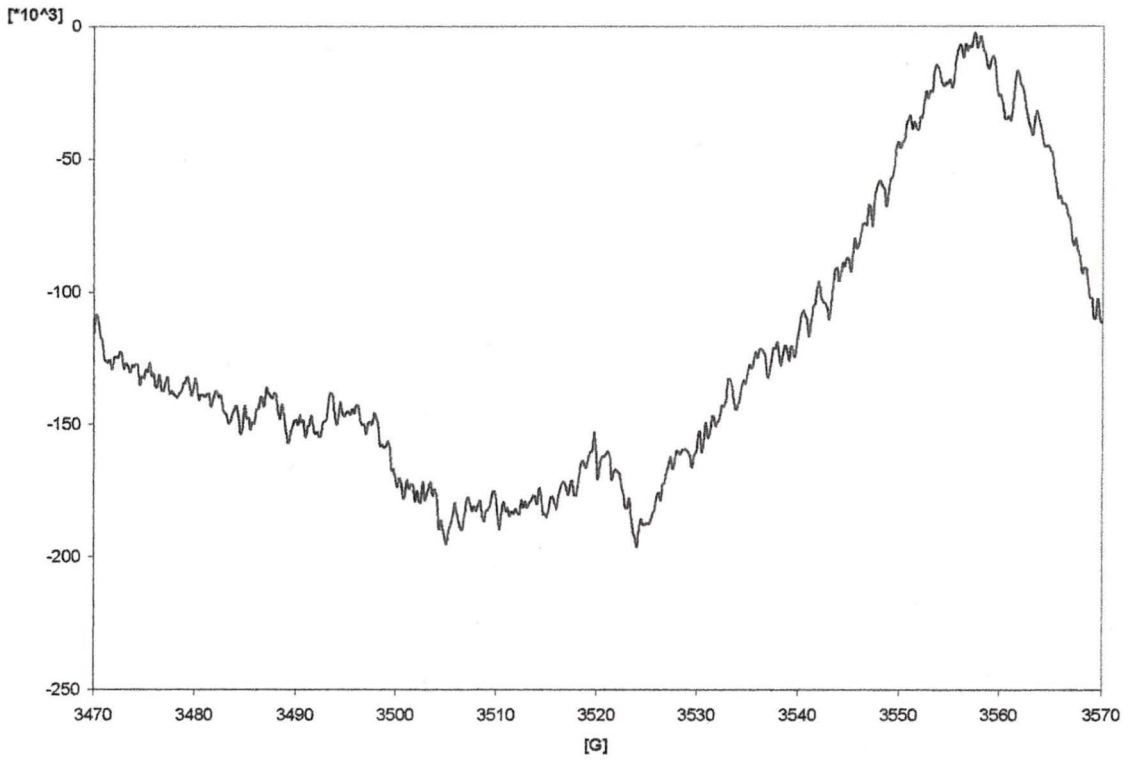

Figure 4.7: Empty capillary tube run at RT

Chapter 5: Results and Discussion

5.1 MTSL

The reaction of MTSL with the SH group of a protein is given in Figure 2.1. MTSL and a protein join together with an S-S bond. The first step in this study was to determine the EPR spectrum of the spin probe in solution. This was a good starting point because it gave a reference point for comparison with future spectra. Parameters of the free probe were determined through simulations, making comparison with other spectra straightforward. Figure 4.4 shows the EPR spectrum of 5 μM MTSL in water.

The spectrum was determined to have a g value of 2.0050 and a(N) value of 16.20 G. The EPR spectra of radicals with the ^{14}N nuclei (I_n=1) are characterized by three components, m_{-1}, m_0, and m_1, with corresponding I_Z values of -1, 0, 1. Recalling that the linewidth is proportional to the mean square of the shift in line positions caused by the mean-square of the fluctuating field, it is clear from Figure 1.13 why the three lines have different widths and why the high-field line is broader than the low-field line. The value of the isotropic hyperfine splitting depends on the structure and properties of the solvent. Values for the linewidth parameters A, B, and C (equation 52) were obtained for this spectrum using SimFonia were 1.1012, -.0331, and 0.0254 respectively. SimFonia simulates a spectrum when one enters the widths of the lines of the spectrum and tells it what spin system is being considered. The A, B, and C values are selected to get reasonable values of g and a(N) for MTSL. In work carried out later in this thesis the B and C values will be determined using the equation 53 given in section 1.5 (page 28). Figure 5.1 shows how well SimFonia was able to simulate Figure 4.4. It shows the difference when the simulation was subtracted from the experimental data.

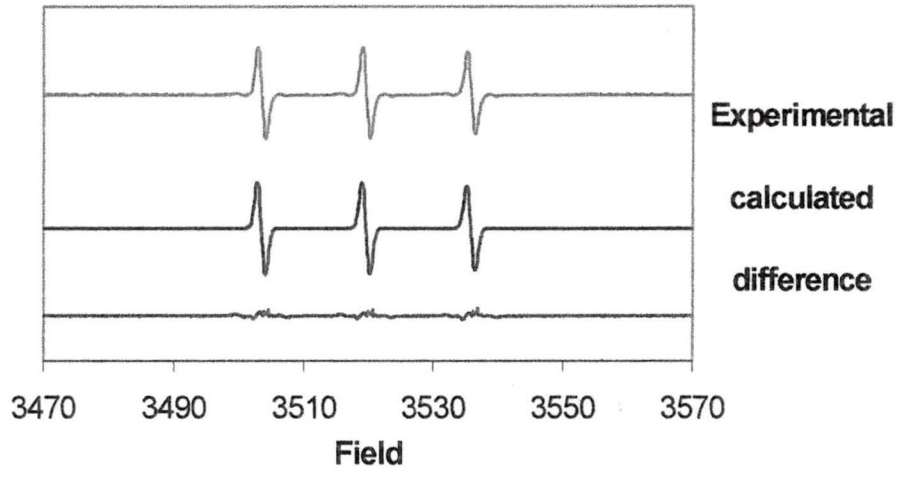

Figure 5.1: Plot of simulation and experimental data from Figure 4.4

5.2 Labeling of Variant 300C PA

The variant 300C PA was chosen as a standard for the experiments that were performed on proaerolysin. The free cysteine at position 300 is in domain 3 of the protein as seen in Figures 1.15 (page 41) and 5.2. Domain 3 is formed by a five-stranded beta-sheet on one face and a long loop with two short strands on the other face (Figure 5.3). The cysteine is on one of the strands, directed outwards into the aqueous environment.[34] It is in a position of low mobility, but because it is exposed to the surrounding solvent it was expected to react very well with the spin label. Variant 300C PA was labeled at a final protein concentration of 5.28 μM in a buffer of 20 mM Hepes, 0.15 M NaCl, 1 mM EDTA, pH 7.4.

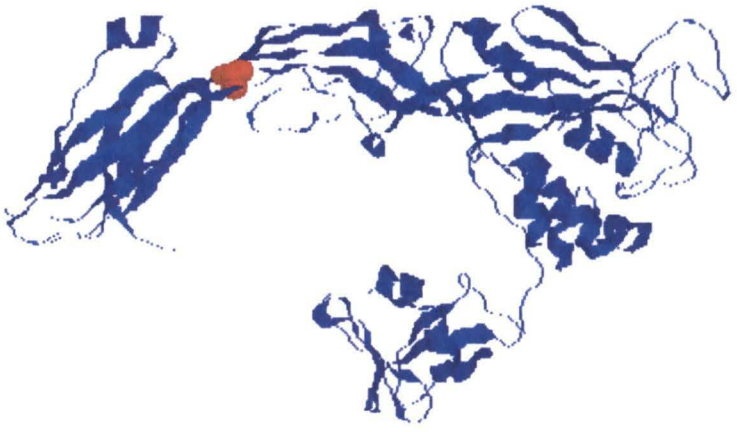

Figure 5.2: The red dot gives the position of 300C PA. It is on one strand of the beta-sheet and is directed outwards into the aqueous environment.

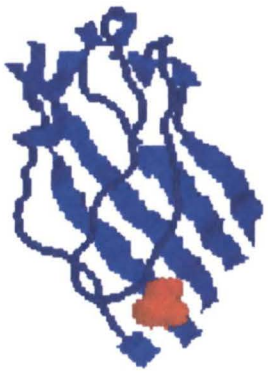

Figure 5.3: Focusing in on Domain 3, 300C PA is the red dots on a beta sheet. It is on one strand of the beta-sheet and is directed outwards into the aqueous environment.

5.2.1 EPR Spectrum and Simulation of Variant 300C PA + MTSL

The EPR spectrum of variant 300C PA + MTSL is shown in Figure 4.5. It appears as expected from the literature spectra.[9, 26, 27, 29] It is a rigid body spectrum, quite different from the three sharp line spectrum of the spin label by itself in solution in Figure 4.4. For comparison Figure 5.4[9] shows PD-Tempone (perdeuterated 2,2,6,6-metramethyl-4-piperidone-1-oxyl); it was investigated in toluene-d_8 because the solution can be cooled sufficiently without any changes in phase until a rigid-limit spectrum can be achieved.[9]

From computer simulations using the computer program SimFonia, values of A and g were determined for 300C PA + MTSL. There was approximately axial symmetry with $A_{xx} = A_{yy} = 11$ G, and A_{zz} was 30.5 G. The g_x, g_y, and g_z values were 2.0055, 2.005, and 2.0035 G respectively. The simulation (Figure 5.5) appeared to be accurate except that it gave an extra peak because A_{yy} was chosen to be 11.0 G. The experimental spectrum had no peak for A_{yy}, but since $A_{xx} = A_{yy}$ no value could be chosen that would give the desired peak for A_{xx} and not give a peak for A_{yy}. The difference spectrum was not a flat line, as one would have hoped for. This could be due to some residual motion of the label that was not accounted for in the simulation. The simulation assumed a completely rigid structure, whereas 300C PA + MTSL may not in fact be 100% rigid and therefore the simulation was not perfect.

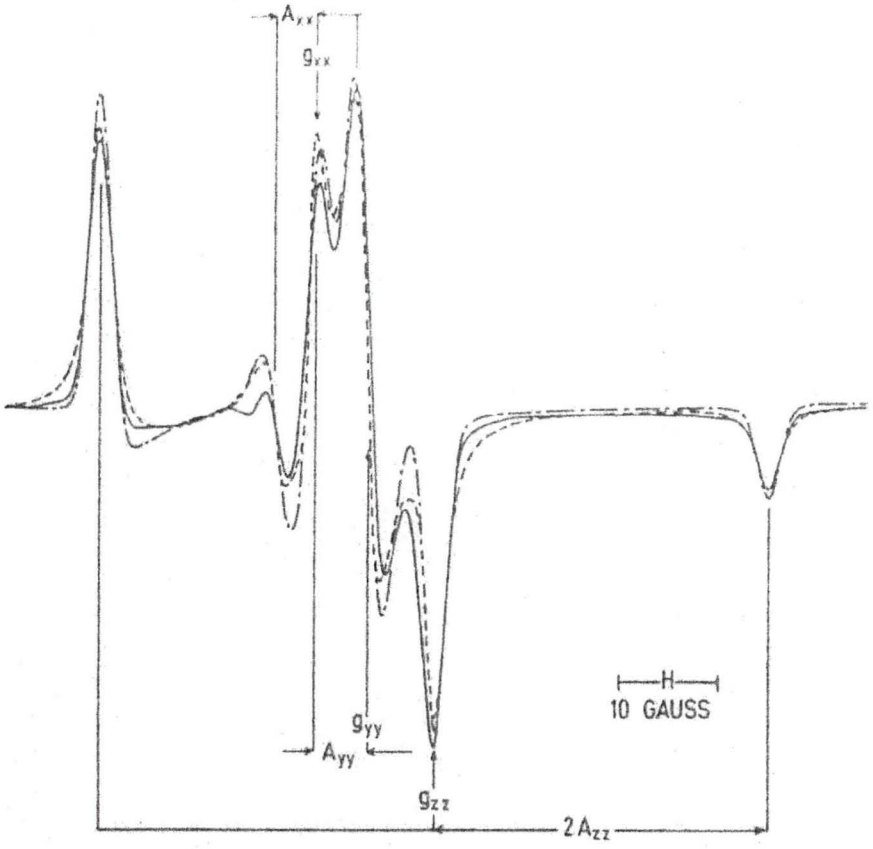

Figure 5.4: Rigid limit spectrum (——) and simulations using Lorentzian (----) and Gaussian (–·–·–) line shapes for PD-TEMPONE in toluene-d_8.[9]

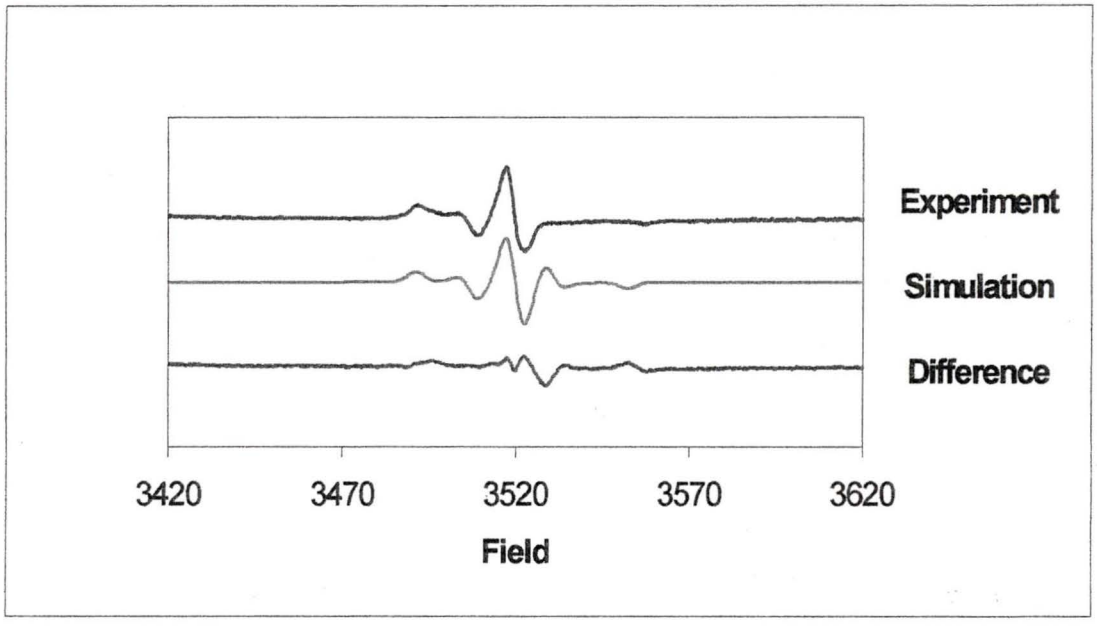

Figure 5.5: Plot of simulation and experimental data for 300C PA + MTSL

5.2.2 Analysis of 300C PA + MTSL

The labeled protein was run on a SDS-PAGE gel and the results showed that it was all in the form of proaerolysin (Figure 4.2). The single band present for 300C PA + MTSL was in the same horizontal plane as the proaerolysin standard. The results in Figure 4.3 showed that the protein had less activity after labeling with MTSL. These two experiments indicate that the labeling process may have had an undesired effect on the protein and that 300C PA + MTSL was in the proaerolysin form and not aerolysin.

5.2.3 Experiments Performed with 300C PA + MTSL

In order to determine if 300C aerolysin + MTSL had a different spectrum from 300C PA + MTSL, trypsin was added to the protein at a concentration of 2 μg/ml. After 20 min of incubation, 2 μg/ml of trypsin inhibitor was added to the solution in order to prevent aerolysin degradation. The protein was nearly entirely converted to the aerolysin form by this treatment (Figure 4.2). When the spectrum in Figure 5.6 was subtracted from the spectrum of 300C PA + MTSL without trypsin a flat line resulted which indicated that the spectra were identical. The subtraction process is illustrated in Figure 5.7. This was what would be expected, since the hydrodynamic radius of the protein would not change much when the 4.5 kDa tail was cut off. Since the protein is 52 kDa a 10% change in mass would not be enough to make a difference in the EPR spectrum.

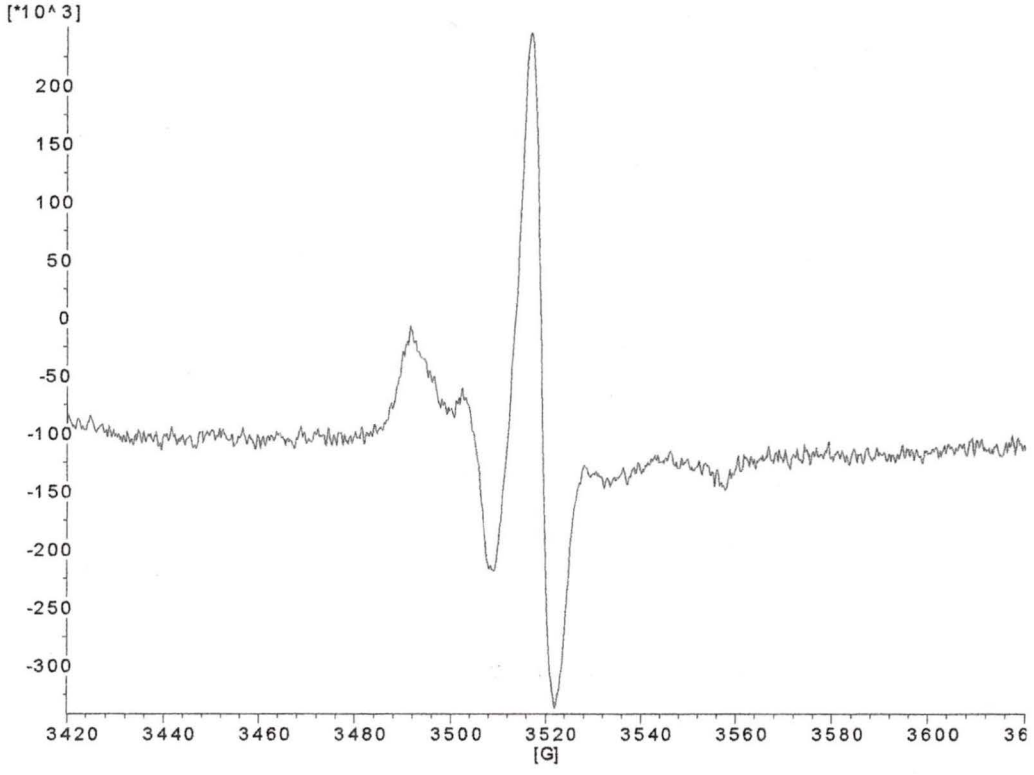

Figure 5.6: Spectrum of 4.33 μM 300C PA + MTSL with 2 μg/ml trypsin added and inhibitor, run in capillary tube at RT

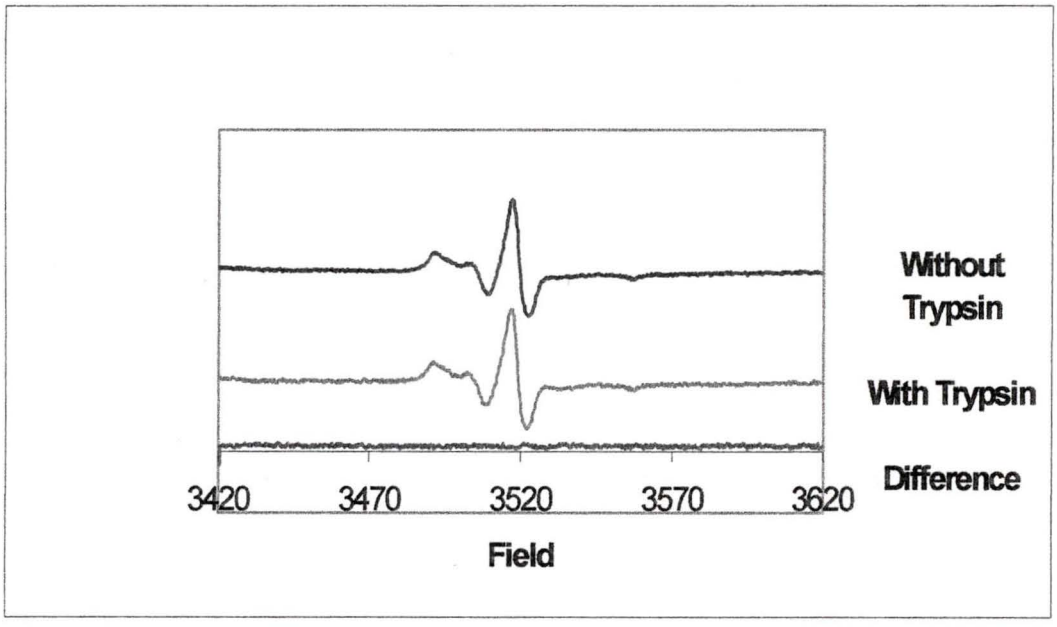

Figure 5.7: Plot of 300C PA without trypsin added and with trypsin added

5.3 Labeling of Variant 445C PA

The variant 445C PA was also labeled. This variant was chosen because the cysteine is on the C-terminal peptide of proaerolysin that is released when trypsin is added. The cysteine is located in domain 4 at one tip of the major lobe as seen in Figure 5.8. The domain adopts a beta-sandwich fold with a short stretch of helix in one of the loops connecting the strands. The sequence distal to the site of processing (to residue 470), covers ~1100Å^2 in domain 4.[12] Proteolysis occurs in the middle of a long, flexible loop formed by residues 422 to 440 at the very tip of the molecule.[34] It was expected that the spectrum of 445C PA + MTSL would look similar to that of 300C PA + MTSL before the addition of trypsin, because the probe should be immobilized by attachment to the protein resulting in a spectrum that will be approximately that of a rigid body. After addition of trypsin the spectrum should look completely different, because the protein would now be attached to a much smaller piece that should be able to rotate much faster in solution than the 52 kDa proaerolysin molecule. Therefore one should obtain an intermediate spectrum between that of the free spin label and a bound spin label.

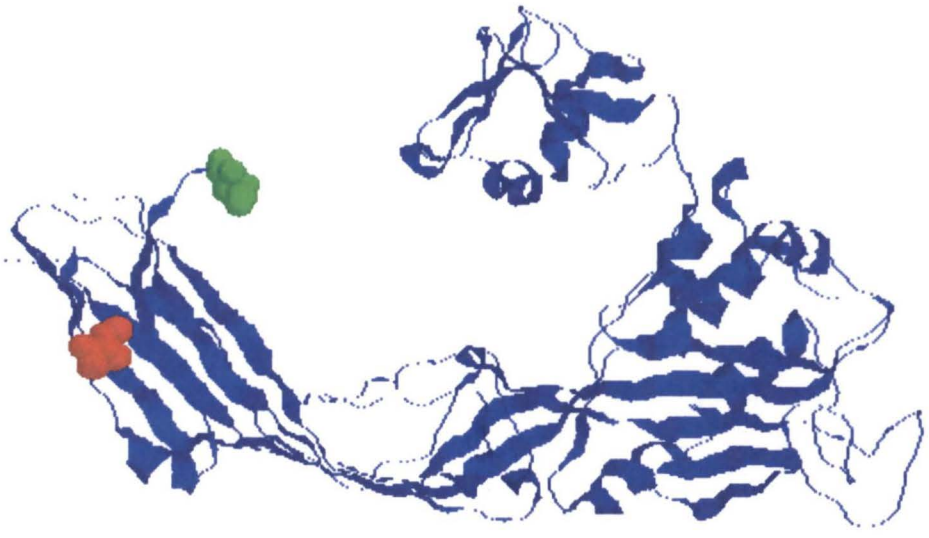

Figure 5.8: Red dots indicate the position of the free cysteine in 445C PA, the green dots represent the C terminal amino acid. 445C PA is on the tail piece that is nicked when trypsin is added thus activating the protein.

Figure 5.9: Red dots indicate the position in domain 4 of 445C PA, the green dots indicate the C terminal amino acid. 445C PA is on the tail piece that is nicked when trypsin is added thus activating the protein.

5.3.1 EPR Spectrum and Simulation of Variant 445C PA + MTSL

Variant 445C PA was labeled at a final protein concentration of 2.71 μM and the EPR spectrum of the purified product was obtained. As expected, Figure 5.10 shows the spectrum of a rigid body. The peaks at 3450 G, 3475 G, and 3516 G matched up well with the spectrum of 300C PA + MTSL. These peaks were indicative of slow motion in the EPR spectrum. There were three peaks that were different in the spectrum for 445C PA + MTSL when compared to 300C PA + MTSL. They occurred at 3465 G, 3480 G, and 3495 G. These peaks will be compared to the peaks of MTSL and trypsin processed 445C PA + MTSL later to see if they may be attributed to either free spin label or to the C-terminal peptide that had been nicked when trypsin was added. The plot of simulation and experimental data for 445C PA + MTSL showed that there were three sharp peaks left over when the powder spectrum was run in SimFonia with $A_{xx} = A_{yy} = 6.0$ G, and A_{zz} was 31.0 G. The g_x, g_y, and g_z values were 2.0080, 2.00525, and 2.00234 G respectively.

The plot of simulation and residual data for 445C PA + MTSL showed that there were three sharp peaks left over when the powder spectrum was run in SimFonia. The residual three sharp lines were simulated and the spectrum was determined to have a g value of 2.0050 and an a value of 16.15 G. Using a Lorentzian lineshape with a linewidth of 1.0 G, the values of A, B, and C were determined. For 445C PA + MTSL, A = 1.0980, B = -0.450, and C = 1.250.

5.3.1 EPR Spectrum and Simulation of Variant 445C PA + MTSL

Variant 445C PA was labeled at a final protein concentration of 2.71 μM and the EPR spectrum of the purified product was obtained. As expected, Figure 5.10 shows the spectrum of a rigid body. The peaks at 3450 G, 3475 G, and 3516 G matched up well with the spectrum of 300C PA + MTSL. These peaks were indicative of slow motion in the EPR spectrum. There were three peaks that were different in the spectrum for 445C PA + MTSL when compared to 300C PA + MTSL. They occurred at 3465 G, 3480 G, and 3495 G. These peaks will be compared to the peaks of MTSL and trypsin processed 445C PA + MTSL later to see if they may be attributed to either free spin label or to the C-terminal peptide that had been nicked when trypsin was added. The plot of simulation and experimental data for 445C PA + MTSL showed that there were three sharp peaks left over when the powder spectrum was run in SimFonia with $A_{xx} = A_{yy} = 6.0$ G, and A_{zz} was 31.0 G. The g_x, g_y, and g_z values were 2.0080, 2.00525, and 2.00234 G respectively.

The plot of simulation and residual data for 445C PA + MTSL showed that there were three sharp peaks left over when the powder spectrum was run in SimFonia. The residual three sharp lines were simulated and the spectrum was determined to have a g value of 2.0050 and an a value of 16.15 G. Using a Lorentzian lineshape with a linewidth of 1.0 G, the values of A, B, and C were determined. For 445C PA + MTSL, A = 1.0980, B = -0.450, and C = 1.250.

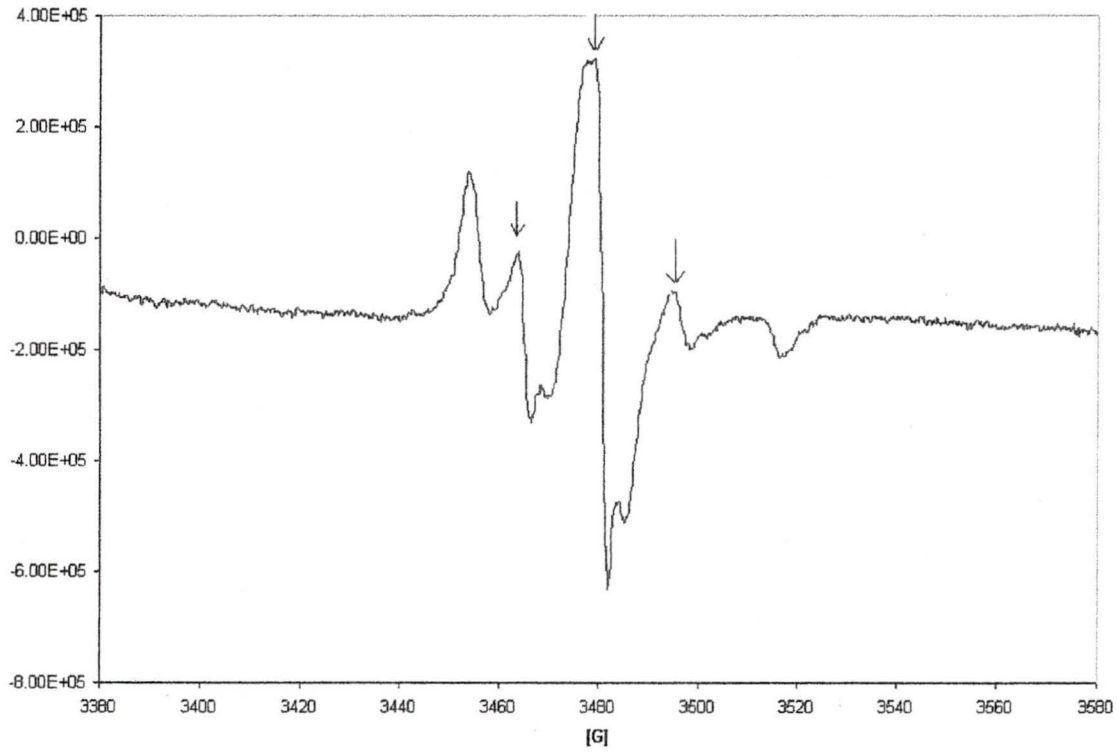

Figure 5.10: Spectrum of 2.71 μM 445C PA + MTSL in solution, run in flat cell at RT with arrows designate the fast component in labeled 445C PA.

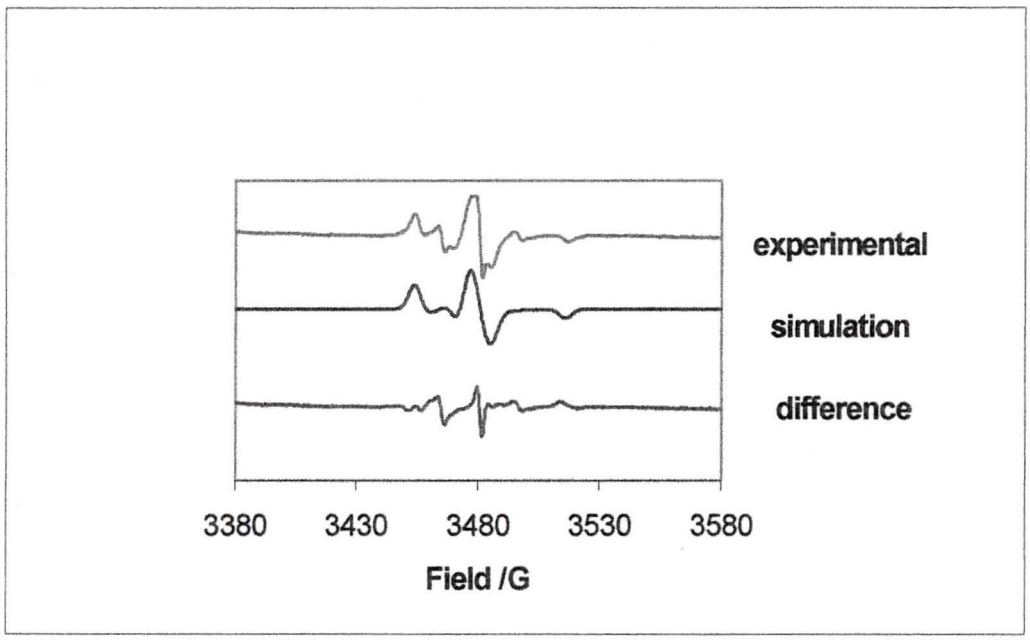

Figure 5.11: Plot of simulation and experimental data for 445C PA + MTSL

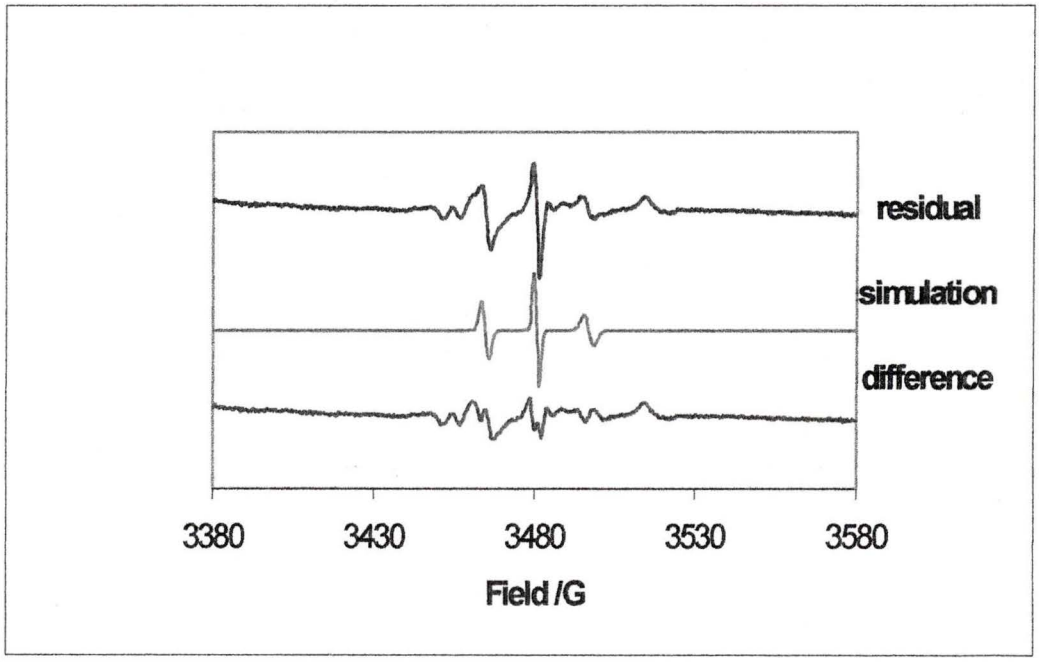

Figure 5.12: Plot of simulation versus residual from 445C PA + MTSL simulation

5.3.2 Analysis of 445C PA + MTSL

The labeled protein was run on a SDS-PAGE gel and the results showed that the protein was all in the form of proaerolysin. The results in Figure 4.3 showed that the protein had more activity after labeling with MTSL. These two experiments indicate that the labeling process may have had an undesired effect on the protein and that 445C PA + MTSL was in the proaerolysin form and not aerolysin.

Figure 5.13: SDS-Page gel of 1.66 μM 445C PA + MTSL with and without trypsin added, LMW Std included 97.4, 66.2, 45.0, 31.0, 21.5, and 14.4 kDa proteins[32], the bottom of the 445C PA + MTSL + trypsin lane has a blue band at the bottom of the gel that denotes the presence of trypsin.

5.3.3 Experiments Performed with 445C PA + MTSL

The effect of activation on the spectrum of 445C PA + MTSL was determined next. Trypsin was added to the protein at a concentration of 2 μg/ml. After 20 min of incubation at RT, 2 μg/ml trypsin inhibitor was added. The protein was nearly entirely converted to the aerolysin form by this treatment (Figure 5.13). In a solution of labeled proaerolysin there was a possibility that two species existed in solution that could have contributed to an EPR spectrum. The two species were the labeled proaerolysin and free label that was not removed in the labeling process. After trypsin treatment there were three species in solution. Unlabeled aerolysin was in solution, along with the label attached to the C-terminal peptide that was produced by trypsin, and free label. It was also possible that the cysteine at 445 generated a fast component when in the proaerolysin form since it is at the end of the protein and in a position where it might have been more mobile. The spectrum produced by trypsin treatment (Figure 5.14) was very different from the spectrum of 445C PA + MTSL that did not have trypsin added to it (Figure 5.15). The plot in Figure 5.15 shows that it is similar to the spectrum of MTSL (Figure 4.4). The percent labeling of 445C PA + MTSL was determined to be approximately 65% from the spectrum. This was determined by integrating twice the spectrum of 445C PA + MTSL with trypsin added and the spectrum of the free spin and comparing the area of each spectrum. The spectrum in Figure 5.14 was simulated in SimFonia and several parameters were obtained from the simulation. The spectrum of 445C PA + MTSL with trypsin added was determined to have a g value of 2.0048 and an a value of 16.20 G. Using a Lorentzian lineshape with a linewidth of 1.0 G, the values of

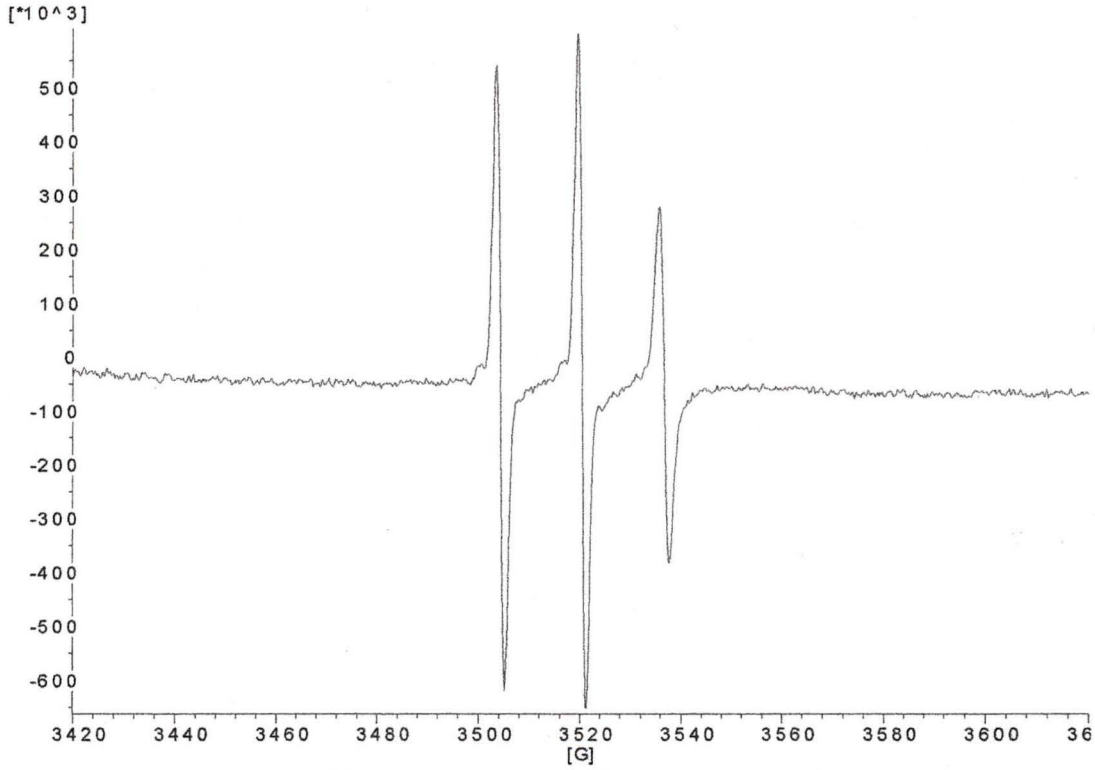

Figure 5.14: Spectrum of 2.22 μM 445C PA + MTSL with trypsin added, run in capillary tube at RT

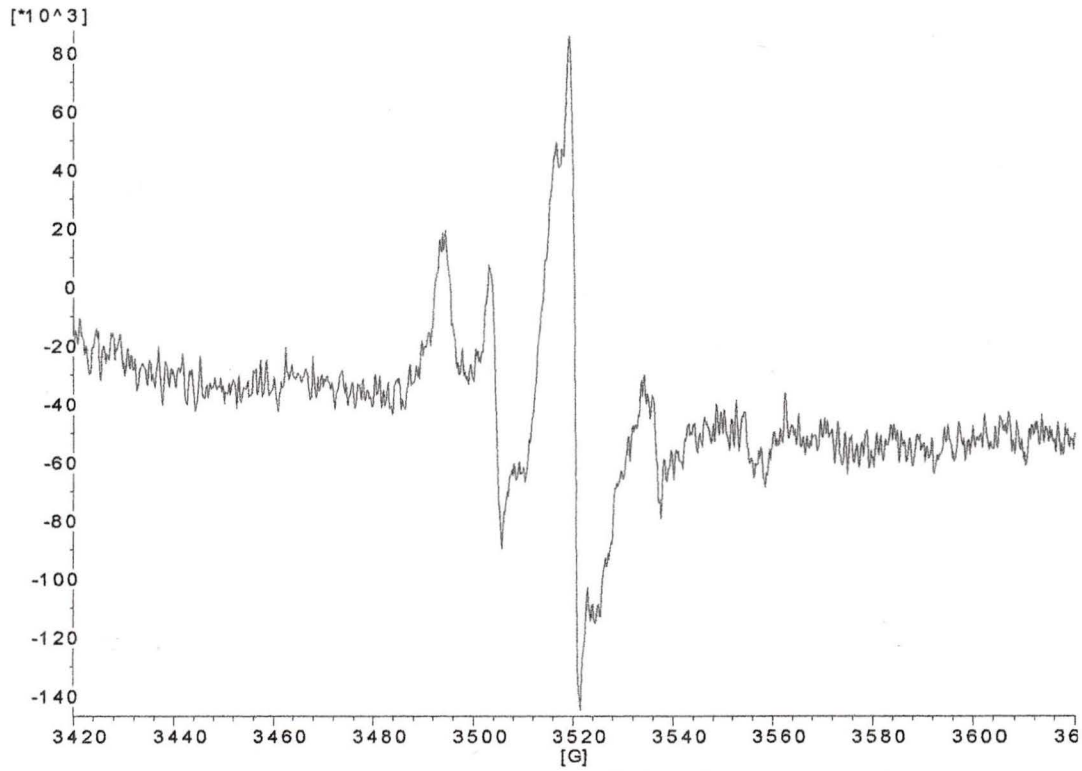

Figure 5.15: Spectrum of 2.22 μM 445C PA + MTSL without trypsin added, run in capillary tube at RT

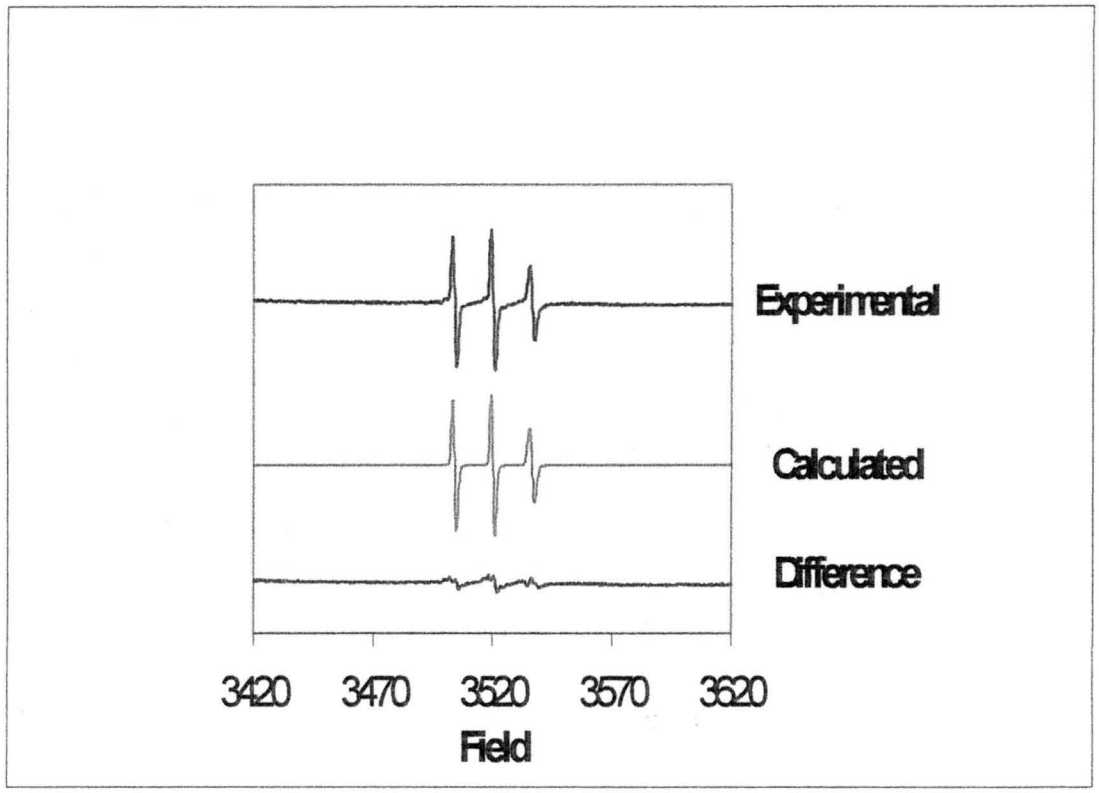

Figure 5.16: Plot of simulation versus experimental data for Figure 5.14

A, B, and C were determined. For 445C PA + MTSL, A = 1.0980, B = -0.3427, and C = 0.4201.

Temperature studies were carried out on 445C PA + MTSL with and without trypsin added and the resulting EPR spectra are illustrated in Figures 5.17 through 5.24.

The correlation times of the trypsin processed 445C PA + MTSL were determined by the method described in section 1.5. The results showed that the correlation time increased with a decrease in temperature, which was as expected since the viscosity of the solution increased, reducing the mobility of the spin label. The correlation times determined using B and C were very close to one another. In the same way the correlation time of the free spin label was determined to be 5.543×10^{-13} seconds at 293 K using the C value, which was approximately 2 times faster than the 445C PA C-terminal peptide. Since the correlation time and the temperature were both known, the Arrhenius equation could be used to determine an activation energy for the rotation of the C-terminal peptide in solution. The Arrhenius equation is $k = Ae^{-E_a/RT}$.[30] According to this equation, a straight line should be obtained when the logarithm of the rate constant, k, is plotted against the reciprocal of the absolute temperature. The rate constant in the present study was determined by the inverse of the correlation time determined from the C value. The activation energy, E_a, could be determined from the slope of this graph.

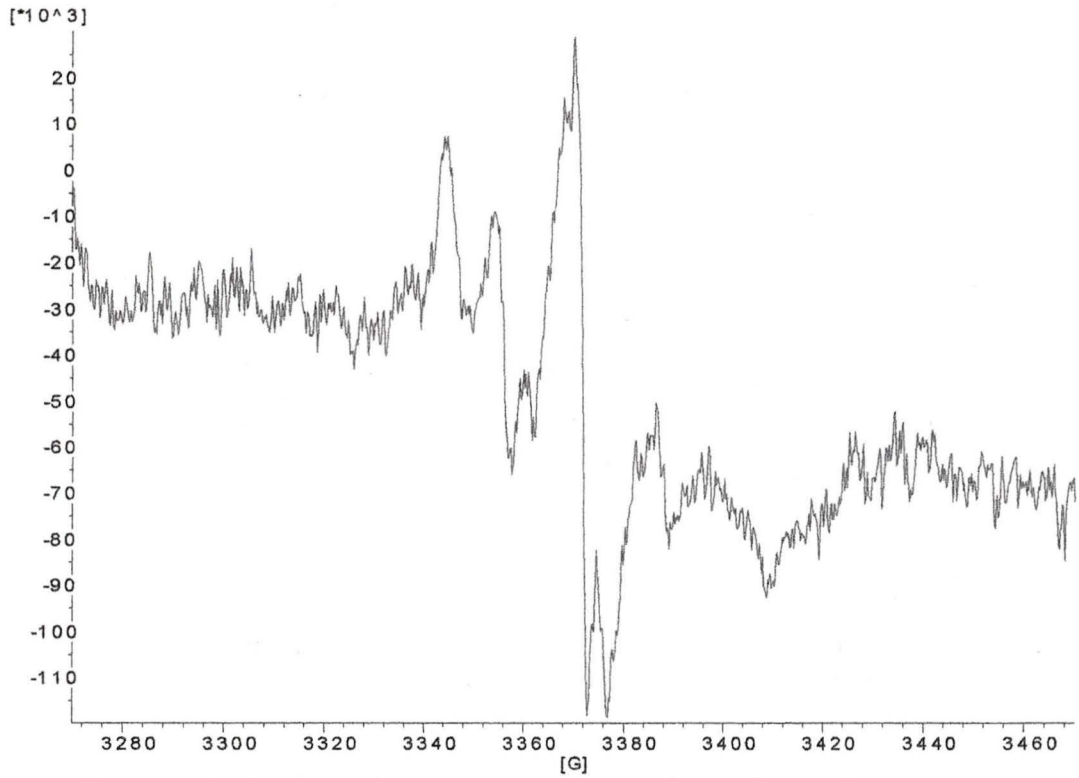

Figure 5.17: 2.22 μM 445C PA + MTSL, run in capillary tube at 273K

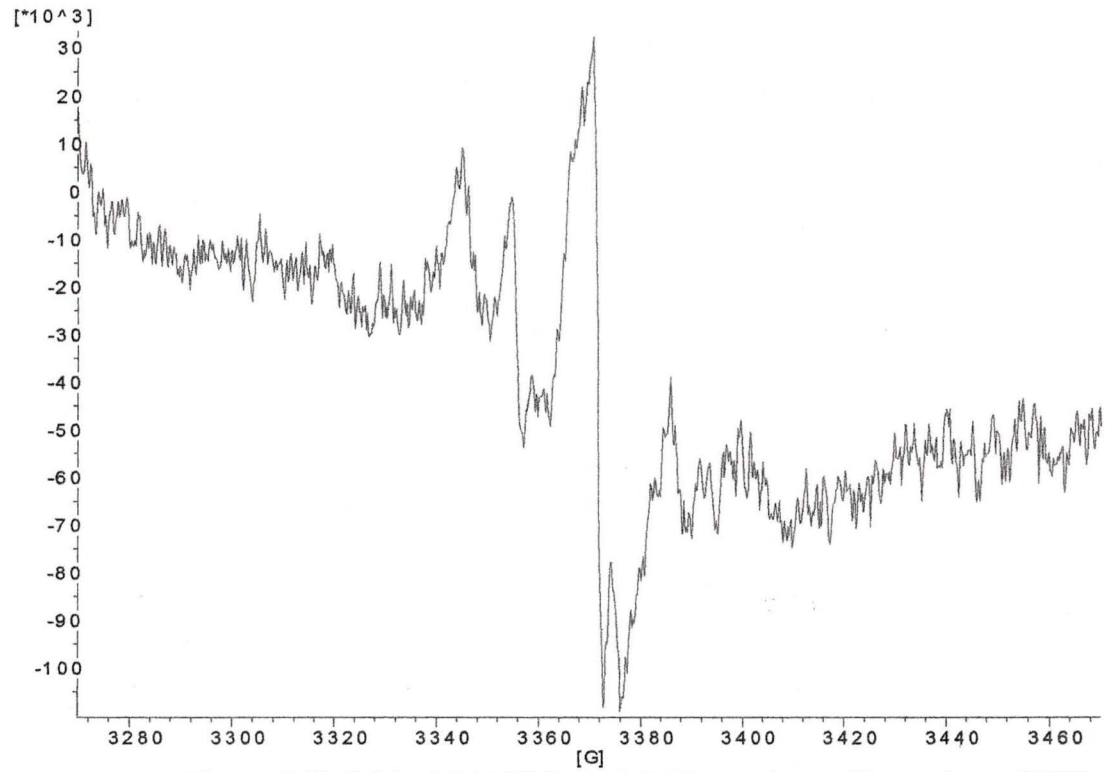

Figure 5.18: 2.22 μM 445C PA + MTSL, run in capillary tube at 283K

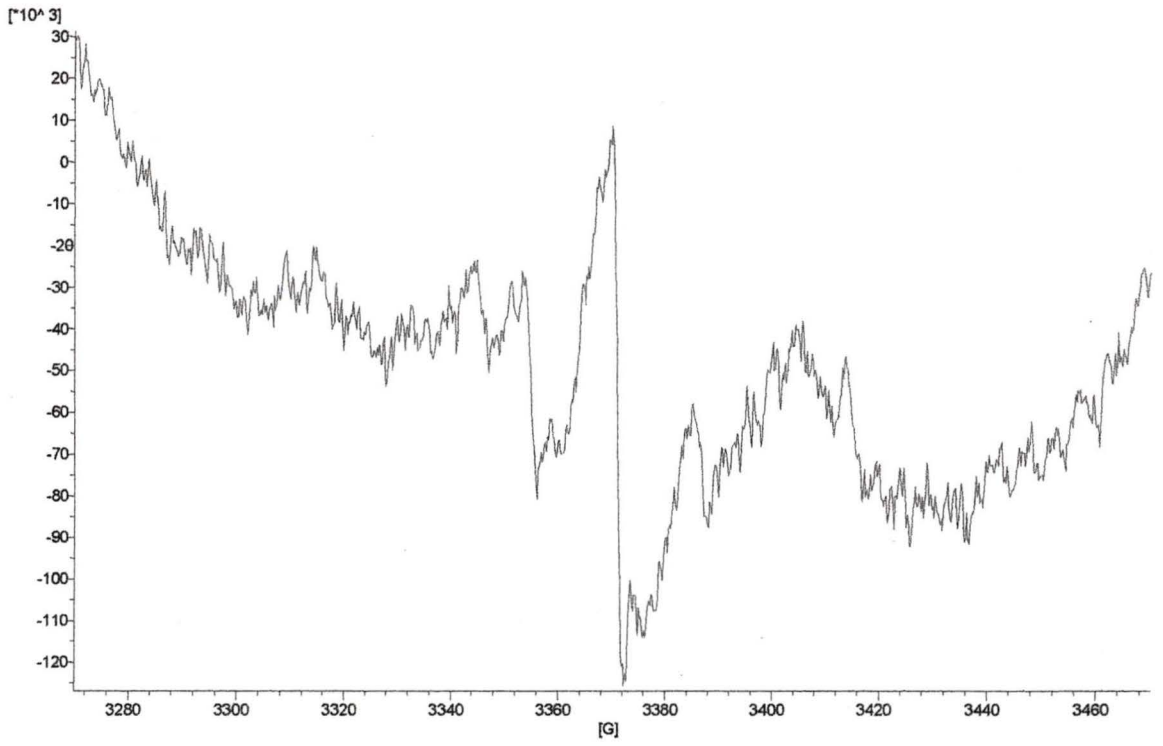

Figure 5.19: 2.22 μM 445C PA + MTSL, run in capillary tube at 293K

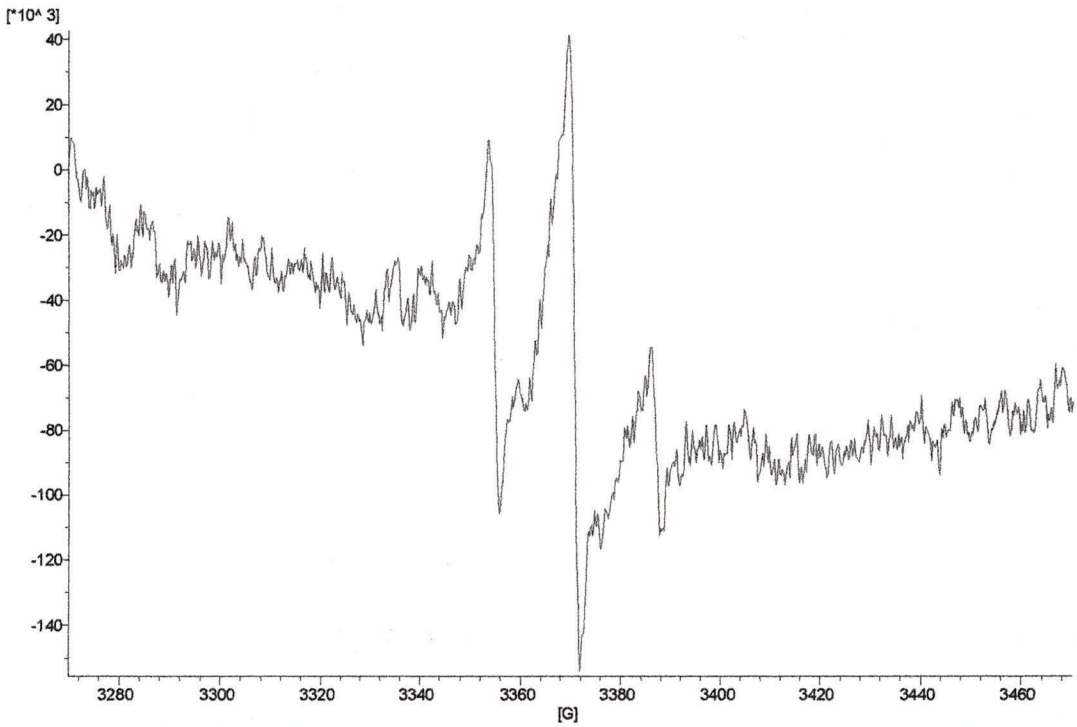

Figure 5.20: 2.22 μM 445C PA + MTSL, run in capillary tube at 303K

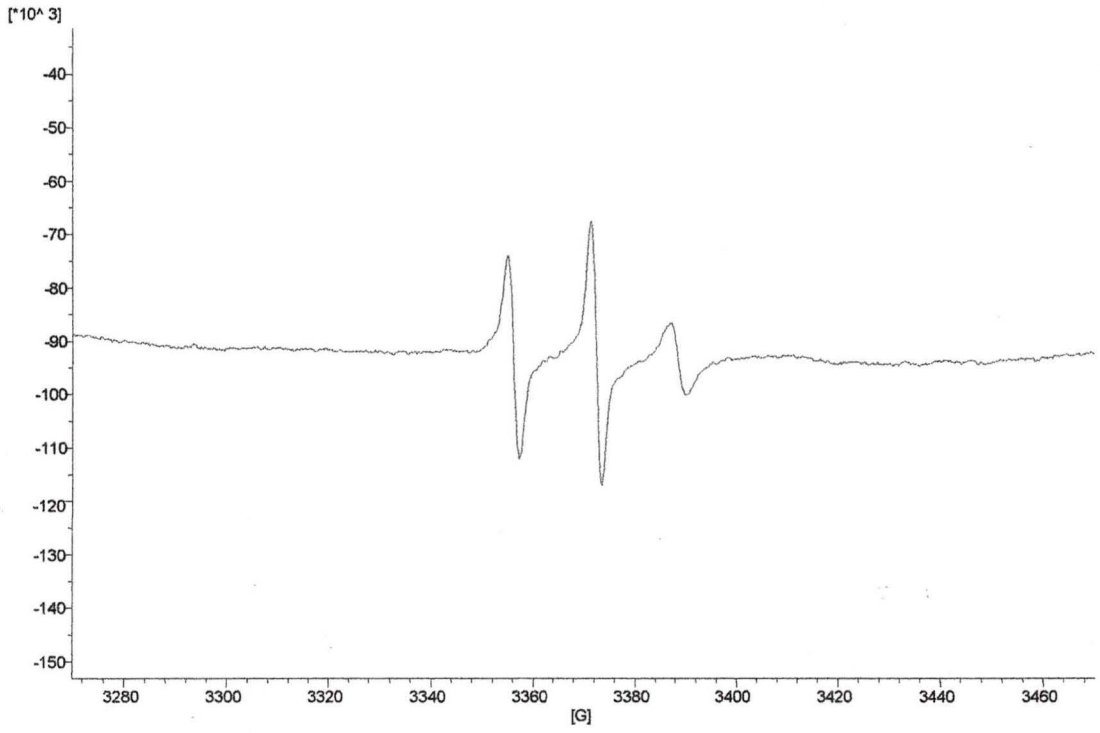

Figure 5.21: 2.22 μM 445C PA + MTSL + trypsin + inhibitor, run in capillary tube at 273K

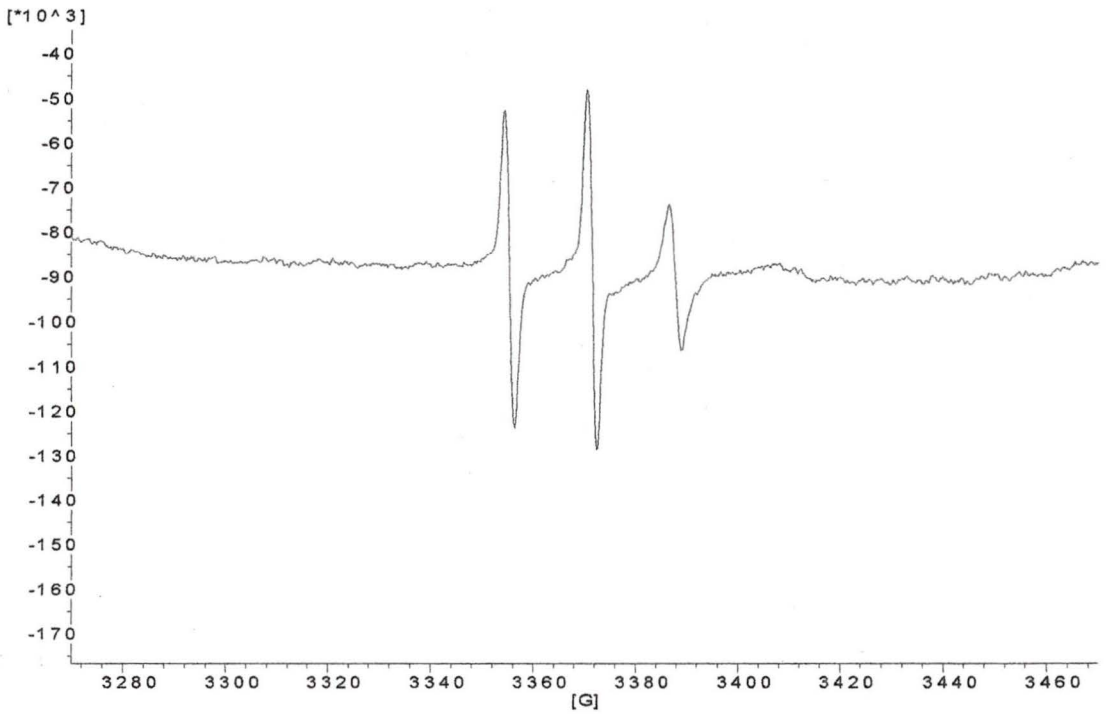

Figure 5.22: 2.22 μM 445C PA + MTSL + trypsin + inhibitor, run in capillary tube at 283K

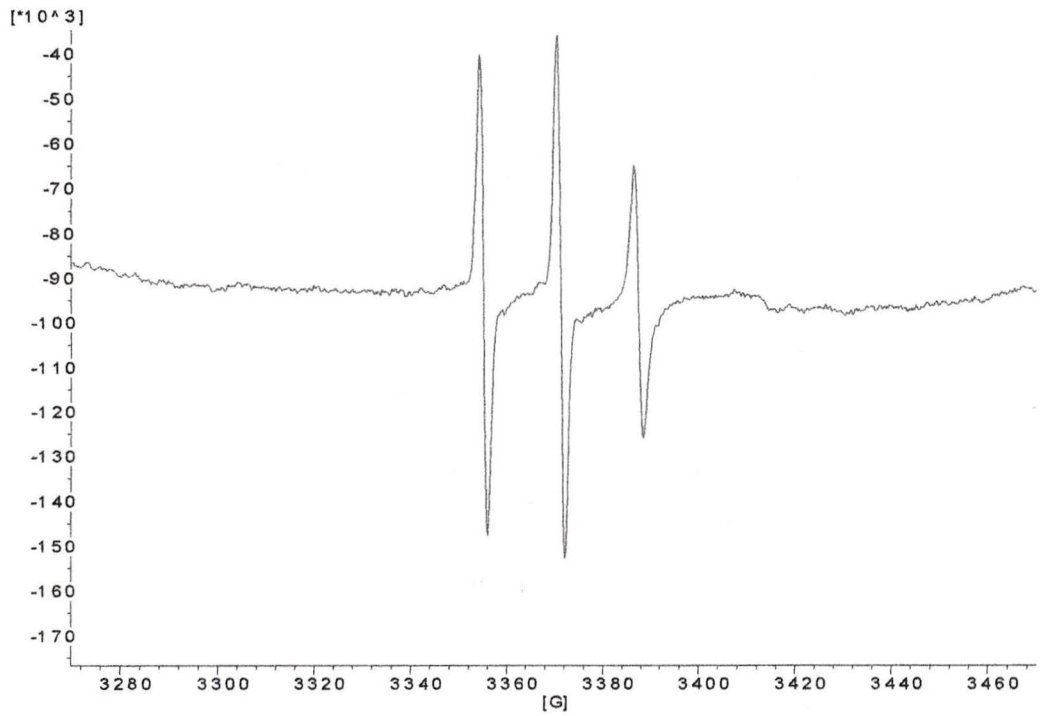

Figure 5.23: 2.22 μM 445C PA + MTSL + trypsin + inhibitor, run in capillary tube at 293K

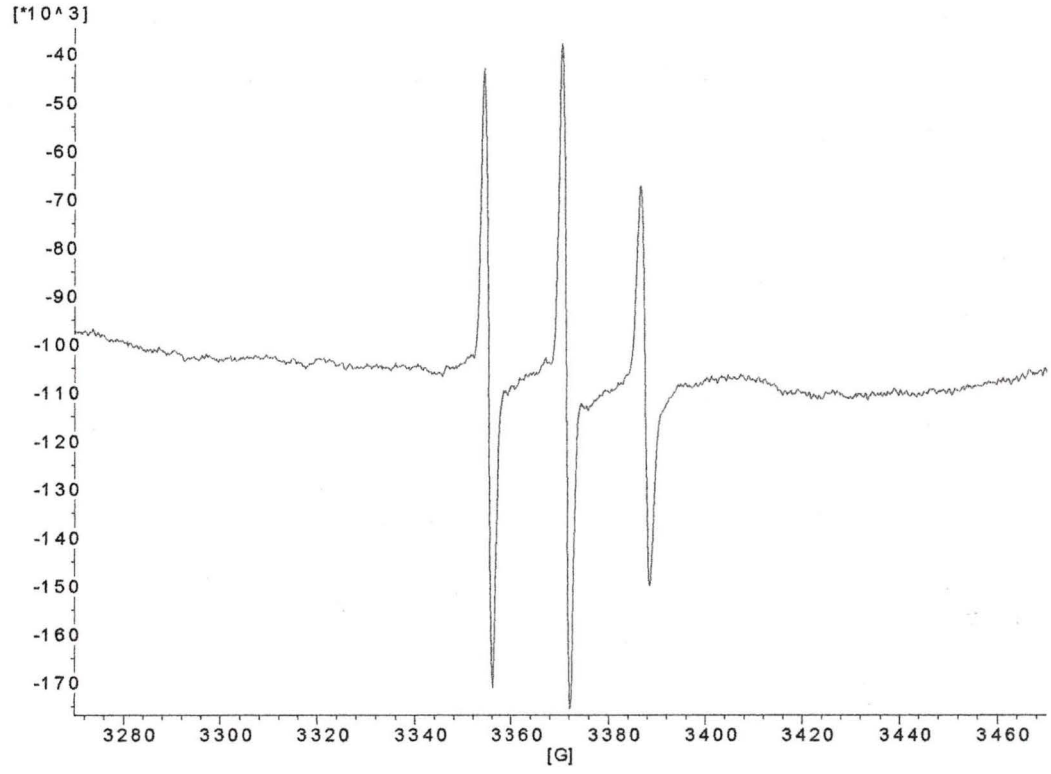

Figure 5.24: 2.22 μM 445C PA + MTSL + trypsin + inhibitor, run in capillary tube at 303K

Table 1: Amplitude of the three lines of the EPR spectrum of trypsin processed 445C PA + MTSL at various temperatures.							
		Temp /K	m_{-1}	m_0	m_1		
		303	127210	137599	82801		
		293	107081	116287	61208		
		283	70995	80085	32939		
		273	76505	98323	27350		
		263	44351	71701	14044		

Table 2: C and B values at various temperatures in units of MHz				
	Temp /K	C	B	
	303	0.264	0.1994	
	293	0.313	0.2506	
	283	0.458	0.3662	
	273	0.665	0.4923	
	263	0.848	0.5472	

Table 3: Correlation time using C and B values		
Temp /K	correlation time using C /second	correlation time using B /second
303	3.113×10^{-12}	2.445×10^{-12}
293	3.702×10^{-12}	3.073×10^{-12}
283	5.407×10^{-12}	4.491×10^{-12}
273	7.854×10^{-12}	6.036×10^{-12}

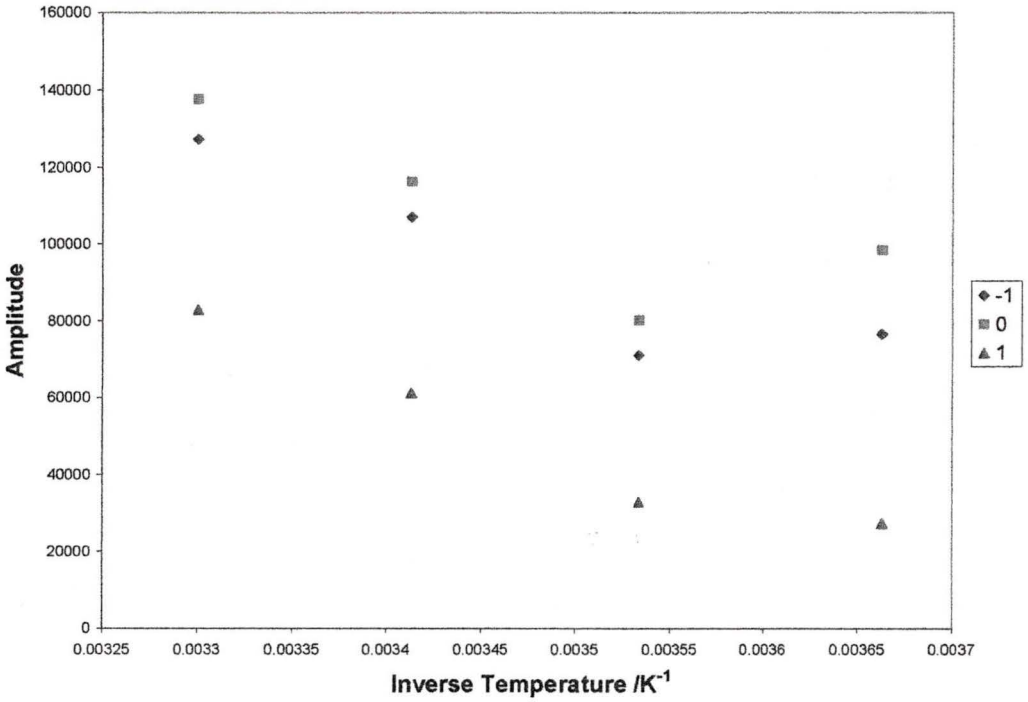

Figure 5.25: Plot of amplitude versus inverse temperature for trypsin processed 445C PA

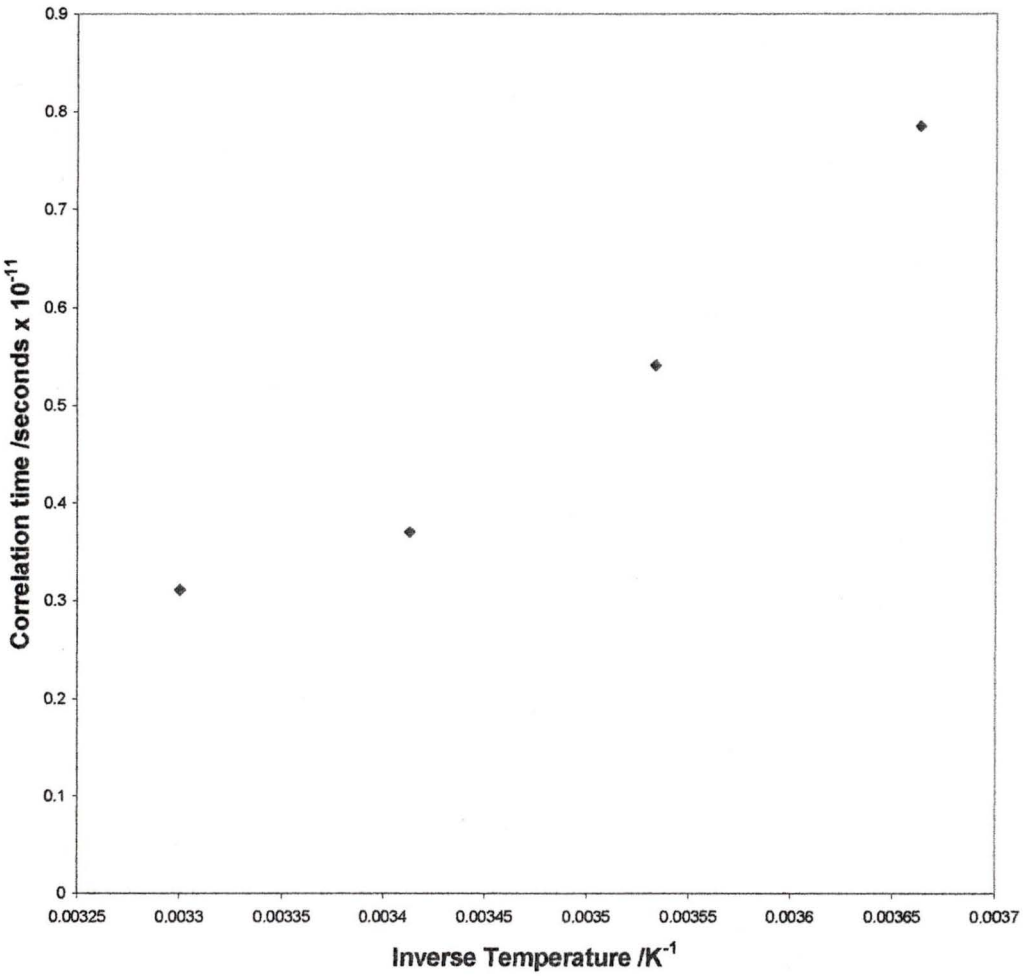

Figure 5.26: Plot of correlation time versus inverse temperature for trypsin processed 445C PA

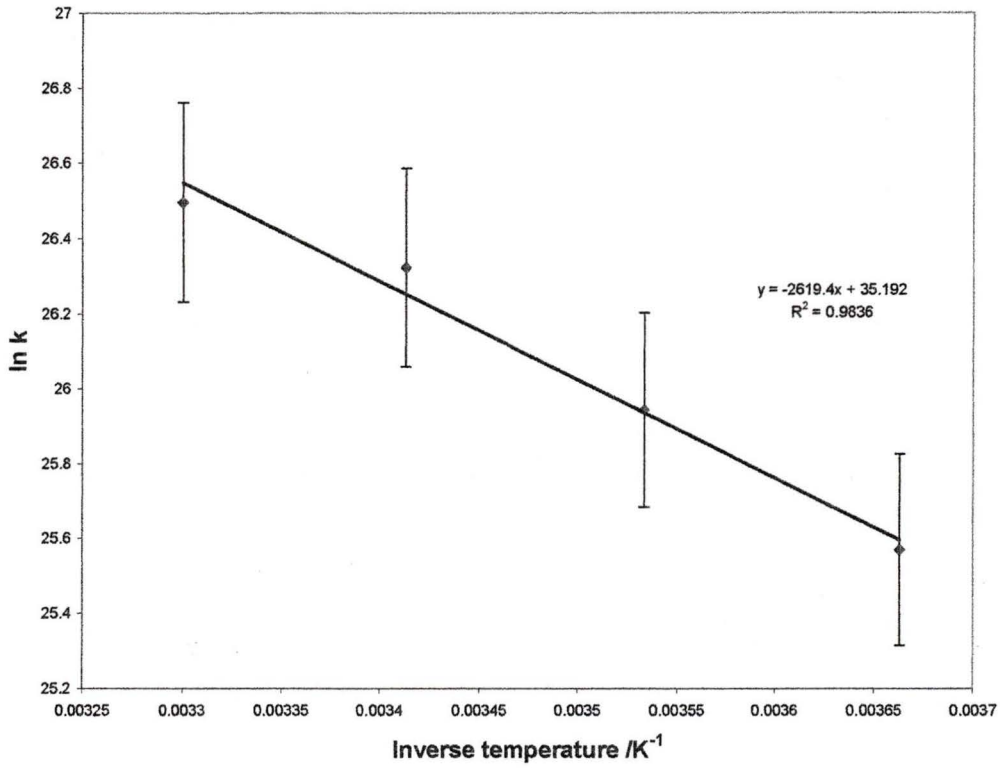

Figure 5.27: Plot of ln k versus 1/T for 445C PA with trypsin added

From the plot of ln k versus 1/T for 445C PA + MTSL with trypsin added the activation energy was determined to be 20 ± 8 kJ/mol. This energy is approximately the energy of a hydrogen bond. This activation energy gave an idea of how much energy was required for the molecule to rotate in solution.

The correlation time was also used to determine the radius of the portion of proaerolysin that was nicked upon activation. According to the Debye diffusion model, the correlation time can be calculated if the molecules are approximated as spheres of radius R:

$$\tau_c = \frac{1}{6D} \tag{66}$$

$$D = \frac{kT}{8\pi\eta R^3} \tag{67}$$

D is the rotational diffusion constant and η is the viscosity.[9] Once the radius of the sphere is known the volume of a sphere is

$$V = \frac{4}{3}\pi R^3. \tag{68}$$

Since the mass of the MTSL is 264.384 g/mol the mass of the C-terminal peptide that included 445C PA + MTSL could be approximated. The mass of the C-terminal peptide was approximately 1.9 kDa.

Trypsin cuts proteins on the C-terminal side of arginines and lysines. Trypsin cuts proaerolysin at amino acid 427 and the peptide that is released may be further cut into smaller peptides.[33] The whole peptide is 43 amino acids long with a weight of 4.5kDa. The solution that was used in Figures 5.21-5.24 contained a combination of chains of various lengths depending on the places where trypsin could cut the protein.

The mass of the fragments was 1.9 kDa, when the weight of the spin label is subtracted; the fragment is approximately 1.65 kDa. A fragment of 1.65 kDa corresponds to a peptide of between 16 and 17 amino acids long since each amino acid weighs approximately 0.1 kDa. The EPR spectrum was made up of any of these chains that contained 445C PA + MTSL.

Since the 445C PA + MTSL proaerolysin spectrum also had three sharp lines it was investigated in the same manner as the processed 445C PA + MTSL spectrum. The correlation times for the fast part of the 445C PA + MTSL spectra were all slower than the corresponding correlation times for the trypsin-treated labeled protein. This showed that the fast part of the 445C PA + MTSL spectrum was not due to the presence of protease-activated protein that may have been formed in the process of labeling. The correlation time was approximately 2-3 times slower for the fast part of the 445C PA + MTSL spectrum than it was for the corresponding part of the spectrum of the protein treated with trypsin. The activation energy of 445C PA + MTSL was determined to be 14 ± 20 kJ/mol (Figure 5.29) which was significantly lower then the activation energy determined when trypsin was added. The lower energy can be attributed to the fact that 445C PA + MTSL was not rotating freely in solution but was restricted in its movement because of its size.

Table 4: Radius, volume, and mass of the C-terminal peptide that included 445C PA + MTSL			
Temp	Radius	Volume	Mass
/K	/m	/m^3	/kDa
303	1.573×10^{-10}	1.633×10^{-29}	1.928
293	1.528×10^{-10}	1.495×10^{-29}	1.765
283	1.569×10^{-10}	1.621×10^{-29}	1.914
273	1.582×10^{-10}	1.657×10^{-29}	1.957
MTSL	8.155×10^{-11}	2.238×10^{-30}	0.264

Table 5: Amplitude of the three sharp lines of the EPR spectrum of 445C PA + MTSL at various temperatures.

			m_{-1}	m_0	m_1		
		303	115600	196593	57800		
		293	54400	131400	28200		
		283	52208	143062	29307		
		273	53810	150614	26300		

Table 6: C and B values at various temperatures in units of MHz

Temp	C	B
303	0.040792	0.113253
293	0.080058	0.167378
283	0.097438	0.17981
273	0.100062	0.207119

Table 7: Correlation Time using C value

Temp /K	Correlation time /seconds
303	0.7145×10^{-11}
293	1.1477×10^{-11}
283	1.2860×10^{-11}
273	1.4248×10^{-11}

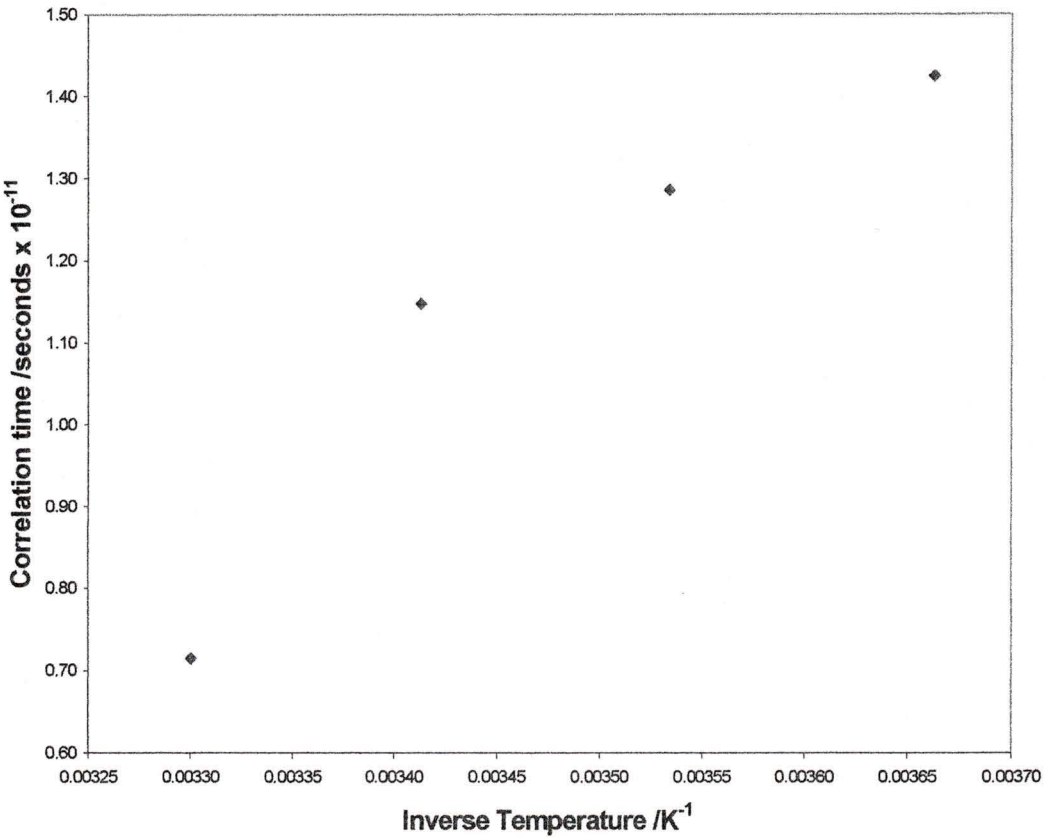

Figure 5.28: Plot of correlation time versus inverse temperature for fast moving component of 445C PA + MTSL

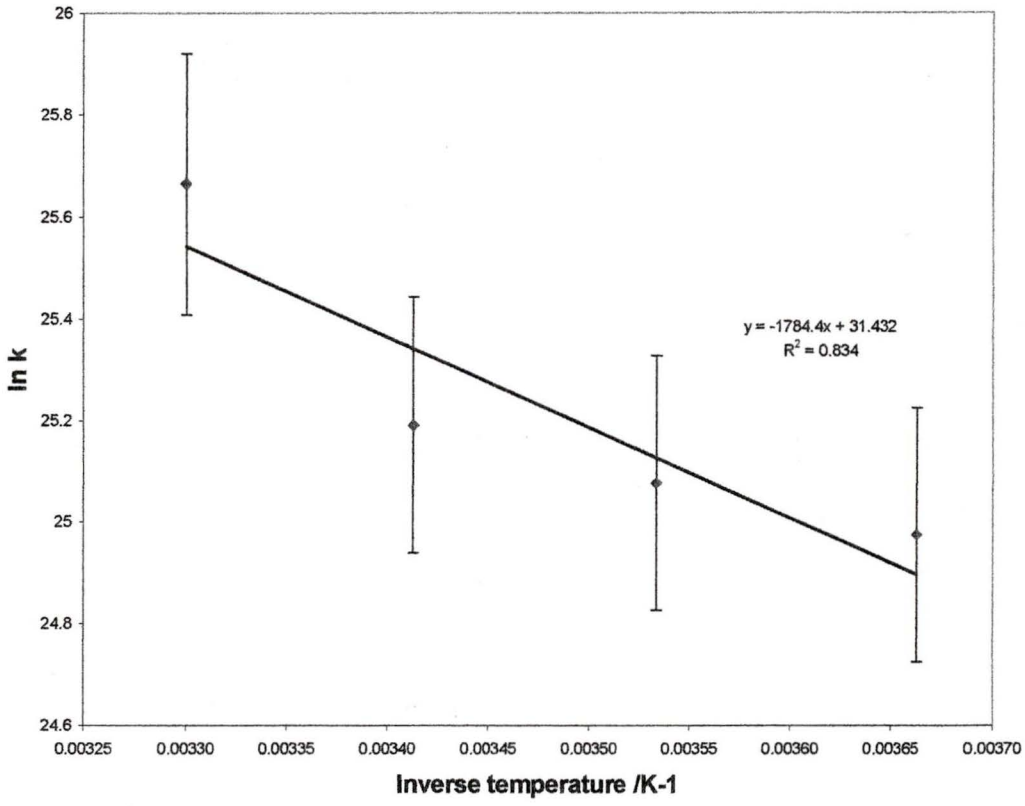

Figure 5.29: Plot of ln k vs inverse temperature for the fast component of 445C PA + MTSL

5.4 Labeling of Variant 241C PA

The free cysteine of the 241C PA variant is on the loop in domain three of the protein and it is on the inside surface of the proaerolysin dimer (Figures 5.30 and 5.31). This variant was chosen for study because it is believed that the loop plays an important role in the formation of the heptamer of aerolysin that inserts into cells.[11] There is evidence that the loop in domain 3 must move during oligomerization.[34]

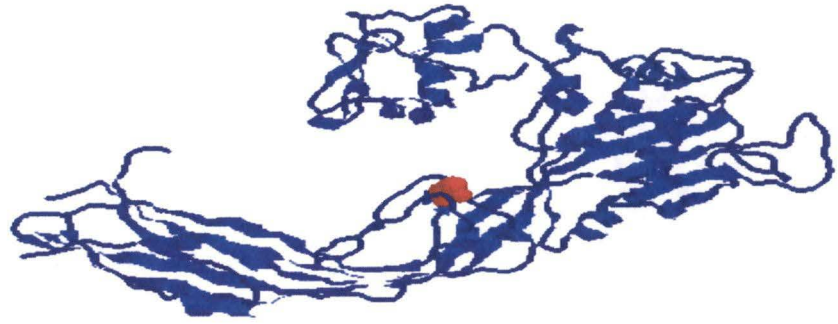

Figure 5.30: Red dots show the location of 241C PA in the protein proaerolysin

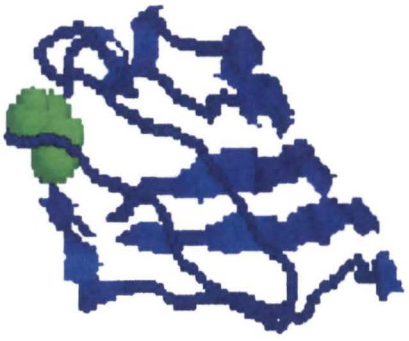

Figure 5.31: The green dots show the location of 241C PA at one end of the long loop.

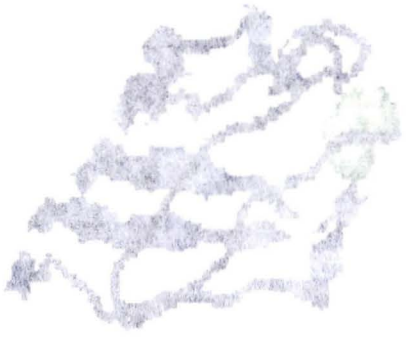

5.4.1 EPR Spectrum of Variant 241C PA + MTSL

Variant 241C PA was labeled at a final protein concentration of 8.16 μM in a buffer of 20 mM Hepes, 0.15 M NaCl, 1 mM EDTA, pH 7.4. The EPR spectrum was run in the flat cell. Figure 5.32 shows the fast component in 241C PA + MTSL. The results indicate that 241C PA + MTSL was more poorly labeled than 300C PA + MTSL or 445C PA+ MTSL. The amount of labeling was determined by adding 1 μg/ml protease K to a solution of the 241C PA + MTSL and comparing the signal to that of the free spin label at the same concentration. Protease K cleaves peptide bonds at the carboxylic sides of aliphatic, aromatic or hydrophobic amino acids, degrading proteins into small peptides, thereby creating a three line spectrum that can be compared to MTSL.[35] Both Figures 5.33 and 5.34 were integrated twice and the area of Figure 5.33 was determined to be 10% the area of Figure 5.34. The SDS-PAGE gel and the titre both showed that the labeling was not detrimental to the protein, even though if there was only 10% labeling then the titre may not have been sensitive enough to differentiate between labeled and unlabeled protein. The residue may be hard to label because it is buried inside the protein.[33] The addition of 6 M urea was tried to improve the labeling. Urea unfolds the protein allowing for easier access to the cysteine. Unfortunately, the hemolytic titre showed that this caused the variant to become inactive. Adding urea did improve the percent labeling but was not explored because of the results of the titre.

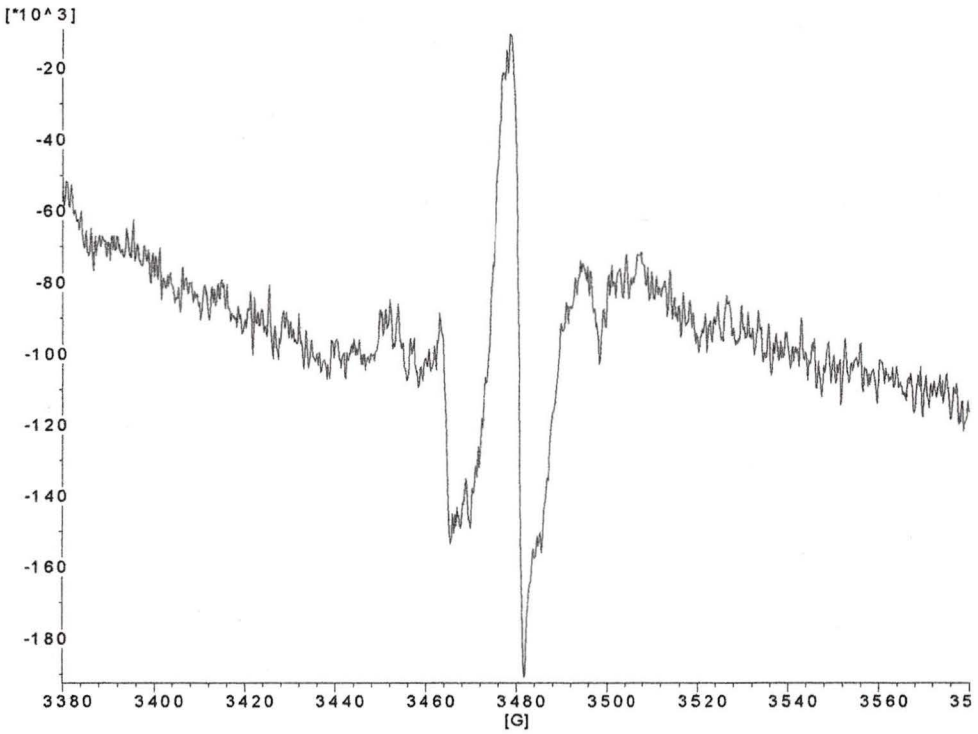

Figure 5.32: 6.67 μM 241C PA + MTSL, run in flat cell at RT

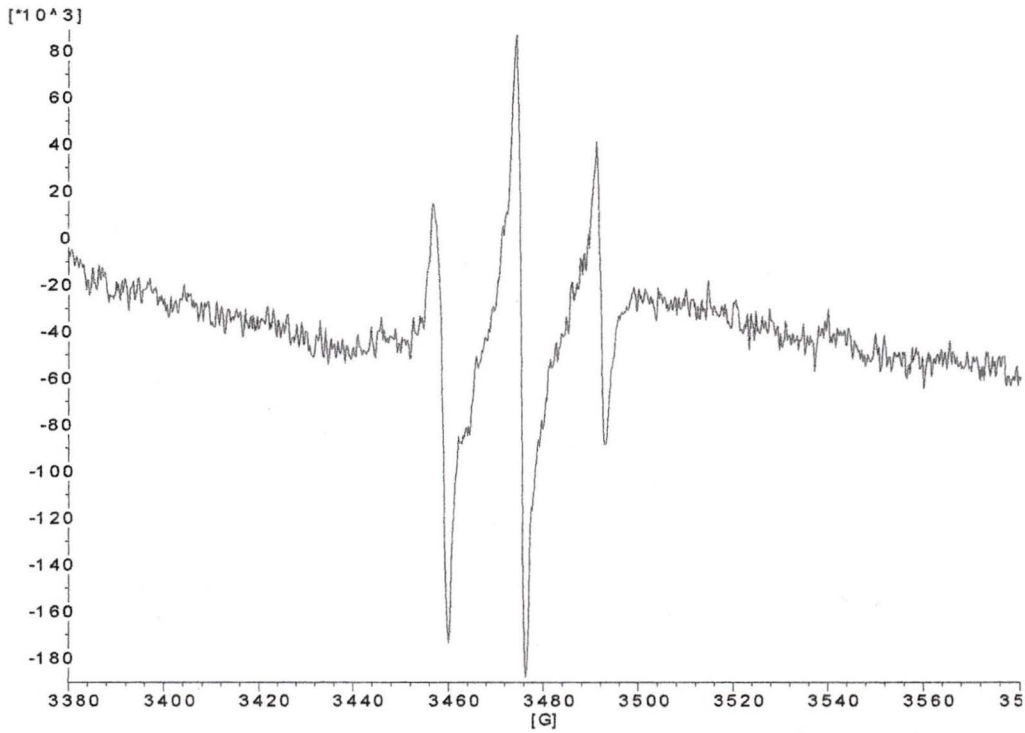

Figure 5.33: 6.67 μM 241C PA + MTSL with protease K added, run in flat cell at RT

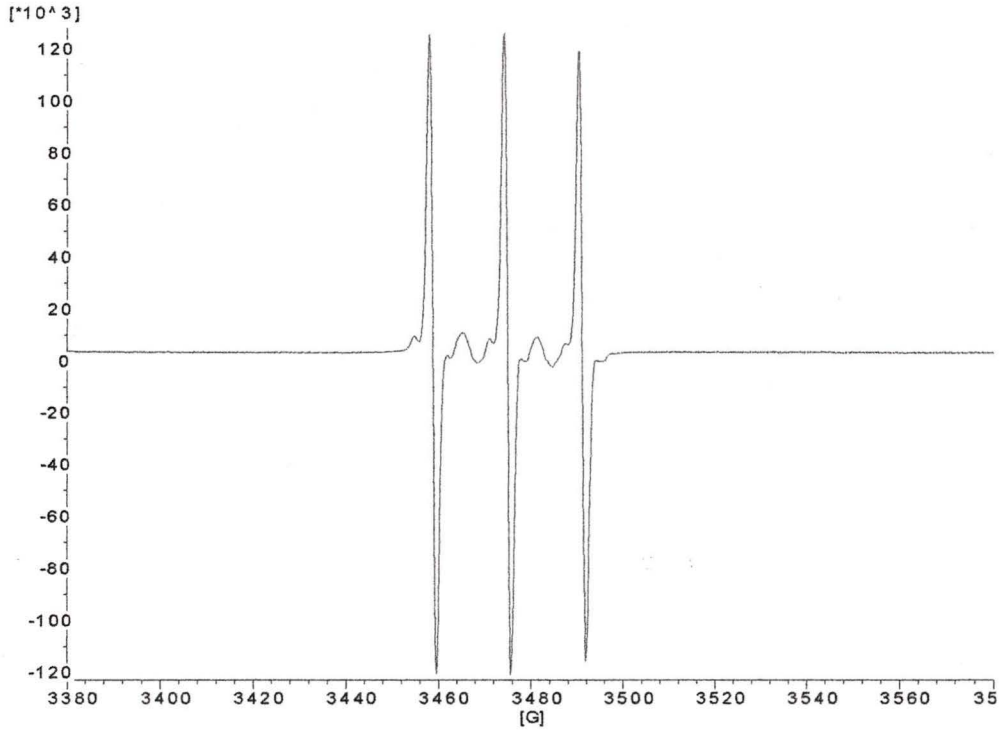

Figure 5.34: 6.67 μM MTSL in buffer solution, run in flat cell at RT

5.4.2 Experiments Performed with 241C PA + MTSL

The labeled 241C PA was next processed with trypsin. The spectrum that was obtained was very similar to the spectrum of the unprocessed protein, except that the peaks at 3450 and 3480 G were a bit larger indicating that this variant is more rigid after processing. The difference was not large, but might be increased by improving the labeling process for this protein, increasing the signal and decreasing background noise.

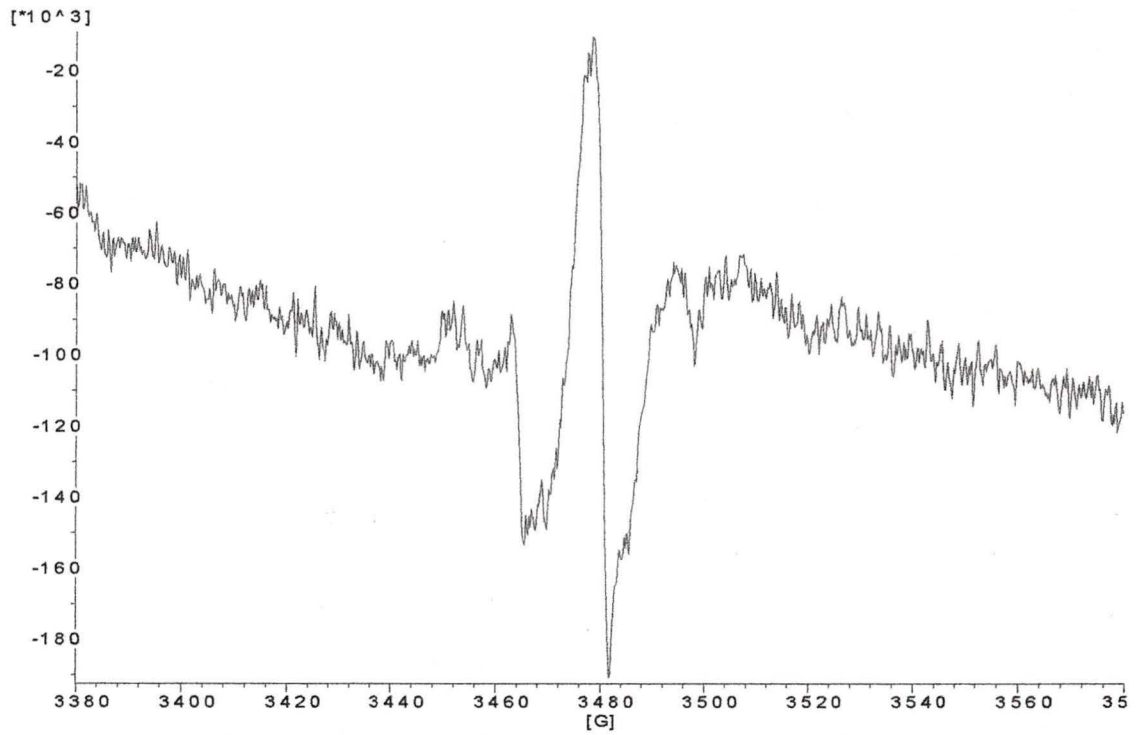

Figure 5.35: 6.67 μM 241C PA + MTSL with 2 μg/ml trypsin added, run in flat cell at RT

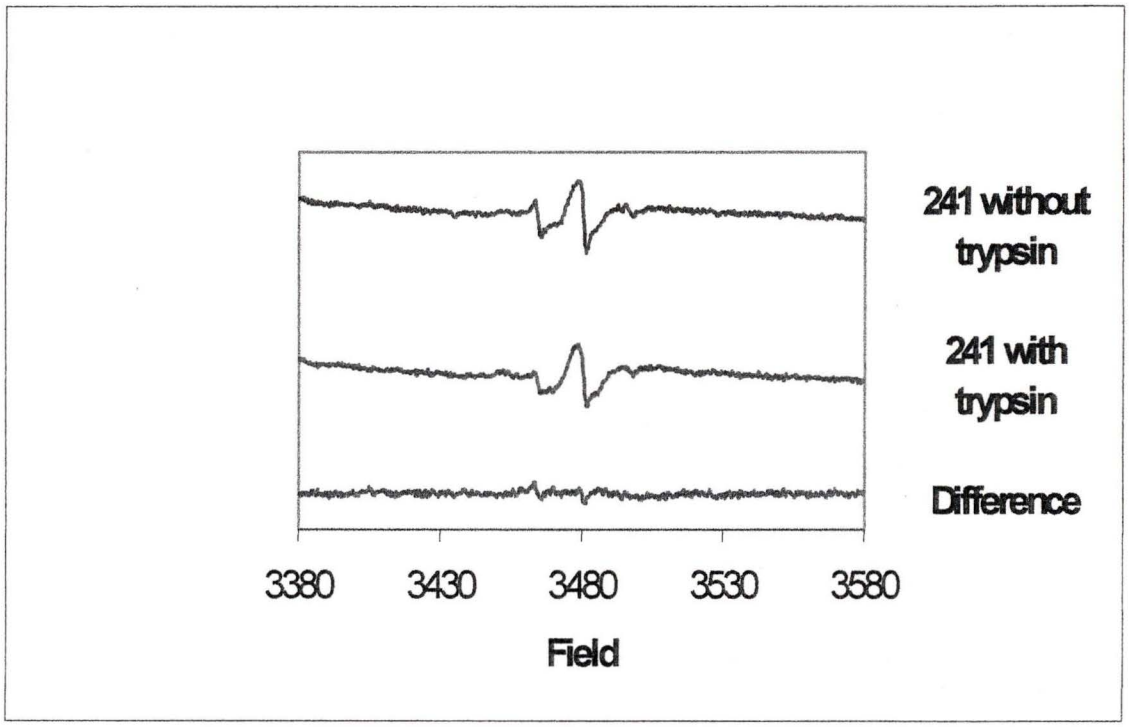

Figure 5.36: Plot of 241C PA + MTSL without and with trypsin added

5.5 Labeling of Variant 242C PA

The cysteine is also on the loop in domain three of the protein (Figures 5.37 and 5.38).

5.5.1 EPR spectrum of Variant 242C PA + MTSL

This variant was labeled at a final protein concentration of 9.68 μM in a buffer of 20 mM Hepes, 0.15 M NaCl, 1 mM EDTA, pH 7.4 and the EPR spectrum was run in the flat cell. The spectrum can be seen in Figure 5.39.

The results in Figure 5.39 show that this variant was in an area of the protein where it could move about. Further work must be carried out to see if this spectrum was labeled protein or whether the label has been nicked during the labeling process. The spectrum does not have the same rigidity that was seen in 300C PA + MTSL, and it seems even more mobile than does 241C PA + MTSL, which was right beside it.

The labeling, approximately 15% for 242C PA, was not terribly efficient. With the concentration of protein that was obtained in the labeling process, one would expect to see a signal at least the size of 300C PA + MTSL. Since it is on the loop on the interior of the protein dimer, it was not as easily labeled as 300C PA+ MTSL. Variant 242C PA will be labeled under different conditions in order to optimize the labeling process.

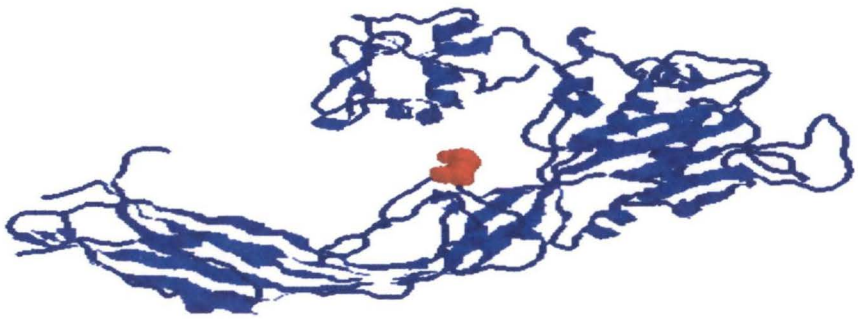

Figure 5.37: Red dots show the location of 242C PA in the protein proaerolysin

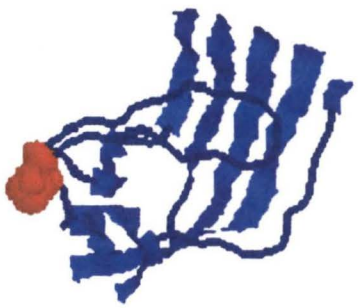

Figure 5.38: Red dots show the location of 242C PA in domain 3

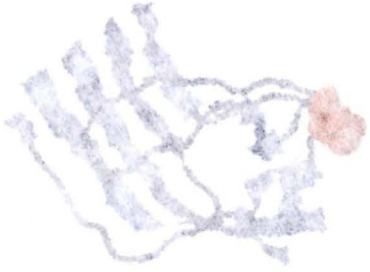

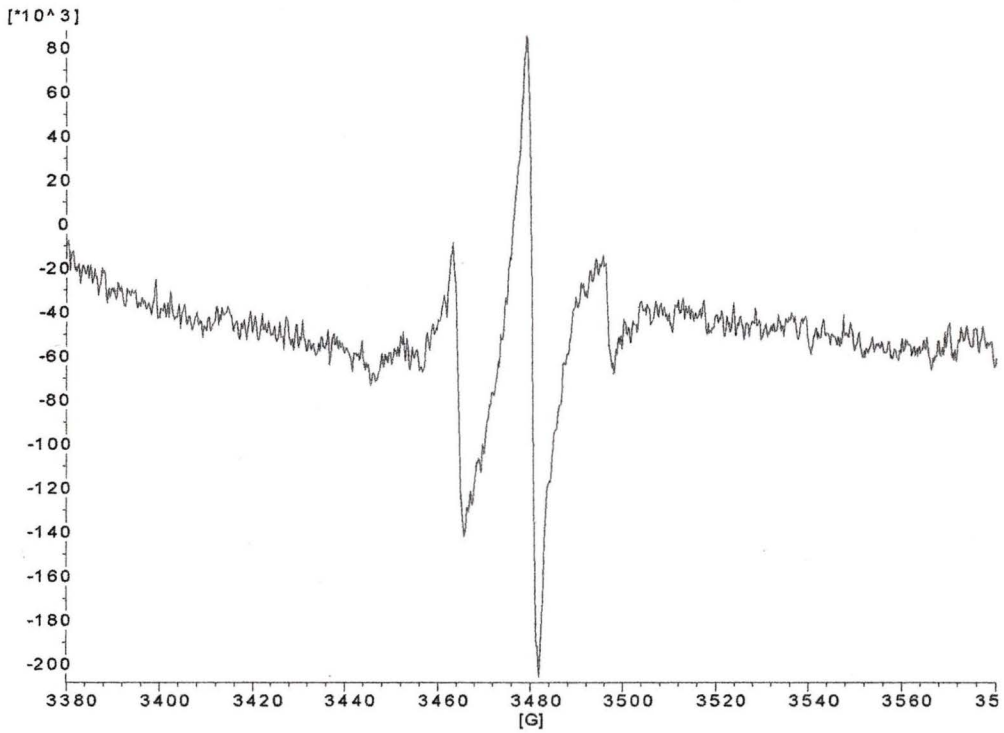

Figure 5.39: 6.67 μM 242C PA + MTSL, run in flat cell at RT

Chapter 6: Conclusions

The free spin label was determined to have a g value of 2.0050 and an a value of 16.20 G. Variants 300C PA, 445C PA, 241C PA, and 242C PA were each labeled with the nitroxyl spin label (1-oxyl-2,2,5,5-tetramethylpyrrolidine-3-yl)methylmethanethiosulfonate. The SDS-PAGE gels and titres for the variants showed that in no case was the protein inactivated or degraded by labeling. In the proaerolysin form, each labeled variant had a rigid EPR spectrum. The spectrum of variant 300C PA + MTSL was the most rigid. It looked very similar to the rigid limit spectra of PD-Tempone (Figure 5.4). There was axial symmetry with $A_{xx} = A_{yy} = 11$ G, and A_{zz} was 30.5 G. The g_x, g_y, and g_z values were 2.0055, 2.005, and 2.0035 G respectively. Variants 242C PA + MTSL and 241C PA + MTSL both had EPR spectra that were a bit more mobile than 300C PA + MTSL. Variant 445C PA + MTSL had an EPR spectrum that was part way between 300C PA + MTSL and 242C PA + MTSL. It was determined to have $A_{xx} = A_{yy} = 6.0$ G, and $A_{zz} = 31.0$ G. The g_x, g_y, and g_z values were 2.0080, 2.00525, and 2.00234 G respectively. It had some of the rigidity that was seen in the 300C PA + MTSL spectrum but it also had peaks that were attributed to a more freely moving label, similar to those in 242C PA + MTSL. Temperature studies were carried out on 445C PA + MTSL with and without trypsin added. These allowed for the determination of correlation times that are on the order of 10^{-12}-10^{-11} seconds. Distances were determined to be on the order of 1-2 Å for the C-terminal peptide of proaerolysin, and from this the mass of the peptide was determined to be approximately 1.9 kDa.

Chapter 7: Future Work

There are many things that can be done on this project in the future. The labeling process could be optimized to give a higher yield of spin labeled mutants. So far only a few areas of the protein have been investigated. Labeling more in key areas of the protein will help answer some of the questions about the heptamer formation of aerolysin. One of the stumbling blocks to date has been a poor signal to noise ratio. Several things could be tried to improve this. Other researchers have used various modifications to the EPR spectrometer to improve signal to noise in the systems that concern them. These modifications can either be in the spectrometer design or in the design of the sample container. Also work should be continued on the labeling process to look at ways of optimizing the process. With improved labeling will come an improved signal to noise ratio.

One thing that could be tried is to label some of the double mutants that exist with spin label. By comparing the spectra of the single mutants with the spectrum of the double mutant one should be able to determine the distance between the two labels. This could be of some use if the distance between molecules changes either when the protein is activated to aerolysin or when the aerolysin combines to form the heptamer that inserts into cells and kills them.

Cu(II) can also be added to the mutant. The hope with this is that if enough mutants can be labeled relatively close to the metal binding site then its exact location can be determined from simple triangulation of distance measurements. It will be interesting to know where the metal binding center is because if it is known where the

metal binds then one may be able to improve the sensitivity of the protein to the metal and thus change its selectivity towards other cells.

Another possible road to travel would be to put a spin labeled protein near a cell membrane and activate it. Since the process of insertion is not completely understood at this time some insight could be obtained. By labeling throughout proaerolysin one may be able to learn which portion goes where when the heptamer forms. There should be a change in the environment when the heptamer forms and hopefully EPR could detect these changes. By doing depth and distance measurements similar to those described in chapter 2 it could be possible to determine where various amino acids are situated in the heptamer.

References

1. J. A. McMillan, "Electron Paramagnetism," (Reinhold Book Corporation, New York, 1968), pp. 14-24, 155-183.

2. J. E. Wertz, J. R. Bolton, "Electron Spin Resonance: Elementary Theory and Applications," (McGraw-Hill Inc., New York, 1972), pp. 2-32, 195-200.

3. P. Atkins, "Physical Chemistry: Fifth Edition," (W. H. Freeman and Company, New York, 1994), p. 457.

4. R. T. Weber, J. J. Jiang, D. P. Barr, "EMX User's Manual," (Bruker Instruments Inc., Billerica, 1998), pp. 19-22.

5. R. T. Weber, J. J. Jiang, D. P. Barr, "EMX Training Manual," (Bruker Instruments Inc., Billerica, 1998).

6. C. P. Jr. Poole, "Electron Spin Resonance: A Comprehensive Treatise on Experimental Techniques," (Wiley-Interscience Publication, New York, 1982), p. 82.

7. N. M. Atherton, "Principles of Electron Spin Resonance," (Ellis Horwood limited, London, 1993), p. 287.

8. J. S. Leigh Jr., "ESR Rigid-Lattice Line Shape in a System of Two Interacting Spins," *The Journal of Chemical Physics,* 52(5), pp. 2608-2612, (1970).

9. L. J. Berliner, "Spin Labeling: Theory and Applications," (Academic Press, New York, 1976), pp. 28-29, 34.

10. J.W. Orton, "Electron Paramagnetic Resonance: An Introduction to Transition Group Ions in Crystals," (London Iliffe Books Ltd., Bath, Somerset, 1968), p. 142.

11. J. T. Buckley, "The Comprehensive Sourcebook of Bacterial Protein Toxins: Chapter 18 The channel-forming toxin aerolysin," (Academic Press, New York, 1999).

12. M. W. Parker, J. T. Buckley, J. P. M. Postma, A. D. Tucker, K. Leonard, F. Pattus, D. Tsernoglou, "Structure of the *Aeromonas* toxin proaerolysin in its water-soluble and membrane-channel states." *Nature*, 367, pp. 292-295, (1994).

13. S. S. Eaton, G. R. Eaton, "Interaction of Spin Labels with Transition Metals," *Coordination Chemistry Reviews,* 26, pp. 207-261, (1978).

14. W. L. Hubbell, H. S. Mchaourab, C. Altenbach, M. A. Lietzow, "Watching proteins move using site-directed spin labeling," *Structure,* 4, pp. 779-783, (1996).

15. C. K. Mathews, K. E. van Holde, "Biochemistry: Second Edition," (The Benjamin/Cummings Publishing Company, Menlo Park, California, 1996).

16. W. L. Hubbell, C. Altenbach, "Investigation of structure and dynamics in membrane proteins using site-directed spin labeling," *Current Opinion in Structural Biology*, 4, pp. 566-573, (1994).

17. C. Altenbach, D. A. Greenhalgh, H. G. Khorana, W. L. Hubbell, "A collision gradient method to determine the immersion depth of nitroxides in lipid bilayers: Application to spin-labeled mutants of bacteriorhodopsin," *Proceedings of the National Academy of Science USA*, 91(5), pp. 1667-1671, (1994).

18. H. S. Mchaourab, M. A. Lietzow, K. Hideg, W. L. Hubbell, "Motion of Spin-Labeled Side Chains in T4 Lysozyme. Correlation with Protein Structure and Dynamics," *Biochemistry*, 35(24), pp. 7692-7704, (June 1996).

19. W. L. Hubbell, D. S. Cafiso, C. Altenbach, "Identifying conformational changes with site-directed spin labeling," *Nature Structural Biology*, 9 (7), pp. 735-739, (September 2000).

20. H. S. Mchaourab, K. Joon Oh, C. J. Fang, W. L. Hubbell, "Conformation of T4 Lysozyme in Solution. Hinge-bending Motion and the Substrate-Induced Conformational Transition Studied by Site-Directed Spin Labeling," *Biochemistry,* 36, pp. 307-316, (1997).

21. G. I. Likhtensktein, "Spin Labeling Methods in Molecular Biology," (Wiley, New York, 1976).

22. H. J. Steinhoff, O. Dombrowsky, C. Karim, C. Schneiderhahn, "Two dimensional diffusion of small molecules on protein surfaces: an EPR study of the restricted translational diffusion of protein-bound spin labels," *European Biophysics Journal,* 20, pp. 293-303, (1991).

23. A. H. Beth, J. H. Park, "Interactions and spatial arrangement of spin labeled NAD^+ bound to glyceraldehydes-3-phosphate dehydrogenase. Comparison of EPR and X-ray modeling data." *Journal of Biological Chemistry,* 259, pp. 9717-9728, (1984).

24. H. S. Mchaourab, C. Fang, W. L. Hubbell, "A site directed spin labeling study of T4 lysozyme in solution," *Biophysics Journal,* 70, pp. 174-180, (1995).

25. J. Sun, J. Voss, W. L. Hubbell, H. R. Kaback, "Proximity between Periplasmic Loops in the Lactose Permease of *Escherichia coli* As determined by Site-Directed Spin Labeling," *Biochemistry,* 38(10), pp. 3100-3105, (1999).

26. C. Altenbach, T. Marti, H. G. Khorana, W. L. Hubbell, "Transmembrane Protein Structure: Spin Labeling of Bacteriorhodopsin Mutants," *Science,* 248, pp.1088-1092, (1990).

27. D. A. Greenhalgh, C. Altenbach, W. L. Hubbell, H. G. Khorana, "Locations of Arg-82, Asp-85, and Asp-96 in helix C of bacteriorhodopsin relative to the aqueous boundaries," *Proceedings of the National Academy of Science USA*, 88, pp. 8626-8630, (1991).

28. J. Voss, L. Salwinski, H. R. Kaback, W. L. Hubbell, "A method for distance determination in proteins using a designed metal ion binding site and site-directed spin labeling: Evaluation with T4 lysozyme," *Proceedings of the National Academy of Science USA*, 92(26), pp.12295-12299, (1995).

29. J. Voss, W. L. Hubbell, H. R. Kaback, "Distance determination in proteins using designed metal ion binding sites and site-directed spin-labeling: Application to the lactose permease of *Escherichia coli*," *Proceedings of the National Academy of Science USA*, 92(26), pp. 12300-12303, (1995).

30. D. L. Nelson, M. M. Cox, "Lehninger Principles of Biochemistry: Third Edition," (Worth Publishers, New York, 2000).

31. D. M. Jr. Neville, H. Glossman, "Plasma membrane protein subunit composition: a comparative study by discontinuous electrophoresis in sodium dodecyl sulfate." *Journal of Biological Chemistry*, 246, pp. 6335-6338, (1971).

32. http://www.biorad.com/

33. S. P. Howard, J. T. Buckley, "Activation of the hole-forming toxin aerolysin by extracellular processing," *Journal of Bacteriology,* 163, pp. 336-340, (1985).

34. J. Rossjohn, S. C. Feil, W. J. McKinstry, D. Tsernoglou, G. Van Der Goot, J. T. Buckley, M. W. Parker, "Aerolsyin – A Paradigm for Membrane Insertion of Beta-Sheet Protein Toxins?" *Journal of Structural Biology,* 121, pp. 92-100, (1998).

35. http://www.fermentas.com/profiles/ModifyingEnzymes/pproteinasek.html

Curriculum Vitae

Date: March 9, 2002

NAME: Michael James McAlduff

ADDRESS: 26 Hillcrest Street

Antigonish, N.S, Canada

B2G 1Z3

DATE & PLACE OF BIRTH: May 10th 1977, Antigonish, N.S.

EDUCATION:

Date	Discipline	Degree	Institution
June 1995		Diploma	Dr. John Hugh Gillis Regional High School
May 1999	Chemistry	B.Sc.	Saint Francis Xavier University

HONORS AND DISTINCTIONS (Year and name of award):

September 1995 $2,000 Entrance Scholarship to St. F.X.

September 1996 $1,000 In-house Scholarship at St. F.X.

September 1999 $12,400 University of Victoria Fellowship

PUBLICATIONS:

1. MacMillan, S.N.; Kennedy, C.A.; McAlduff, M.J.; Marangoni, D.G. The Interaction of Isomeric Hexanediols with Anionic and Cationic Micelles; Colloid Polymer Sci., 2001 279, 1-7.

University of Victoria Partial Copyright License

I hereby grant the right to lend my thesis to users of the University of Victoria Library, and to make single copies only for such users or in response to a request from the Library of any other university, or similar institution, on its behalf or for one of its users. I further agree that permission for extensive copying of this thesis for scholarly purposes may be granted by me or a member of the University designated by me. It is understood that copying or publication of this thesis for financial gain by the University of Victoria shall not be allowed without my written permission.

Title of Thesis:

An EPR Study of the Protein Proaerolysin

Author 

Michael James McAlduff

July 7, 2002